# plag.docx

Delhi Technological University

## Document Details

Submission ID
trn:oid:::27535:123871143

Submission Date
Dec 7, 2025, 1:54 AM GMT+5:30

Download Date
Dec 7, 2025, 2:07 AM GMT+5:30

File Name
plag.docx

File Size
10.4 MB

140 Pages

35,468 Words

195,271 Characters

# 9% Overall Similarity

The combined total of all matches, including overlapping sources, for each database.

## Filtered from the Report

- Bibliography
- Small Matches (less than 8 words)

## Match Groups

**447** Not Cited or Quoted 12%
Matches with neither in-text citation nor quotation marks

**63** Missing Quotations 2%
Matches that are still very similar to source material

**4** Missing Citation 0%
Matches that have quotation marks, but no in-text citation

**2** Cited and Quoted 0%
Matches with in-text citation present, but no quotation marks

## Top Sources

5% Internet sources
8% Publications
9% Submitted works (Student Papers)

## Integrity Flags

**1 Integrity Flag for Review**

**Replaced Characters**
83 suspect characters on 20 pages
Letters are swapped with similar characters from another alphabet.

Our system's algorithms look deeply at a document for any inconsistencies that would set it apart from a normal submission. If we notice something strange, we flag it for you to review.

A Flag is not necessarily an indicator of a problem. However, we'd recommend you focus your attention there for further review.

## Match Groups

- **447** Not Cited or Quoted 12%
  Matches with neither in-text citation nor quotation marks
- **63** Missing Quotations 2%
  Matches that are still very similar to source material
- **4** Missing Citation 0%
  Matches that have quotation marks, but no in-text citation
- **2** Cited and Quoted 0%
  Matches with in-text citation present, but no quotation marks

## Top Sources

5% Internet sources
8% Publications
9% Submitted works (Student Papers)

## Top Sources

The sources with the highest number of matches within the submission. Overlapping sources will not be displayed.

| | | |
|---|---|---|
| 1 | Internet | hdl.handle.net <1% |
| 2 | Internet | www.mdpi.com <1% |
| 3 | Publication | Manar Abdelhamid, Nazri Ali, Tareq Abdelaziz. "A Literature Review of Factors Aff... <1% |
| 4 | Internet | www.schweizerbart.de <1% |
| 5 | Submitted works | universititeknologimara on 2024-07-15 <1% |
| 6 | Submitted works | University of Cape Town on 2021-01-15 <1% |
| 7 | Submitted works | University of Hong Kong on 2015-04-30 <1% |
| 8 | Submitted works | Universiti Malaysia Pahang on 2019-05-26 <1% |
| 9 | Publication | "Proceedings of the Indian Geotechnical Conference (IGC 2024), Volume 1", Sprin... <1% |
| 10 | Publication | Elsawy, Mohamed(Boley, C. and Richwien, Werner). "Highway Embankment Const... <1% |

| | | |
|---|---|---|
| 11 | Publication | Meenakshi Singh, Ashutosh Trivedi, Sanjay Kumar Shukla. "Evaluation of geosynt... <1% |
| 12 | Internet | 123docz.net <1% |
| 13 | Submitted works | Jaypee University of Information Technology on 2021-03-10 <1% |
| 14 | Publication | "Proceedings of the Indian Geotechnical Conference 2019", Springer Science and ... <1% |
| 15 | Submitted works | University Tun Hussein Onn Malaysia on 2018-07-03 <1% |
| 16 | Internet | pdfcoffee.com <1% |
| 17 | Submitted works | University of Mosul on 2023-06-01 <1% |
| 18 | Publication | Ashish Juneja, Anil Joseph, Dasaka S. Murty. "GeoVadis - The Future of Geotechnic... <1% |
| 19 | Publication | Geosynthetics in Civil and Environmental Engineering, 2009. <1% |
| 20 | Submitted works | University of Birmingham on 2017-01-06 <1% |
| 21 | Internet | etheses.bham.ac.uk <1% |
| 22 | Internet | www.issmge.org <1% |
| 23 | Publication | "Proceedings of GeoMandu 2024 Volume 4", Springer Science and Business Media... <1% |
| 24 | Publication | Benz, . "Performance of geogrid-encased stone columns as a reinforcement of sof... <1% |

25 Submitted works
National Institute Of Technology, Tiruchirappalli on 2023-07-20 <1%

26 Publication
Al-Saadi, Ali Nashat Shukur. "Numerical Simulation of Geosynthetic Encased Ston... <1%

27 Publication
Ghazavi, Mahmoud, and Javad Nazari Afshar. "Bearing capacity of geosynthetic e... <1%

28 Publication
Manita Das, Ashim Kanti Dey. "Use of Soil Cement Bed in Improvement of Load C... <1%

29 Publication
Deb, K.. "Laboratory model studies on unreinforced and geogrid-reinforced sand ... <1%

30 Publication
"Technologies for Sustainable Transportation Infrastructures", Springer Science a... <1%

31 Internet
usir.salford.ac.uk <1%

32 Submitted works
Birla Institute of Technology and Science Pilani on 2025-06-24 <1%

33 Internet
www.ijert.org <1%

34 Submitted works
Nottingham Trent University on 2025-09-11 <1%

35 Internet
dspace.dtu.ac.in:8080 <1%

36 Internet
lib.buet.ac.bd:8080 <1%

37 Publication
K. Ali, J.T. Shahu, K.G. Sharma. "Model tests on geosynthetic-reinforced stone colu... <1%

38 Publication
Kim Chan, Bosco Poon. "New Analytical Approach for Predicting Horizontal Displa... <1%

39 Submitted works
Middle East Technical University on 2013-09-04 <1%

40 Publication
"Ground Engineering and Applications", Springer Science and Business Media LLC... <1%

41 Submitted works
Dr. B R Ambedkar National Institute of Technology, Jalandhar on 2020-05-25 <1%

42 Publication
Meixiang Gu, Xiaocong Cai, Yi Lu, Daoling Han. "Numerical investigation of cyclic ... <1%

43 Publication
Sitaram Nayak, M. P. Vibhoosha, Anjana Bhasi. "Effect of Column Configuration o... <1%

44 Publication
A. P. Ambily, Shailesh R. Gandhi. "Behavior of Stone Columns Based on Experimen... <1%

45 Submitted works
De La Salle University - Manila on 2025-08-07 <1%

46 Submitted works
National Institute Of Technology, Tiruchirappalli on 2021-12-31 <1%

47 Publication
Mohammad Reza Malekpoor, Gholamreza Poorebrahim. "Behavior of Compacted ... <1%

48 Internet
www.ir.juit.ac.in:8080 <1%

49 Publication
"Advances in Geoengineering along the Belt and Road", Springer Science and Bus... <1%

50 Publication
"Ground Improvement and Reinforced Soil Structures", Springer Science and Busi... <1%

51 Publication
"Proceedings of the 7th Indian Young Geotechnical Engineers Conference", Sprin... <1%

52 Publication
Amit Kumar Das, Kousik Deb. "Experimental and 3D Numerical Study on Time-De... <1%

53 Publication

Anandha Raj Lenin Kumar, Sanjay Nimbalkar, G R Dodagoudar. "Performance of ... <1%

54 Submitted works

National Institute of Technology, Rourkela on 2018-05-20 <1%

55 Publication

Kirsch, Klaus, and Fabian Kirsch. "Improvement of fine-grained and cohesive soils... <1%

56 Publication

Shakeel Abid Mohammed, Deendayal Rathod, Sai K. Vanapalli. "Experimental and ... <1%

57 Publication

"Geocells", Springer Science and Business Media LLC, 2020 <1%

58 Submitted works

University of Birmingham on 2015-09-28 <1%

59 Submitted works

Indian Institute of Technology, Bombay on 2015-03-11 <1%

60 Publication

Sanjoli Gupta, Suresh Kumar, N. Muni Pradeep, Mayank Nishant. "Performance a... <1%

61 Submitted works

Gujarat Technological University on 2018-10-22 <1%

62 Submitted works

University of Newcastle on 2015-06-19 <1%

63 Submitted works

University of Technology on 2020-12-16 <1%

64 Submitted works

Indian School of Mines on 2025-07-15 <1%

65 Publication

J. T. Shahu, Suresh Kumar, Riya Bhowmik. "Behaviour of Geogrid-Encased Group o... <1%

66 Publication

Joel Gniel, Abdelmalek Bouazza. "Improvement of soft soils using geogrid encase... <1%

67 Submitted works
University of Leeds on 2013-04-29 <1%

68 Internet
espace.rmc.ca <1%

69 Internet
etd.aau.edu.et <1%

70 Publication
Fang Xu, Hossein Moayedi, Loke Kok Foong, Mohamad Jamali Moghadam, Milad Z... <1%

71 Submitted works
Jawaharlal Nehru Technological University on 2025-09-26 <1%

72 Publication
Lateef Ahmad Dar, Mohammad Yousuf Shah. "Three Dimensional Numerical Stud... <1%

73 Submitted works
Universiti Teknologi Malaysia on 2022-03-11 <1%

74 Submitted works
University of Birmingham on 2021-01-15 <1%

75 Submitted works
University of Nottingham on 2022-04-20 <1%

76 Internet
gcris.iyte.edu.tr <1%

77 Submitted works
universititeknologimara on 2024-07-09 <1%

78 Publication
J Black, V Sivakumar, J D McKinley. "Performance of clay samples reinforced with ... <1%

79 Publication
Maryam Gaber, Anuar Kasa, Norinah Abdul Rahman, Jamal Alsharef. "Compariso... <1%

80 Submitted works
Napier University on 2015-09-04 <1%

81 Submitted works
Napier University on 2017-03-24 <1%

82 Publication
Srijan Srijan. "Enhancing ground stability with quarry dust columns: A comparati... <1%

83 Submitted works
Trinity College Dublin on 2022-04-28 <1%

84 Submitted works
Universiti Teknologi Malaysia on 2024-09-08 <1%

85 Submitted works
University of Glasgow on 2016-01-13 <1%

86 Submitted works
University of Portsmouth on 2017-09-11 <1%

87 Internet
worldwidescience.org <1%

88 Publication
"Recent Advances in Civil Engineering", Springer Science and Business Media LLC,... <1%

89 Publication
A. M. Hanna, M. Etezad, T. Ayadat. "Mode of Failure of a Group of Stone Columns i... <1%

90 Publication
Mahdavi, Hamed. "Three-Dimensional Numerical and Physical Modelling of Soft S... <1%

91 Publication
Muhammad Syamsul Imran Zaini, Muzamir Hasan, Wan Nursyafiqah Binti Wan Ju... <1%

92 Submitted works
National Institute Of Technology, Tiruchirappalli on 2023-01-06 <1%

93 Submitted works
National Institute of Technology, Rourkela on 2014-05-30 <1%

94 Submitted works
University of Southern Queensland on 2023-11-15 <1%

95 Submitted works
University of Technology on 2017-06-18 <1%

96 Submitted works
University of Wollongong on 2014-06-13 <1%

97 Internet
spectrum.library.concordia.ca <1%

98 Publication
"Latest Thoughts on Ground Improvement Techniques", Springer Science and Bu... <1%

99 Publication
Abas, Hassan Ali. "Performance and Design Optimization of Stone Column in Sab... <1%

100 Publication
Boštjan Pulko, Bojan Majes, Janko Logar. "Geosynthetic-encased stone columns: ... <1%

101 Submitted works
Maulana Azad National Institute of Technology Bhopal on 2020-10-17 <1%

102 Submitted works
University of Bradford on 2022-04-08 <1%

103 Submitted works
University of Bradford on 2023-03-22 <1%

104 Submitted works
University of Technology on 2023-04-03 <1%

105 Internet
khazna.ku.ac.ae <1%

106 Submitted works
nith on 2023-05-17 <1%

107 Publication
Jang, I.S.. "Lateral and consolidation behaviors of seabed-type breakwater for ver... <1%

108 Publication
M. Alamgir, N. Miura, H.B. Poorooshasb, M.R. Madhav. "Deformation analysis of s... <1%

109 Submitted works
University of Birmingham on 2015-01-12 <1%

110 Submitted works
Universiti Malaysia Perlis on 2023-07-19 <1%

111 Submitted works
University of Birmingham on 2014-05-12 <1%

112 Publication
Andrea Brito, Laura Maria Mello Saraiva Caldeira, João Ribas Maranha. "Hydrome... <1%

113 Publication
Arvind Kumar Jha, Dhanraj Kumar, P. V. Sivapullaiah. "Influence of Fly Ash on Geo... <1%

114 Submitted works
Jawaharlal Nehru Technological University on 2025-09-15 <1%

115 Publication
Leung, C.. "An experimental study of the effect of local contact loss on the earth ... <1%

116 Submitted works
University of Southampton on 2021-05-03 <1%

117 Publication
Yaolin Yi, Songyu Liu, Anand J. Puppala, Fei Jing. "Variable-diameter deep mixing ... <1%

118 Internet
daneshyari.com <1%

119 Internet
www.nature.com <1%

120 Submitted works
Asian Institute of Technology on 2009-05-05 <1%

121 Publication
Bo Yang, Zexi Yin, Araz Hasheminezhad, Mohammad Ahmad Alsheyab, Halil Ceyla... <1%

122 Submitted works
Liverpool John Moores University on 2025-06-15 <1%

123 Submitted works
Universiti Malaysia Sabah on 2018-05-16 <1%

124 Submitted works
University of Birmingham on 2009-09-01 <1%

125 Submitted works
University of East London on 2024-09-02 <1%

126 Submitted works
University of Pretoria on 2018-07-24 <1%

127 Internet
core.ac.uk <1%

128 Submitted works
A'Sharqiyah University, Oman on 2025-05-11 <1%

129 Publication
Ankur Mudgal, Bibek Jha, Raju Sarkar, Amit Kumar Srivastava, Akshit Mittal, Neh... <1%

130 Publication
Pallavi Verma*, A. K. Sahu. "Effect of Grouted Granular Column on the Load Carryi... <1%

131 Publication
S. T. Kadhim, R. L. Parsons, J. Han. "Vertical Stability of Individual Geotextile-Encas... <1%

132 Publication
Sanjay Kumar Shukla. "Fundamentals of Fibre-Reinforced Soil Engineering", Sprin... <1%

133 Submitted works
Universiti Malaysia Pahang on 2018-09-13 <1%

134 Submitted works
University of Portsmouth on 2013-09-18 <1%

135 Internet
bentleysystems.service-now.com <1%

136 Internet
www.science.gov <1%

137 Publication
"Recent Developments in Sustainable Infrastructure", Springer Science and Busin... <1%

138 Publication
Ahad Ehsaniyamchi, Mahmoud Ghazavi. "Short-term and long-term behavior of g... <1%

139 Submitted works
Asian Institute of Technology on 2010-05-09 <1%

140 Publication
Engineering Computations, Volume 27, Issue 5 (2010-07-03) <1%

141 Submitted works
Engineers Australia on 2016-08-05 <1%

142 Submitted works
European University of Lefke on 2020-06-08 <1%

143 Publication
Huifang Zhang, Lei Wang, Jie Chen, Haiyang Chen, Wei Wu, Jinzhu Li, Henan Lu, D... <1%

144 Submitted works
Indian Institute of Technology, Bombay on 2015-03-26 <1%

145 Submitted works
Institute of Graduate Studies, UiTM on 2013-06-04 <1%

146 Publication
J. Obradors-Prats, M. Rouainia, A. C. Aplin, A. J. L. Crook. "Hydromechanical Modeli... <1%

147 Publication
Kousik Deb, P. K. Basudhar, Sarvesh Chandra. "Generalized Model for Geosynthet... <1%

148 Submitted works
Ohio University on 2006-02-27 <1%

149 Publication
Sitaram Nayak, M. R. Dheerendra Babu, R. Shivashankar, Naveen James. "Perfor... <1%

150 Submitted works
University of East London on 2013-09-13 <1%

151 Publication

Wei Guo, Xin Wang, Yuxiao Ren, Yifei Kang, Keshen Yu, Hao Xu, Changyi Yu. "Expe... <1%

152 Internet

digitalcommons.wayne.edu <1%

153 Internet

www.teses.usp.br <1%

154 Submitted works

Curtin University of Technology on 2013-05-19 <1%

155 Publication

Gurbhej Singh. "Multifunctional and Smart Materials - Advances in Sustainable En... <1%

156 Publication

Jayapal Jayarajan, Rajagopal Karpurapu. "Bearing Capacity and Settlement Respo... <1%

157 Submitted works

Middle East Technical University on 2014-06-13 <1%

158 Publication

Miura, . "Soft clay engineering", Soft Clay Behaviour Analysis and Assessment, 20... <1%

159 Publication

Mohammed Y. Fattah, Bushra S. Zabar, Hanan A. Hassan. "Experimental Analysis ... <1%

160 Submitted works

Queen's University of Belfast on 2024-09-16 <1%

161 Submitted works

University of Auckland on 2018-12-10 <1%

162 Submitted works

University of Portsmouth on 2017-09-11 <1%

163 Submitted works

University of Stellenbosch, South Africa on 2013-10-26 <1%

164 Submitted works

University of Technology on 2022-11-03 <1%

165 Internet
ir.canterbury.ac.nz <1%

166 Internet
ir.uz.ac.zw <1%

167 Internet
iris.polito.it <1%

168 Internet
kipdf.com <1%

169 Internet
network.bepress.com <1%

170 Internet
tudr.thapar.edu:8080 <1%

171 Internet
www.cedd.gov.hk <1%

172 Publication
"Advances in Civil Engineering", Springer Science and Business Media LLC, 2021 <1%

173 Publication
"Scanning Auger Electron Microscopy", Wiley, 2005 <1%

174 Submitted works
76830 on 2014-10-26 <1%

175 Submitted works
8779 on 2015-04-24 <1%

176 Submitted works
Birla Institute of Technology and Science Pilani on 2021-04-22 <1%

177 Submitted works
Cape Peninsula University of Technology on 2009-04-26 <1%

178 Submitted works
Central Queensland University on 2024-09-29 <1%

179 Submitted works
City University of New York System on 2025-04-12 <1%

180 Submitted works
Curtin University of Technology on 2015-10-27 <1%

181 Submitted works
Engineers Australia on 2023-01-10 <1%

182 Submitted works
Indian Institute of Science, Bangalore on 2023-11-27 <1%

183 Submitted works
Indian Institute of Technology, Madras on 2022-03-07 <1%

184 Submitted works
Indian School of Mines on 2017-12-07 <1%

185 Publication
Jian-Feng Chen, Liang-Yong Li, Zhen Zhang, Xu Zhang, Chao Xu, Sathiyamoorthy R... <1%

186 Publication
Khabbazian, M. "Numerical simulation of geosynthetic encased columns used ind... <1%

187 Publication
Liang-Yong Li, Sathiyamoorthy Rajesh, Jian-Feng Chen. "Centrifuge model tests o... <1%

188 Publication
Ling Zhang, Minghua Zhao. "Deformation Analysis of Geotextile-Encased Stone C... <1%

189 Submitted works
Napier University on 2017-08-17 <1%

190 Publication
S. H. Lajevardi, H. R. Shamsi, M. Hamidi, S. Enami. "Numerical and Experimental St... <1%

191 Publication
Sudip Basack, Buddhima Indraratna, Cholachat Rujikiatkamjorn. "Modeling the P... <1%

192 Submitted works
Swinburne University of Technology on 2021-04-30 <1%

193 Publication
Sünnetçioglu, Mehmet Emrah. "A Laboratory Model Study on Settlement Reducti... <1%

194 Submitted works
UC, San Diego on 2024-06-10 <1%

195 Submitted works
Universiti Malaysia Pahang on 2022-06-28 <1%

196 Submitted works
Universiti Tenaga Nasional on 2019-02-16 <1%

197 Submitted works
University of Birmingham on 2008-09-01 <1%

198 Submitted works
University of Birmingham on 2024-05-31 <1%

199 Submitted works
University of Canterbury on 2014-05-22 <1%

200 Submitted works
University of Leeds on 2012-05-04 <1%

201 Submitted works
University of Liverpool on 2023-08-31 <1%

202 Submitted works
University of Nottingham on 2018-05-01 <1%

203 Submitted works
University of Nottingham on 2023-09-08 <1%

204 Submitted works
University of Strathclyde on 2011-08-26 <1%

205 Publication
Wagdi Hamid, Ahmed Alnuaim. "Effect of geopolymer treatment on the ultimate ... <1%

206 Submitted works
Yildirim Beyazit Universitesi on 2025-05-14 <1%

207 Internet
ascelibrary.org <1%

208 Internet
assets-eu.researchsquare.com <1%

209 Internet
doczz.net <1%

210 Internet
download.bibis.ir <1%

211 Internet
era.library.ualberta.ca <1%

212 Internet
kuscholarworks.ku.edu <1%

213 Internet
mediatum.ub.tum.de <1%

214 Submitted works
nith on 2024-05-25 <1%

215 Internet
theses.hal.science <1%

216 Internet
www.icevirtuallibrary.com <1%

217 Internet
www.jkcs.or.kr <1%

218 Internet
www.onlime.co.nz <1%

219 Internet
www.sctce.ac.in <1%

220 Internet
zone.biblio.laurentian.ca <1%

# CHAPTER 1

# INTRODUCTION

## 1.1 General

The nation's economy, urbanization, and population growth are all contributing to the enormous expansion of its civil infrastructure. The number of appropriate sites for construction is gradually declining. This necessitates improving and honing marginal sites that would not have been considered fit for building otherwise. Soft clay, loose sand, silt, expanding soil, frozen soil, collapsible soil, organic soil, loess, and other types of soil are considered poor and challenging for construction purposes. Shear strength, compressibility, volume change, creep deformation, and permeability are the main issues with these soils (Han, 2015).

The process utilized to enhance the characteristics of soil, namely its behavior in terms of strength, compressibility, and permeability, is known as ground augmentation. Many techniques for ground enhancement have been applied extensively and shown to be effective in raising the caliber of soft deposits. The stone column is a commonly used method for increasing the stability of loose sandy soils, such as silty or clayey sands, as well as soils with poor undrained shear strength. In this process, boreholes are made in the malleable soil at predetermined spots. Granular particles of various sizes fill the area. For construction projects such as liquid storage tanks and embankments, the composite earth provides a semi-rigid and flexible base. The application of stone columns results in improved stiffness, increased bearing ability, and decreased settlement. Consolidation proceeds more quickly as a result of improved soil drainage.

Around 1830, the usage of stone columns was first implemented in France, a European nation. They have been extensively used in Europe for site improvement since the late 1950s (Barksdale and Bachus, 1983). Basarkar et al. (2009) reported that the vibro-flot technique was first applied to the construction of stone columns in India in 1961 in Ennore, Madras. Since then, the strategy has been widely used in numerous locations around the nation.

The stone column transmits the upcoming load to the nearby earth by acting as an interconnected framework. Each stone column has a tributary area of soil encircling it that forms a regular hexagon. A comparable circular region with the same total area as the hexagon can be used to roughly represent this hexagon. The identical circle has a diameter that almost encompasses both the tributary dirt and one stone column.

This is frequently called a unit cell. When examining the operation of the column group, the unit cell concept is particularly useful.

Either the displacement method or the replacement approach can be used to finish the construction of the stone column. With the displacement method, the surrounding dirt is moved and a hole is made in the ground using a closed casing pipe. The hole that the casing produced is then filled with stones. In the replacement procedure, a hole or cavity of the desired depth is dug out of the ground and filled with stones. The displacement method works well for both unsaturated cohesive and cohesionless soils, while the replacement strategy works well for cohesive soils (Han, 2015).

The case studies of Indian foundations that use stone columns have been reported by Datye and Madhav (1988). The effectiveness of foundations for a range of uses, such as pipe pedestals, small and large groups of isolated footings, bridge abutments, and stone columns for area treatment, was examined. These cases cover a wide range of projects, including the footings for pipe rack work at IFFCO, Kandla in 1972, the treatment of foundations for the Belapur and Kasheli Bridge abutments in 1975, the improvement of soil for lagoon embankment and foundations for a sewage treatment plant near Bhandup, Bombay in 1982, the ground treatment for a pipeline at Sion-Koliwada, Bombay, and the hazardous storage liquid tanks at Manglore Chemical and Fertilizers, Manglore, as well as at IFFCO, Kandla.

Barksdale and Bachus (1983) state that the stone column design loads typically range from 20 to 50 tons. In contrast to the nearby soft soils, a composite structure with greater shear strength and less compressibility was formed inside the soft ground after a stone column was constructed. The column material is contained by the malleable earth. Stress concentration occurs in the column as a result of the superstructure's tension causing the column and the surrounding earth to slide downward simultaneously. The stiffness of the column material causes the concentration of stress. The column is under more stress than the surrounding soil due to the difference in modulus between the column material and the surrounding soil. The stress concentration ratio, or SCR, is the ratio of the stress on the nearby soil to the stress across the column. It is commonly used to illustrate the transmission of load between columns and soft soils. IS 15284 (Part I) provides a stress concentration ratio of 2.5–5, but Barksdale and Bachus (1983) suggest a ratio of 1–5.

When a single stone column is subjected to loads over its area, its length significantly affects how it fails. In general, a stone column will collapse in the bulging state if its length exceeds the critical length, which is four times its diameter. On the other hand, if the column's length is less than the critical length, punching shear failure or general shear failure may occur. (IS15284 Part 1).

Two elements contribute to the strength of traditional stone columns: the limitation supplied by the loose soil in the area and the friction between the granular components that comprise the column. The properties of higher bearing capacity and less settling are observed in the loaded ground in comparison to the original native soil. Nevertheless, the following reasons might cause its performance to still fall short of expectations (Murugesan and Rajagopal, 2009).

The stone columns' frictional properties may be reduced if the nearby loose dirt were to seep inside.

The stones may not make as much of an effect as they would have in their original, undisturbed form since they can move laterally into the soft nearby soil.

A different strategy has been investigated to solve this problem, which involves reinforcing rammed stone columns with a geogrid-encased tube. This method has been found to increase the strength and compressibility of the stone columns. Numerous experiments have been carried out in a small number of projects to apply the positioning of a geogrid casing, followed by the charging of stones into it (Deshpande and Vyas, 1996; Richard and Yogesh, 2005; Raithel et al., 2006). The resultant columns have a constant diameter throughout, despite the departure from the traditional vibro-technique, and the addition of a geogrid offers the necessary lateral confinement. Laboratory model stone columns with encasement have been the subject of several studies (Sivakumar et al., 2004; Bauer and Nabil, 1996). These studies, which primarily use sand in combination with stone particles, have shown an increase in bearing capacity, which helps to explain the scaled-down effect. By adding an encasement, a stone column's stiffness and structural integrity are improved. It also helps to lessen the lateral compression that stones experience during installation, especially in low-bearing soils. This enables quicker installation procedures without compromising the column's ability to drain or the frictional properties of the stones used. Even with all of the benefits that enclosed stone columns offer, this method is not as often used as stone columns. The main cause of this is a lack of knowledge about how applied loads affect encased stone columns.

Therefore, it is thought that a thorough study of encased type stone columns is necessary to clarify the process by which the encasement increases the column's strength and pinpoint the factors influencing its behavior.

Comparing encased and unencased stone columns is important to ascertain how encasement impacts the strength of a bed supported by stone columns. To make it easier to quantify the previously described impact, this investigation should be carried out under similar testing settings. As a result, the goals and scope of the study have been established.

### 1.2 Inspiration

The availability of building sites with appropriate soil qualities has decreased as a result of the quick speed of urbanization and industrial growth. As a result, field engineers often face constraints when selecting locations that contain weak soil layers with complex behaviours, mainly due to the existence of troublesome soils with varying geotechnical characteristics. Soft clay with high compressibility, poor shear strength, and substantial settlement potential makes up a large portion of these underutilized or abandoned sites, or loose, cohesionless soils lacking sufficient load-bearing capacity. Such conditions make these sites vulnerable to issues like landslides, liquefaction, or instability due to the presence of uncontrolled fill materials. Therefore, thorough site preparation is necessary to guarantee building projects' feasibility and safety. When exploring different ground improvement or modification techniques, it is crucial to select and apply a method that meets both the economic constraints and the structural design requirements.

In recent years, a widely adopted ground improvement technique involves inserting granular aggregates into weak soil layers in the form of cylindrical columns. This method is typically executed through either vibration or dynamic compaction. The use of stone columns—where columns of granular material are introduced into loose sands, alluvial silty clays, sandy silts, and soft cohesive soils—has proven to be an effective reinforcement strategy (Ketkar and Telang, 1994; Kumar et al., 2002). Since its introduction in the 1970s, Stone column technology has been used to improve, stabilize, and rehabilitate soil foundations for a broad range of structures, including high-rise buildings, industrial facilities, towers, and oil storage tanks.

JBF Petrochemical Industries Ltd proposed the development of a new paraxylene terephthalic acid (PTA) plant in Mangalore, India, with an anticipated annual output of 1.25 million

metric tonnes. The facility was designed to include storage tanks, processing units, substations, and various support structures. Keller was commissioned to design and execute ground improvement solutions for three paraxylene tanks and two fire water tanks, measuring 64 meters and 35 meters in diameter, respectively. Alongside these tanks, construction of the corresponding tank pads was also required. Subsurface investigations revealed varying layers of sand with differing consistencies—from soft to dense—underlain by tightly packed silty sand or weathered rock. The main objective of the project was to limit both total and differential settlement while increasing the tank pad foundations' load-bearing capability. To achieve this, Keller implemented a ground improvement strategy using bottom feed vibro stone columns, which effectively enhanced the bearing strength of the soil and reduced settlement issues. The tank pad construction involved several critical elements, including a stone blanket, HDPE membrane, sand pad, stone ring beam, and bituminous surfacing.

Similarly, Cochin International Airport Ltd. (CIAL) proposed an expansion project to upgrade apron areas adjacent to the existing facilities, including associated airfield infrastructure. The major contractor hired Keller to carry out ground renovation using vibro stone columns to support the building of new airplane parking bays. The site posed several geotechnical challenges, notably the presence of highly compressible plastic clay and loosely filled soil layers over an area of approximately 41,000 m². Additionally, a subsurface nallah posed a risk of uneven settlement. Given the complexities of working in an operational airport environment, careful coordination and planning of rig movements were essential.

To address these challenges, Keller implemented an optimized foundation solution using vibro stone columns. This technique successfully enhanced the soil's settling properties and bearing capacity, while also enhancing drainage for rapid consolidation. The solution not only reduced project costs for the client but also resulted in significant time savings. The treatment zone was extended beyond the apron’s footprint to provide lateral confinement and ensure a smooth transition between treated and untreated soils. The project was successfully completed within the scheduled timeframe using four rigs.

Beyond this, geotechnical experts have successfully applied the stone column technique in various notable projects. In Rohtak, Haryana, a temple foundation was constructed using granular piles with a 12-meter diameter and 500 mm rammed stone columns. Likewise, the restoration of approximately 1,000 pillars at the Kalyana Mandapa in Hanuma Konda,

Warangal, involved 400 mm diameter rammed stone columns and 7-meter-long granular piles. The construction of a picture tube manufacturing facility in Karzan, Vadodara, incorporated gravel piles between 300 and 400 mm in diameter. Additionally, the fire water tank at the Indian Oil Corporation Ltd.'s LPG Bottling Plant in Madanpur Khadar was supported by a foundation consisting of a group of gravel columns measuring 3 × 22 meters.

The use of vibro stone columns to support the raft foundation was most recently suggested by the foundation committee for the Ram Temple in Ayodhya. These examples demonstrate the widespread adoption of stone column techniques across a variety of soil conditions and structural applications, demonstrating that it is a dependable and economical way to increase the stability of poor soils.

### 1.3 Significance of the Research

Soft clay formations, which are geologically young deposits, are commonly located all across the world, including several regions in India. Notable examples include the Thane Creek area in Mumbai, where thick layers of highly deformable clay—ranging from 15 to 20 metres—are prevalent. Similarly, Cochin is underlain by a significant marine clay deposit exceeding 20 metres in thickness, posing challenges even for constructing relatively light structures such as two-storey buildings. This soft clay is typically found beneath surface fills of about 2 to 3 metres. In Vishakapatnam, particularly near the port, there exists an offshore clay deposit with a depth of approximately 100 metres, characterized by high compressibility. Likewise, the coastal region of Chennai features a soft clay layer varying in thickness from a few metres up to more than 20 metres, located beneath a crustal layer of 2 to 3 metres, which presents substantial difficulties in ensuring foundation stability.

These deposits are predominantly composed of fine-grained soils, with moderate to high clay content. The clay fractions typically display high plasticity, low shear strength, and significant compressibility. In many cases, The amount of natural moisture is about or even exceeds the liquid limit, further reducing the soil’s load-bearing capacity. These characteristics often lead to foundation failures, particularly when surface loads from embankments or shallow foundations are applied—resulting in large settlements that must be considered during design and may require ongoing structural maintenance.

Due to these challenges, ground improvement becomes essential for ensuring the safe and stable performance of civil engineering structures on such weak soils. A common scenario encountered by field engineers involves loose, soft soil overlying a more competent layer, such as dense sand or stiff clay. There is a great need for more research on the efficacy of this method in improving the performance of soft clay foundations given the frequency of studies and real-world applications involving the usage of stone columns for cohesive soil reinforcement.

## 1.4 SCOPE AND OBJECTIVES OF THIS STUDY

The main goal of this thesis is to evaluate the possibilities of using ordinary stone columns (OSC) and vertically enclosed stone columns (VESC) to increase the load carrying capacity of soft soil. Additionally, by testing scaled models in the lab, the current study seeks to examine the impact of different parameters. Numerical analyses were also carried out to confirm the experiment's results.

Hence, the primary aims of this study are as follows:

- Identification of expansive soil, column filling materials and the encasing material.
- To investigate how stone columns behave in terms of strength, either individually or in groups.
- Comparison of the performance of geosynthetic encased column with unencased column in individual or in groups.
- Compare relative efficiency of different types of geosynthetics i.e. geotextile and geogrid.
- Validation of the findings of the laboratory tests results against the numerical modelling done by Plaxis 3D software.

## 1.5 METHODOLOGY

To fulfill the goals of the study, a dedicated laboratory setup was designed and fabricated for this study. In this configuration, a rigid circular plate acting as a model footing was used to evaluate a single stone column—built regardless of its geosynthetic encasement—under load in a soft clay base. The experimental program explored the influence of several key factors, including column diameter, encasement length, encasement material stiffness, stone column group configurations, and the ratio of spacing to diameter (S/D).

The aim was to evaluate how these parameters affect the load-bearing performance compared to traditional, unencased stone columns. Similar investigations were carried out for stone columns arranged in group patterns.

The finite element approach was used in PLAXIS to conduct numerical simulations of the model tests, and the numerical results were verified against the results obtained in the laboratory. The modified cam clay model was used for the stone column material, and the Mohr–Coulomb model was used to depict the behavior of the clay. In order to capture the tensile stiffness of enclosed stone columns, the encasement was modeled using PLAXIS's Geogrid element in conjunction with the soil and stone column models. The impact of the chosen parameters on the performance of stone columns were thoroughly evaluated thanks to this experimental and numerical technique.

To examine the particles of the soil and stone column mix XRD and SEM was also done.

## 1.6 THESIS STRUCTURE

The following sections provide a brief summary of each of the seven separate chapters that make up the thesis.

Chapter 1 a concise explanation is provided on the importance of ground improvement, the specific constraints associated with the use of stone column approach, and the requirement for encasing the conventional stone column. Additionally, the motivation, need and objectives of the present research is also presented.

The behavior and operation of regular stone columns and geosynthetics-encased stone columns are covered in detail in Chapter 2, which includes analytical, experimental, and computational studies.

Chapter 3 offers a thorough account of the experimental inquiries conducted on stone columns and enclosed stone columns. The fundamental characteristics of the materials employed in the experiments are provided, alongside the facilities that have been constructed for the purpose of conducting model testing. The details regarding the PLAXIS 3D used for simulating experimental investigations has also been explained in current chapter. The crystalline structure of the materials and column mix is shown by using SEM and XRD tests.

Chapter 4 the findings of the experiments that were carried out on conventional stone columns, vertically encased stone columns (VESC) are presented. Another aspect of the stone columns that was investigated was their failure mechanism. Both individual stone columns and groupings of stone columns were used in the inquiry.

Numerical modeling with PLAXIS 3D was used to validate the experimental results for each of the several experimental tests whose outcomes are reported in this chapter. Furthermore, a comparison of the experimental and numerical results has been presented. The SEM and XRD results also shown.

Chapter 5 An outline of the conclusions drawn from the investigation is provided in this chapter. Numerous behaviors were examined, including column lateral deformation, excess pore water pressure, stress concentration ratio, and settlement.

Chapter 6 presents an additional work methodology, results and conclusions performed to stabilize the soil using stone columns in expansive soil.

Chapter 7 significant findings that have been derived from a combination of experimental and numerical investigations on the stabilisation of soft soil beds using typical stone columns and enclosed columns of stone are presented. This chapter also highlights potential areas for upcoming studies.

# CHAPTER 2
# LITERATURE REVIEW

## 2.1 GENERAL

This chapter offers foundational knowledge on soft soils and various ground improvement methods. As outlined in the previous chapter, stone columns represent a practical, rapid, and cost-effective technique for enhancing ground conditions. This method is commonly applied in the construction of embankments, liquid storage tanks, and offshore infrastructure, and it helps mitigate the risk of soil liquefaction. To illustrate the effectiveness of this technique, several brief case studies showcasing successful applications are included. However, in cases involving extremely soft soils, the settlement of the improved ground may still pose challenges even after the installation of standard stone columns. To address this, research has indicated that wrapping the granular material with geosynthetics can enhance the performance of the columns. Consequently, this chapter includes a literature review focusing on the layout, construction, and functionality of both traditional and geosynthetic-enclosed stone columns.

## 2.2 SOFT SOILS

Soft soils are characterized by high compressibility and low shear strength, which can lead to structural issues both during construction and after a project is completed. These soils are often geologically young and fine-grained, including normally consolidated, under-consolidated, or lightly over-consolidated materials. They may also include weathered surface clays and quick clays—soils that appear stable but have not experienced significant delayed or secondary consolidation since their formation. Common examples of soft soils include loose sands, soft clays, and silty materials, typically found in areas with recurring wetting and drying cycles, such as near rivers, lakes, and coastal zones. These environments are where such soils naturally develop. In India, soft soils are prevalent in marine and river delta regions, including the Gulf of Kutch, Gulf of Cambay, and along the Eastern and Western coastal belts. The soil classifications generally associated with soft soils—excluding SP (poorly graded sand)—are MI, MH, CI, CH, MI-MH, CI-CH, MI-CI, and MH-CH.

The German Geotechnical Society has introduced a set of standards aimed at defining and

evaluating soft soils for use in construction. These guidelines are intended to help classify such soils based on their physical and mechanical properties, ensuring their suitability for building purposes.

a. A consistency index (Ic) of less than 0.75 indicates a very soft to soft consistency.
b. Nearly or at full saturation
c. c. Cu ≤40 kN/m², the undrained shear strength
d. Low to medium plastic property
e. Inclined to flow
f. Thixotropic property
g. Very sensitive to vibrations

### 2.2.1 Soft soil properties

Soft soils possess certain key characteristics that contribute to their low shear strength and high compressibility:

a. Over 50% of their particles pass through a 75µm sieve.
b. They are typically found among organic and inorganic clays and silts, displaying low to moderate plasticity.
c. Their shear strength is generally less than 25 kPa, as supported by several studies (Madhav and Miura, 1994; Priebe, 1995; Muir-Wood et al., 2000; Alexiew et al., 2005; Wehr, 2006; Gniel and Bouazza, 2009; Mohanty and Samanta, 2015; Fattah et al., 2014; Dutta et al., 2016; Mehrannia, 2018).
d. According to Ranjan and Rao (2000), these soils typically exhibit low Standard Penetration Test (SPT) "N" values—less than 8 for cohesive soils ranging from medium to very soft, and less than 10 for cohesionless types.
e. The activity index is commonly used to assess the compressibility and swell-shrink potential of clayey soils; values over 1.25 indicate active clays.
f. They often contain a high amount of organic material, which further increases their compressibility.

### 2.2.2 Problems Associated with Soft Soils

a. Bearing Capacity Failure: Soft soils are typically weak and may undergo bearing failure when the applied pressure from structures exceeds their ultimate bearing capacity. This failure is more pronounced when the applied loads are inclined or eccentric, leading to instability or tilting of foundations.

b. Excessive Settlement (Total and Differential): Due to their high compressibility, soft soils can experience significant settlement under loading. This includes both:

    a. Total settlement, which affects the entire structure, and
    b. Differential settlement, which affects parts of the structure unevenly and can result in structural damage such wall, slab, or beam cracking.
    c. Shrinkage and Swelling (Volume Change): Soft soils rich in expansive clay minerals like montmorillonite can absorb large amounts of water, leading to swelling or ground heave during wet conditions. Conversely, during dry conditions, these soils may shrink, causing shrinkage fissures. These volumetric changes can lead to long-term structural instability.

### 2.2.3 Remediation of soft soil

The problem of soft soil can be resolved using the following strategies (Hausmann, 1990):

a. Permanently alter the construction site.
b. Likewise, superstructure planning.
c. Remove any damaged soils and use sturdy materials in their stead.
d. Using the proper techniques to develop the characteristics of the surrounding terrain and soil.

Various improvement techniques on the ground are:

1. Replacement
2. Drainage and consolidation
3. Chemical stabilisation
4. Thermal and biological treatment
5. Reinforcement

Below, we briefly review each of the previously listed techniques:

1. Replacement

Both shallow and deep replacement techniques are used to address soft soil issues. For shallow depths (up to 3 meters) above the groundwater table, problematic soil is replaced with stronger, more compact materials, improving the ground's stability. Deep replacement methods involve the use of stone columns, sand compaction columns, rammed aggregate columns, vibroconcrete columns, and geosynthetic encased columns. These methods replace loose, soft soil with hard, stiff materials, typically at depths of 5 to 10 meters. Sand columns can reach depths of 5 to 15 meters, while stone columns can go as deep as 30 meters (Han, 2015). Deep replacement helps reduce the likelihood of settlement and liquefaction, while also enhancing bearing capacity, stability, and speeding up consolidation.

2. Drainage and consolidation

Drainage – Applying a top layer of permeable materials, nonwoven geotextile, or geomaterials can increase the load-bearing capacity and hasten consolidation settlement on soft soils.

Consolidation – Soft soils, particularly those with saturated inorganic clays and silts, can be temporarily subjected to vacuum pressure or surcharge techniques to strengthen the soil and reduce settlement.

3. Chemical Stabilization

Soft soil deposits, whether shallow or deep, can undergo chemical stabilization. At shallow depths (up to 0.3 meters), unsaturated clays and silts can be mixed with materials like fly ash, cement, or lime. For deeper stabilization, techniques like grouting and deep mixing are used, where cement-based fluids are injected into the soil under high pressure. The treatment depths for grouting and deep mixing are typically 30 meters and 70 meters, respectively.

4. Thermal and Biological Treatment

The temperature of the earth can be lowered to below freezing, reducing the amount of heat escaping from beneath the surface, which causes the soil to solidify. This leads to less soil movement and reduced water flow, making it useful for short-term soil improvement, particularly in saturated clay and sand during tasks like soil excavation. Biological treatment involves using plants and their roots, or modifying soil properties through bio-

mediated geochemical processes such as mineral formation, gas generation, biofilm construction, and biopolymer production. This method can be applied to both cohesive and non-cohesive soils, though it is still not widely established.

5. Reinforcement

This treatment consists of two main components: fill reinforcement and in-situ reinforcement. Enhancing ground stability is the main objective of reinforcement. For both temporary and permanent slopes in soil and rock, steel bars combined with grout have been used, while in- situ reinforcement methods include ground anchors, soil nails, and micropiles. High-strength geosynthetics are also placed in slopes, embankments, earth walls, foundations, and roadways for tensile resistance and other applications. This treatment helps reduce settlement and improves both stability and bearing capacity.

Geotechnical experts are well-versed in these corrective measures, but they often come with limitations and may not always be practical for field applications. Stone columns play an essential role in various geotechnical tasks, such as drainage, reinforcement, and densification. This technique is particularly innovative for improving a variety of problematic soils, including waste fills, ash ponds, soft clays, and loose sands.

## 2.3 STONE COLUMNS

Stone columns are compressed hard rock fragments placed vertically into the soil layers beneath the surface. These columns are created in situ using ground improvement techniques such as replacement, displacement, or other methods. They function as a sub-structural component that transfers the weight transferred from the superstructure to the nearby soil through compression, shear, or rotation, interacting with the geo-material above, below, and around them.

21 197 Vibro techniques were first used in the 1800s by French military engineers first employed them, though they were initially forgotten. However, these methods were revived in the 1930s in Germany to construct a racetrack (McKelvey and Sivakumar, 2000). Since Vibro stone columns are now among the most significant deep compaction techniques used worldwide (Serridge, 2005; McCabe et al., 2009). This method has become a cost-effective

alternative to traditional piling techniques for construction projects that are less prone to settlement (Weber et al., 2006).

The following section explores the factors that influence the strength of stone columns.

10

### 1. Stress Variation in the Stone Column's Boundaries

The surrounding earth is compressed and displaced radially when stone columns are installed. The ground pressure at rest ($K_0$) is frequently used as a reference to measure the tensions surrounding the stone column. The surrounding soil experiences horizontal displacement and compression once stone columns are installed, which raises the $K_0$ value. In the case of clay, radial displacement occurs around the stone column's periphery, aiding in vibrocompaction until the material fully expands horizontally to the column's radius. Changes in stress values can be measured by calculating the ratio of effective horizontal stresses to vertical stresses (Chobbasti, 2011; Rao, 1992). Results from 3D modeling tests

99

indicate significant variations in stress concentration at the point where the stone column and the soil meet.

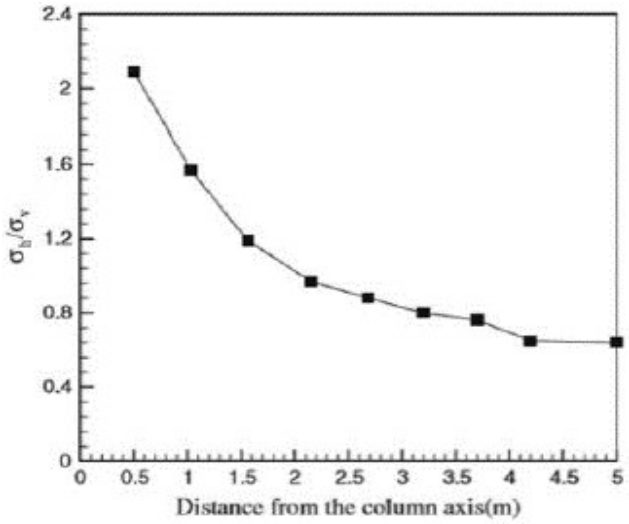


**Figure 2.1.** Stress variation in soft clay as a function of distance from the column (Choobasti, 2011)

In the Perm, Russia region, the effectiveness of stone column technology has been analyzed

for improving foundation stability and reducing subgrade deformation. To prevent financial losses, the ideal pile depth is always chosen within the calculated foundation depth. Since the soil near the borehole compresses during stone column installation, any deformation in this area must be accounted for before the column shell is installed (Shenkman and Ponomaryov, 2016).

As the load on the structure increases, the column material begins to expand laterally. However, the geosynthetic encasement and lateral soil pressure prevent the fill material from moving horizontally. Studies that plot the effective vertical stress over time for both Geosynthetic Enclosed Stone Columns (GESC) and Ordinary Stone Columns (OSC) have shown that the effective stress for the GESC is 1.25 times more than that of the OSC. This variation in effective stress is explained by the geogrid encasement's increased lateral confinement (Rajesh, 2017).

## 1. Confining Pressure

214 25 19 The capacity of stone columns to support applied loads is significantly influenced by the amount of confining pressure. The load-bearing capacity of stone columns is improved by raising the confining pressure, particularly when they are covered in geosynthetic materials. Extensive triaxial and uniaxial tests on Ordinary Stone Columns (OSC) and Geosynthetic Enclosed Stone Columns (GESC) show that the confining pressure for regular stone columns is limited to around 200 kPa, while the residual strength of geotextile-encased columns can reach approximately 800 kPa. Due to this higher confining pressure, GESCs are able to withstand substantial loads even after experiencing failure or deformation (Chen et al., 2009). There is a correlation between the rise in axial stress for encased columns and that of traditional stone columns, which aids in figuring out how much stronger the encased columns are. The improvement is more pronounced at lower confining pressures, with the effect being more noticeable at these lower levels compared to the higher range (Miranda and Costa, 2016). Additionally, the effect of encasing the stone columns is demonstrated by the fact that the strain rate for encased stone columns is lower than for uncased columns, where the strain rate tends to be higher.

## 2. Settlement / Consolidation Behavior

Settlement is an important consideration when dealing with soil reinforced by stone columns since it reduces settlement and increases consolidation rates, which are two of the main advantages of stone columns. According to research, settlement reduces as stone columns get deeper into the soil strata. The area replacement ratio and the settlement characteristics of stone column group designs were found to be correlated by Black et al. (2011). Settlement improvement rises as the area replacement ratio does, although this effect is most pronounced when the area replacement is between 30 and 40 percent. Shahu and Reddy's study (2011) found similar outcomes. The area replacement ratio (Ar), relative density, column length, and water content of the stone material are some of the variables that affect the consolidation behavior of typical stone columns. For a given vertical load, a higher Ar causes a higher failure stress, which reduces settling.

The Response Spectra Methodology shows that settlement of stone columns depends on their diameter and depth. During the first stage of construction, there is an improvement in soil behavior, which acts as preloading for the second stage and improves soil stiffness and shear strength (Elsawy, 2013).

The settlement improvement factor is used to examine floating stone columns' performance under uniform loading. This factor is the ratio of ultimate settlement with and without columns, and β, the proportion of column length to soft soil thickness, is also important (Ng and Tan, 2014). The study by Priebe (1995) is a widely used semi-empirical method for this analysis. As the value of β decreases, pore pressure dissipation reduces, and pore water flows radially from the nearby soil to the column.

The efficiency of stone columns is heavily influenced by the permeability of soft clays (Rajesh and Jain, 2015). In a study by Yoo and Kim (2009), the construction of a 6-meter-high embankment in three increments revealed that the final settlement of unsupervised soft clay was over three times higher than the soil supervised with stone columns.. The ultimate settlement of Ordinary Stone Columns (OSC) and Geosynthetic Enclosed Stone Columns (GESC) was reduced by 43% and 61%, respectively, compared to untreated soft clay. (Figure 2.2).

When considering cyclic loading from transportation loads, elastic deformations in the column and soil occur immediately after load application due to embankment, leading to undrained settlements (Basack et al., 2016). The embankment on soft soil gradually bends because of the column-soil interaction's rigidity (Indraratna et al., 2013). The amount of deformation is influenced by the surcharge load applied before, during, and after consolidation. For regular soil, OSC, and GESC, the dissipation of pore pressure takes 7000, 52, and 30 days on average, respectively. Rajesh (2017) found that the maximum immediate settlement of GESC was 21% less than OSC and 42% less than untreated clay.

The shear deformation of stone columns often results in complex localized bands that challenge traditional analytical models. Singh et al. (2019) found that, even with coupled formulations, refining the mesh reduced the shear band thickness inside the stone column, with no significant effect on the overall settlement profile. The load carried by undisturbed soil is higher than that carried by disturbed soil when compressibility varies along the smear zone. According to Deb and Behera (2017), the smear zone experiences the least consolidation. If the diameter ratio increases from two to five times or the smear zone radius increases from one to three times, the time for 90% consolidation can increase two to three times.

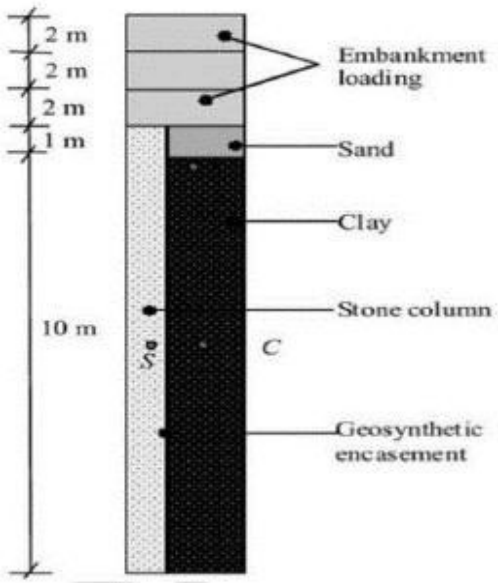


**Figure 2.2.** Schematic Illustration of GESC Modelling Specifications. (Rajesh, 2014)

Research using the Fast Lagrangian Finite-Difference method (Basack et al., 2017) has shown that the stone column-soil system's settlement increases hyperbolically with applied vertical stress. Similarly, the Discrete Element Finite Difference (DEM-FEM) model by Indraratna et al. (2015) showed that applied vertical stress causes a hyperbolic increase in the stone column-soil system's settlement.

15

The impact of the diameter and length of stone columns on settlement was analyzed using Response Surface Methodology (RSM) software (Madun et al., 2018). The RSM provided optimal relationships between the column's diameter and settlement. Singh et al. (2018) proposed a regularized solution for shear localization in geomaterials analysis, noting that mesh refinement affects stress-strain response and shear band thickness. After refining the mesh, total settlement increased by 0.02 m.

Finally, the type of material used for stone columns affects the speed of settlement and consolidation in the surrounding soil. Laboratory studies on pebble gravel, crushed pebble gravel, and quarry stones showed that pebble gravel took the longest to consolidate, while quarry stones had the quickest consolidation time and the least settlement (Stacho and Sulovska, 2017). Quarry stones are thus considered the ideal choice for stone material.

## 3. The Surrounding Soil's Bearing Capacity

Enhancing the soil's bearing capacity is a critical step in using stone columns to strengthen soft soils for engineering purposes. Stone columns significantly improve the soil's load-bearing capacity by creating a composite soil-column system that acts as a support layer for the structure above (Jadid, 2013).

The bearing capacities of reinforced and unreinforced soil are compared using the bearing capacity ratio (BCR). The size of the footing is one of the main elements affecting the carrying capacity of stone columns (Choobbasti, 2011; Nazaruddin, 2013). Although the stability and deformation of stone columns are slightly impacted by the roughness of the footing, the bearing capacity difference between smooth and rough footings is minimal and can be ignored in the majority of designs.

The bearing capacity of stone columns is notably enhanced when encased with geogrid. Research indicates that the end-bearing soil has minimal influence on the strength of ordinary stone columns, as failure in these columns typically occurs through lateral bulging, which is mainly influenced by the surrounding soil. In contrast, punching—which is mostly impacted by the end-bearing soil—causes failure in encased stone columns. (Fattah and Majeed, 2012).

Based on experimental data, Fattah and Majeed (2012) created a regression equation using the Statistical Package for the Social Sciences (SPSS) that connects bearing capacity to variables like cu (undrained shear strength of the soil), Ar (area replacement ratio), L/D ratio, and Ns (number of stone columns). The formula is as follows:

$$q_u = 15.34 \times cu^{0.401} \times As^{0.266} \times Ns^{0.084} \times (L/D)^{0.526}$$

Additionally, Bowels (1996) and Bouassida et al. (1995) proposed various other formulas for calculating the stone columns' carrying capacity.

Response Surface Methodology (RSM) and Design Expert software were used to further evaluate the link between bearing capacity and influencing parameters. An ideal correlation between the diameter, length, and load-bearing capacity of the stone column was revealed by the RSM response plots. The ANOVA results showed that a diameter of 44 mm and a length of 10 cm produced the maximum carrying capacity of 3260.7 N, resulting in a desirability of 77% (Madun et al., 2018).

### 4. Area Replacement Ratio (Ar)

The area of the stone column divided by the area of the surrounding soil is known as the Area Replacement Ratio (Ar). Increasing the stone columns' diameter is one method of raising this ratio.

Two distinct stone column sizes, 8.47 cm and 6.35 cm, were compared by Cimentada et al. (2011). The computed Ar values were 6.25% and 11.11%, respectively. For these sizes, the Stress Concentration Ratio (SCR) varied between 0.68 and 0.75. As the pressure increased, the stiffness ratio between the surrounding soil and the stone column decreased, resulting in this fluctuation. When Ar increases, the bearing capacity enhancement begins even at low Length/Diameter (L/D) ratios. This implies that Ar has a greater impact than column length on increasing the bearing capacity of stone columns (Fattah and Majeed, 2012).

Shahu and Reddy (2011) discovered that floating columns become more rigid than end-bearing columns as Ar rises. Other factors, such as the angle of internal friction, loading intensity, and post-installation pressure, also affect the consolidation rate. However, Ar has the most significant impact. A design equation that illustrates how Ar, the internal friction angle, loading intensity, and post-construction pressure affect stone column settlement was presented by Ng and Tan (2014).

### 5. Depth of Penetration or L/D Ratio

The stiffness of a stone column improves as ratio Length to Diameter (L/D) increases. Furthermore, increasing the column's burial depth enhances the soil's overall bearing capacity, while enlarging the diameter helps reduce the risk of the stone column bulging (Shahu and Reddy, 2011).

According to Black et al. (2011), a rise in the L/D ratio leads to a better settlement profile for the stone column. The optimal L/D ratio for a typical column range from 7 to 8. However, beyond an L/D ratio of 8, there is no significant change in the q treated/q untreated ratio. In contrast, for Geosynthetic Encased Stone Columns (GESCs), this ratio continues to increase even when L/D = 8, suggesting that in the case of reinforced stone columns, the L/D ratio has no upper limit (Fattah and Majeed, 2012).

Madun (2018) conducted a separate analysis using Design Expert software to assess the effects of the stone column's height and diameter on bearing capacity and settlement. The maximum bearing capacity, which was 3260.7 N, was achieved at a 44 mm diameter and 10 cm length, with 77% desirability.

## 6. Stress Concentration Ratio

The Stress Concentration Ratio (SCR), or the ratio of the stress carried by the surrounding soil to that carried by the stone column itself, is an important consideration when designing stone columns. Since the stone column will bear a larger share of the load, the main goal of adding stone columns to soft soil is to lessen the stress on the surrounding soil. As a result, the stone column's efficiency increases with a larger SCR.

Elsawy (2013) found that the SCR in Geosynthetic Encased Stone Columns (GESCs) increases with load, while it remains nearly unchanged in Ordinary Stone Columns (OSC). The SCR for GESCs increases steadily throughout the consolidation period, while for OSCs, the effective stress concentration ratio increases during the initial loading phase, then gradually decreases after reaching the saturation limits, stabilizing at a constant value (Rajesh, 2017). GESCs experience an effective stress that is 1.25 times higher than that of OSCs. Early in the loading process, stress concentration is lower, but as the load increases, the stress in the columns rises, stabilizing after reaching a certain point. Stress concentration is notably higher at low stress levels during the initial phase of loading.

Rajesh and Jain (2015) investigated how permeability affected stone columns' performance and strength, discovering that the Effective Stress Concentration Ratio (ESCR) for GESCs rises as consolidation progresses. Soil permeability plays a significant role in the treated ground's behavior and the soft clays' post-construction settling.

## 2.4 STONE COLUMN CONSTRUCTION METHODS

There are two primary techniques for creating a stone column: the displacement method and the non-displacement method, also known as the replacement method. The replacement method involves backfilling the borehole with granular material, while the displacement method involves laterally displacing the surrounding soil and backfilling it with the new material. These techniques are detailed in IS 15284 (Part -1): 2003. Other commonly used construction methods include the rammed stone column (Datye and Nagaraju, 1981), the simple boring method (Ranjan and Rao, 1983), and the vibro-compaction approach.

### 2.4.1 Displacement Method of Construction



In the displacement method of stone column construction, the process begins by lowering a vibrator into the soft soil. This action creates a void in the ground, which is then filled with stone aggregates. The aggregates are compacted by vibrating them into a dense state as the vibrator is reinserted. This technique reduces the compressibility and settlement of the ground, while simultaneously improving its stiffness, shear strength, and bearing capacity (Charles and Watts, 1983). When a bearing stratum is present, the best outcomes are usually obtained (Barksdale and Bachus, 1983).

### 2.4.2 Replacement Method of Construction

As illustrated in figure 2.3, the replacement method, involves the creation of a cavity using strong air or hydraulic pressure, which removes the weak soil. After that, stone aggregates are used to replace this soil. The remaining steps are similar to the displacement method: stone aggregates are backfilled gradually and compacted using a vibrator to ensure uniform density.

A simple technique developed by Rao (1982) and Ranjan and Rao (1983) is particularly beneficial for use in developing countries. In this method, a borehole is made using a spiral auger and manual labor. When the borehole reaches the necessary depth, it is thoroughly cleaned. Layers of powdered material are placed in the borehole, with each layer measuring 300–500 mm and separated by 50–100 mm layers of sand. To provide the necessary compaction, a power winch operates a 125 kg cast-iron hammer with a diameter smaller than the borehole. This hammer applies compactive force to the granular material,

while sand fills the gaps left during the compaction process, causing the surrounding soil to become fully compacted. Figure 2.4 displays a layout of the procedure.

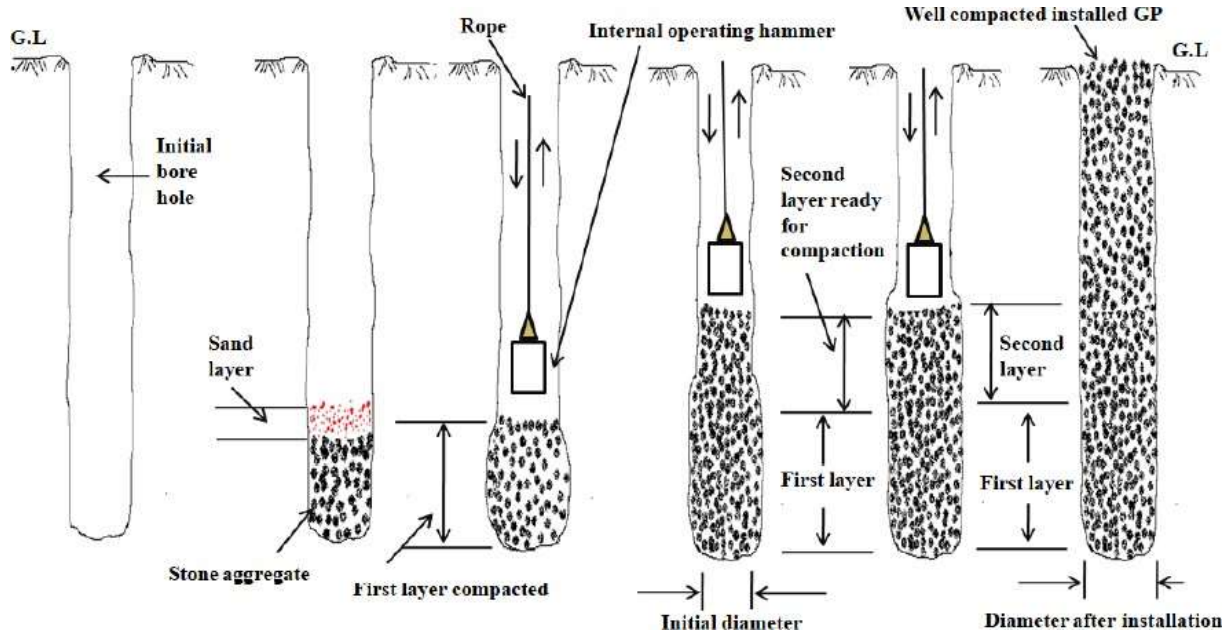


**Figure 2.3.** Granular pile construction using an easy auger boring technique (Rao, 1982)

## 2.5 FAILURE MECHANISM OF STONE COLUMNS

### 2.5.1 Mechanism of Load Transfer of Stone Columns

In geotechnical analysis, two key loading and displacement conditions are considered optimal: equal strain and equal stress. These conditions are commonly encountered in both flexible and rigid loading scenarios. Flexible loading, such as tire pressure, and rigid loading, such as a rigid footing, are examples of these conditions.

The ratio of the stress over the column ($\sigma_c$) to the stress over the soil ($\sigma_s$) is called the stress concentration ratio (n), which is commonly used to describe the transfer of load between columns and soft soils. In contrast, under an equal stress condition, the soil and columns have different settlements (i.e., $S_{sl} > S_{cl}$) but bear the equal stress (i.e., n = 1). The consequence is a difference in settlement between the soil and the columns. (Figure 2.4)

In practical terms, the stone columns undergo more stress than the surrounding soil because they are stiffer and more resistant to deformation. This increases the overall load-bearing capacity and decreases foundation settlement since a larger portion of the applied load is carried to the columns rather than the surrounding soil.

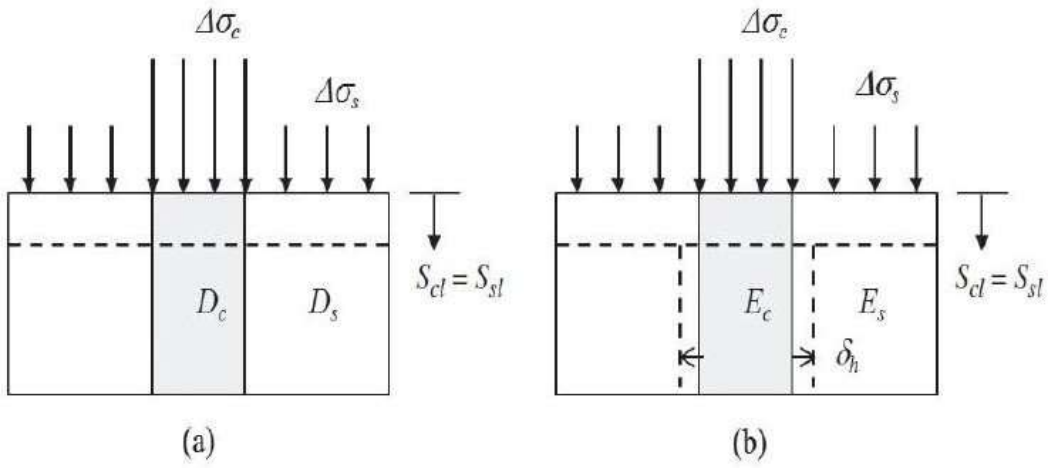


**Figure 2.4.** (a) Unit cells that are not deformed laterally (b) Unit cells that are deformed laterally (Han, 2015)

### 2.5.2 Failure Modes of Stone Columns

Generally, two different sorts of columns that are built, depending on their length and the resistance forces that are created within them (Barksdale and Bachus, 1983):

- End-bearing, or reaching the entire depth of a hard, sustaining stratum and
- Floating (partial depth), resisting pressures by side friction

The slenderness ratio, or the ratio of the column's diameter to its length, is displayed in Figure 2.5, determines whether the columns are long or short (McKelvey et al., 2004). Failures of the following kind might occur:

a. Bulging failure: the column has been limited from the top to the lower solid layer. The column's lateral length increases as a result of its resistance to the approaching load. Equilibrium has been achieved as the surrounding material is now under stress rather than the bulged area.

b. Short columns (L/D<6) situated above a bearing stratum may experience local shear

failure. In these columns, L and D represent the column's length and diameter, respectively. (McKelvey et al., 2004).

c. Both floating and end-bearing columns may fail in bulging, and short columns in weak strata may fail in end bearing or punching before the bulging happens inside the critical length (Hughes and Withers, 1974). When building a short end bearing column, it is important to take into account the possibility of local bearing capacity failure prior to bulging, particularly if the column is supported by weak strata. If the columns are not lowered to the proper depth, punching shear failure could happen (Barksdale and Bachus, 1983).

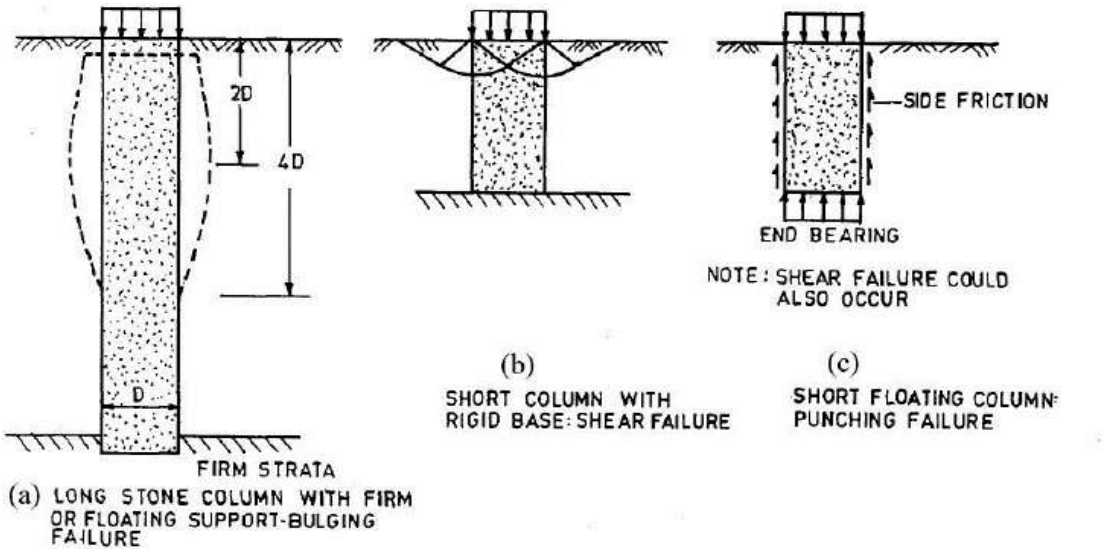


**Figure 2.5.** Breakdown process for a stone column in cohesive soil that is not homogeneous (IS 15284)

An ordinary column may help a stone column in many ways if it is encased in the proper geosynthetic material. According to Murugesan and Rajagopal (2009), it can, for instance, provide more lateral confinement, function as a semirigid element to facilitate load transfer to deeper depths, minimize stone loss by preventing stones from being squeezed into nearby soft clays, allow for a higher degree of compaction than with traditional stone columns, promote vertical drainage by acting as an efficient filter, maintain the aggregates' frictional qualities, and increase the shear resistance of the stone column.

## 2.6 DESIGN OF STONE COLUMNS

Conventional (unencased) and geosynthetic-enclosed stone columns are the two main varieties of stone columns. Bearing capacity and settling studies ought to be divided into the two groups described above.

### 2.6.1 Ordinary Stone Columns

#### 2.6.1.1 Enhanced Bearing Capacity in Stone Columns: A Review

Numerous studies have looked into how stone columns can enhance foundations' capacity to support loads. Their studies indicate a clear correlation between the frictional characteristics of the column material and the degree of lateral support provided by the encircling soil. In an experimental study, Hughes and Withers (1974) examined the deformation behavior around a stone column embedded in kaolin clay. They noticed that inside a zone that extends up to four times its diameter from the top of the column, the column tends to bulge. Furthermore, the surrounding soil and the stone column work together to support the vertical weight. Future advancements in the design and research of stone columns were made possible by these discoveries.

Hughes et al. (1975) proposed a failure mechanism involving both the surrounding soil and the stone column itself, characterized by a triaxial stress condition within the column. Hughes and Withers's earlier laboratory model testing served as the foundation for this theory (1974). According to their framework, the greatest radial pressure that the surrounding soil may apply to maintain the column laterally is known as the confining stress ($\sigma_{rL}$). This confining stress is then multiplied by the passive earth pressure coefficient ($K_{ps}$) unique to the column's granular material to find the ultimate vertical stress the column can support ($\sigma_v$).The load-settlement curve that was acquired for their investigation is presented in the Figure 2.6 and the setup in Figure 2.7.

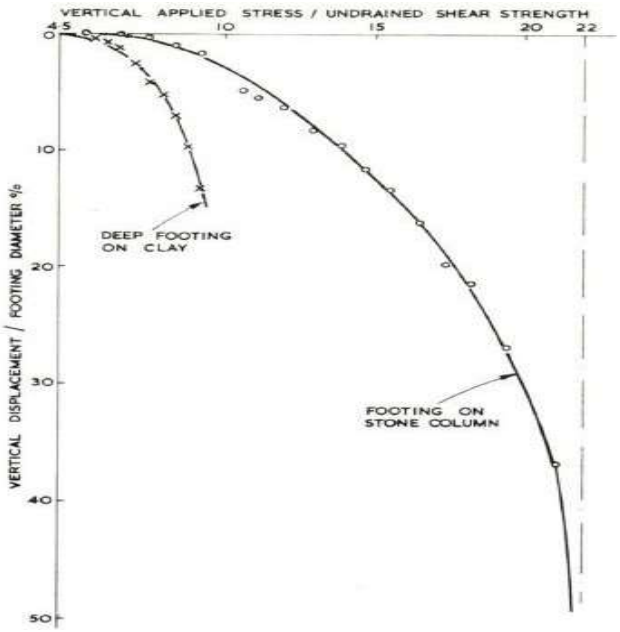


**Figure 2.6.** Load-Settlement curve (Hughes and Withers, 1974)

$$\sigma_v = \sigma_{rL} \frac{(1 - sin\phi')}{(1 + sin\phi')}$$

$$K_{ps} = \frac{(1 - sin\phi')}{(1 + sin\phi')}$$

Where, $\sigma_{rL}$ = Limiting radial stress,

$\phi'$ = Frictional angle of stone column aggregates,

K*ps* = Coefficient of passive earth pressure of the soil.

$$\sigma_{rL} = 4c_u + \sigma_{ro}' + u_o$$

where, $\sigma_{ro}'$ = Initial radial effective stress around the column,

$\sigma_{rL}$ = Total limiting radial stress of the column,

$u_o$ = Initial excess pore-pressure,

$c_u$ = Undrained shear strength of soil.

Brauns (1978) proposed a practical way to determine the confining stress of the nearby soil for the examination of a single stone column found in a saturated soft clay stratum under undrained conditions.

$$\sigma_r = \left(\Delta\sigma_s + \frac{\Delta c_u}{sin2\Psi}\right)\left(1+\frac{tan\Psi_p}{tan\Psi}\right)$$

where, $\sigma_r$ = Lateral confinement from the neighbouring soil,

$\Psi p$ = Column passive failure plane angle,

$\Psi$ = Angle of surrounding soil failure plane,

$c_u$ = The surrounding soil's undrained shear strength.

According to equation (),The angle of the soil failure plane affects the confining stress. Lastly, by calculating the derivative of the preceding equation with respect to the failure plane angle and setting it to zero, the confining stress may be found. The maximum vertical stress that the granular column can withstand ($\sigma_c$) is calculated by multiplying the confining stress by the coefficient of passive earth pressure ($K_p$).

$$\sigma_c = K_p \times \sigma_r$$

where, $\sigma_c$ = Ultimate vertical stress,

$K_p$ = Coefficient of passive earth pressure of the stone column

Barksdale (1987) suggested that both the stone column and the neighbouring soil reach their ability to withstand the same degree of stress, a condition known as the equal strain approach. Based on this assumption, he expressed the composite foundation's ultimate bearing capacity ($q_{ult}$) with the following equation:

$$qult = qult,c \times As + qult,s \times (1 - As)$$

Here, qult,s is the ultimate bearing capacity of the surrounding soil, qult,c is the ultimate bearing capacity of the column, and As is the area replacement ratio. Barksdale has suggested estimating qult,s as $5c_u$, where $c_u$ represents the surrounding clay's undrained shear strength. This can be substituted into the equation to make it simpler:

$$q_{ult} = 5c_u \times (3A_s + 1)$$

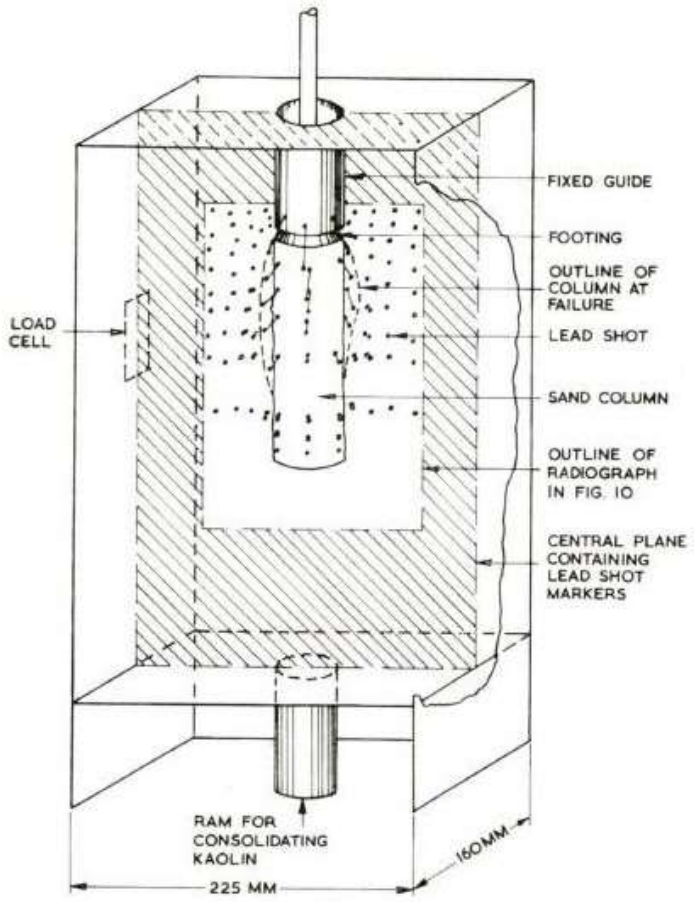


**Figure 2.7.** Consolidometer test on single stone column (Hughes and Withers, 1974)

**IS Code Method (IS 15284 Part 1: 2003)**

(1) Capacity Determined by Column Bulging

$$\sigma_v = \sigma_{rl} \cdot K_{pcol}$$

where, $\sigma_v$ = reducing the axial tension that bulging causes in the column as it approaches shear failure,

$\sigma_{rl}$ = Limiting radial stress

$$\sigma_{rl} = \sigma_{ro} + 4c_u$$

$K_{pcol}$ = Column's passive earth pressure coefficient

$$\sigma_v = (\sigma_{ro} + 4c_u)\, K_{pcol}$$

$\sigma_{ro}$ = Initial effective radial stress

$c_u$ = Undisturbed undrained shear strength of the clay around the column.

$$\sigma_{ro} = K_o \ \sigma_{vo}$$

Ko = For clay soils, the mean lateral earth pressure coefficient has a value of 0.6, or alternatively, it can be calculated using the formula Ko = 1-sin$\phi_s$, where $\phi_s$ is the effective angle of soil's internal friction.

$\sigma_{vo}$ is the average initial effective vertical stress, calculated by taking the column's diameter ($\gamma$2D) twice as the average bulging depth.

$\gamma$ = The soil's effective unit weight in the influence zone,

D = Diameter of the column.

$$Ko = 1\text{-}\sin\phi$$

$$K_{pcol} = \tan^2 (45° + \phi_c/2)$$

Safe load on column alone, $Q_1 = (\sigma_v . \frac{\pi}{4} D^2) /2$

where, 2 is the factor of safety.

(2) Surcharge Effect

$$\Delta \sigma_{ro} = q_{safe} (1 + 2 K_o) / 3$$

$q_{safe}$ = Soil safe bearing pressure with a 2.5 safety factor

$q_{safe} = C_u N_c / 2.5$

Cu = Undrained shear strength,

Nc = Terzgahi bearing capacity factor.

For a safety factor value of 2, increase in the safe load due to surcharge,

$$Q_2 = Kpcol . \Delta \sigma ro. As / 2$$

(3) Intervening soil support

For a column, area of the intervening soil, $Ag = 0.866 S^2 - \frac{\pi}{4} D^2$

Safe load supported by the intervening soil, Q3 = Ag. Qsafe

(4) Total safe load on every column and the surrounding soil

$$Q = Q1 + Q2 + Q3$$

The behavior of both single and group end-bearing stone columns under a variety of influencing parameters, including column spacing, the undrained shear strength of soft clay, and varied loading circumstances, was thoroughly studied by Ambily and Gandhi (2007). Two types of loading scenarios were tested: (i) loading applied throughout the entire unit cell area (to assess increased ground stiffness) and (ii) loading restricted to the stone column area (to assess its load-bearing capacity).

The study's stone columns measured 450 mm in height and 100 mm in diameter. In order to maintain the necessary spacing, model experiments were carried out using tanks with diameters ranging from 210 mm to 420 mm for single columns and a big tank with a diameter of 835 mm for a group of seven columns. The foundation material was soft clay with undrained shear strengths of 7, 14, and 30 kPa. To reduce bulging during construction, mild compaction was used to place stone aggregates (2–10 mm in size).

Axial stresses between 100 and 150 kPa were applied until settlements exceeded 10 mm. When just the column was loaded, bulging was seen to a depth of 0.5 times the column diameter, but not when the full area was loaded—indicating the effectiveness of confinement from surrounding soil in group scenarios.

Finite Element Method (FEM) analysis using PLAXIS (with 15-noded triangular elements) was performed to validate experimental results. The stress-settlement relationship was found to be consistent across different shear strengths for single column loading at a constant spacing-to- diameter (s/d) ratio. The limiting axial stress was found to dramatically drop when the s/d ratio rose to 3, after which the change was insignificant.

A stiffness improvement factor, which is the ratio of treated to untreated ground stiffness, was introduced in the study. This factor was influenced by the s/d ratio but remained unaffected by the clay's shear strength. For s/d ratios greater than 3, no substantial stiffness improvement was observed. Behavior of column groups was found to closely align with that of single columns for s/d ratios up to 3, confirming the modeling application of the unit cell notion.

FEM study also helped in evaluating the stress concentration ratio across both single and group column setups. Results showed consistent stress concentration in both cases, further supporting the reliability of the unit cell approach. Furthermore, it was found that when the shear strength of the surrounding soil declined, stress concentration on the stone column increased.

### 2.6.1.2 Studies on the reduction of settlement in ordinary stone columns

Many techniques have been developed during the past thirty years to forecast how weak soil layers reinforced with stone columns would settle. Priebe (1976) presented one of the fundamental methods, viewing the stone column as an end-bearing, incompressible, rigid-plastic component. He showed that, under these assumptions, the ratio of stress carried by the column to that borne by the surrounding soil, or the stress concentration ratio (n = qp/qs), drops proportionately with 1/α, where α is the earthquake design reduction factor.

Using the unit cell concept, Priebe formulated a fundamental improvement factor method illustrated in Figure 2.8, This method accounted for the following key parameters:

- Poisson's ratio (μ) of the surrounding soil
- Friction angle (φ) of the column material
- Area replacement ratio (Ar), which is the column area divided by the unit cell area.

A simplified expression for the settlement reduction or improvement factor, which calculates the amount that the addition of stone columns reduces ground settlement, was derived by assuming that the elastic soil in the unit cell underwent oedometric (one-dimensional) settlement. Following the previous figure's improvement factor ($I_f$) computation, the decreased settlement can be computed using the formula below:

$$S' = \frac{S_u}{I_f} \qquad (2.21)$$

$$I_f = 1 + A_r \left[\frac{0.5 + f(\mu, A_r)}{(K_a)_s \, f(\mu, A_r)}\right] \qquad (2.22)$$

$$f(\mu, A_r) = \left[\frac{1-\mu^2}{1-\mu-2\mu^2}\right]\left[\frac{(1-2\mu)+(1-A_r)}{1-2\mu+A_r}\right]$$

$$K_a = \tan^2(45 - \phi/2)$$

Where, S′ = The introduction of granular columns results in lesser settlement,

$S_u$ = Untreated settlement in the foundation

Under the influence of larger loading area, $S_u$ can be obtained as:

$$S_u = m_v . \Delta\sigma_z . h$$

Where, $m_v$ = Soil's volumetric compressibility coefficient,

h = Thickness of the soil layer,

$\Delta\sigma_z$ = Pressure due to surcharge.

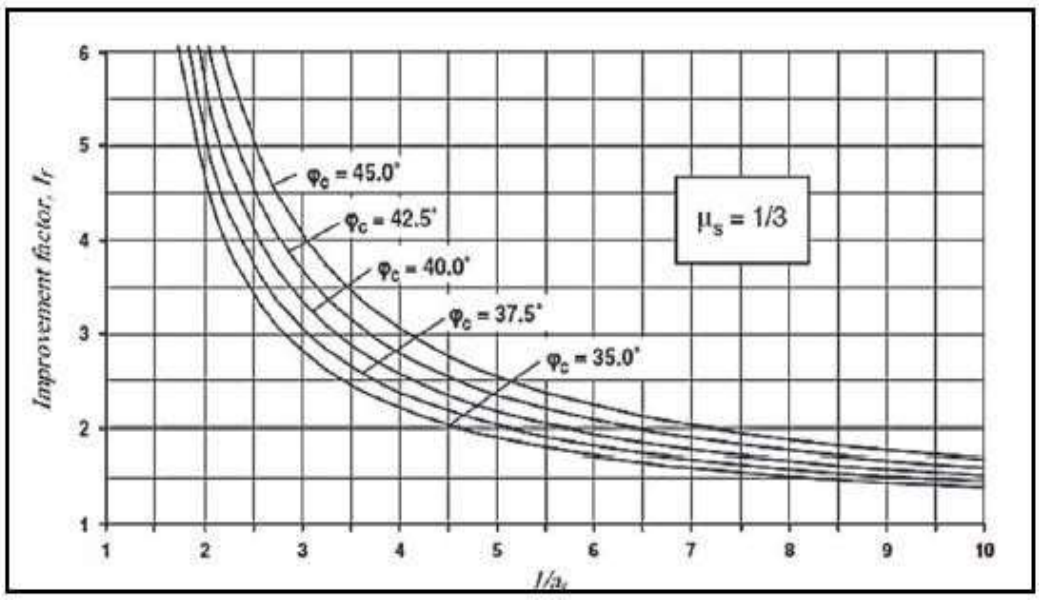


**Figure 2.8**. Chart for Improvement Factor (Priebe, 1976)

Building on the idea of the unit-cell, Aboshi et al. (1979) examined a situation in which it is assumed that the vertical displacement in the surrounding soil and the stone column is equal, suggesting an equal settling condition. Additionally, they took into account that the column and the earth share the entire vertical weight imposed at the surface, preserving equilibrium. Their study relied heavily on the assumption that the vertical stress is constant throughout the stone column's whole length. By following the equal strain concept, this simplification made it simpler to calculate the load distribution between the column and the surrounding soft soil.

The replacement factor ($A_r$) and stress concentration ratio (n) have been linked to the settlement reduction ratio (R). The total settlement ($S_t$) is determined as:

$$S_t = m_v (\mu_c.\sigma) H$$

Where, $m_v$ = Soil's volumetric compressibility coefficient,

$\sigma$ = Unit normal stress,

H = the height of stone column.

The settlement reduction ratio, R was given by

$$R = \mu_c = \frac{1}{1+(n-1)A_r} \qquad (2.27)$$

**IS Code Method (IS 15284 Part1:2003)**

Consolidation settlement of the treated composite soil $S_t$, is given as:

$$S_c = m_v \sigma_z h$$

$$\sigma_z = \sigma / \{1 (n - 1) a_s\}$$

Where, $m_v$ = Coefficient of volume compressibility,

$\sigma_z$ = Vertical stress in the neighbouring ground,

h = Thickness of the treated soil,

$\sigma$ = Applied stress,

n = Stress concentration factor / ratio,

$a_s$ = Area replacement ratio.

A theoretical approach to calculate the consolidation rate of foundations reinforced with granular (stone) columns was devised by Han and Ye (2001, 2002). Their approach notably takes into account two crucial elements that are frequently disregarded in more straightforward models:

41

1. Smear Zone – This is the area of soil that has been disturbed around the stone column as a result of column material seeping into the surrounding soft soil during installation. This disturbed zone has lower permeability, affecting the rate at which pore water dissipates during consolidation.
2. Well Resistance – This accounts for the reduction in permeability within the stone column itself, caused by clay particles migrating into the column material, which can restrict water flow and delay consolidation.

In order to more properly mimic the drainage and consolidation behavior of the improved ground, Han and Ye extended on their earlier simplified model (2001) in their 2002 study by adopting a more thorough unit cell model that incorporates these real-world phenomena. (Fig. 2.9)

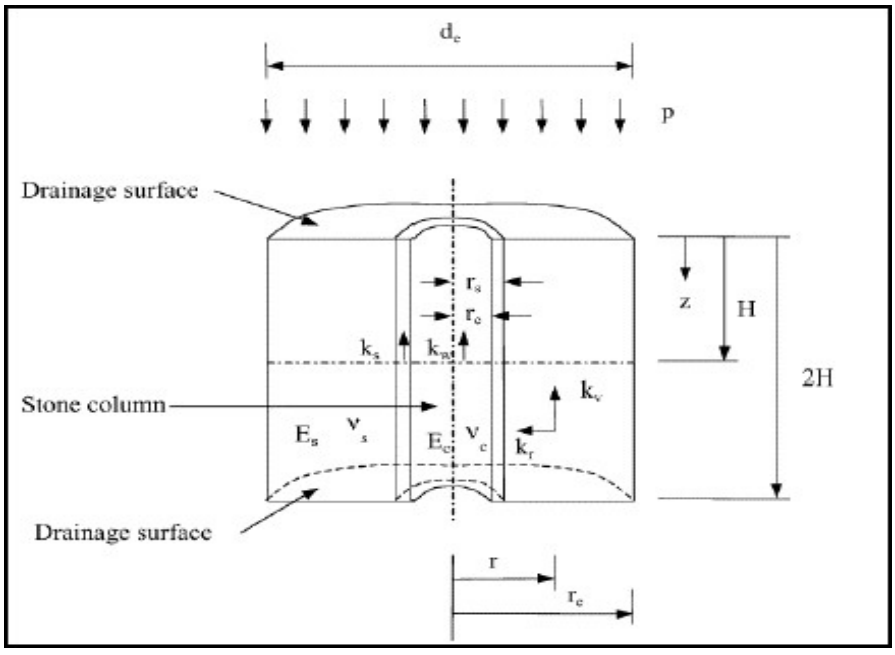


**Figure 2.9.** Unit cell model (Han and Ye, 2002)

In order to assess the consolidation rate of foundations reinforced with granular columns, Han and Ye (2002) devised a theoretical technique that takes into consideration important real-world characteristics including the smear zone and well resistance. Their model includes various unit cell components such as the equivalent diameter (*de*), elastic moduli of the soil (*Es*) and column (*Ec*), and permeabilities in both the radial and vertical directions (*kr* and *kv*), along with those of the stone column (*kc*) and the smear zone (*ks*). The radius of the stone column (rc), the equivalent radius of the unit cell (re), the radius of the smear zone (ds), and the thickness of the soil layer undergoing consolidation (H), with pore pressure depth denoted by *z* are examples of geometric parameters. A parametric analysis was carried out to assess six variables affecting the consolidation rate. First, an increase in column diameter reduces the diameter ratio ($N = de/dc$), thereby shortening the drainage path and accelerating consolidation. Second, the permeability of the stone column (*kc*) may decrease due to clogging by fine soil particles during installation, which raises the *kr/kc* ratio and slows the consolidation process. Third, the stress concentration ratio ($ns = \sigma c/\sigma s$) increases as more load is taken by the column, promoting faster radial consolidation. Fourth, a larger smear zone ($S = ds/dc$) reduces the surrounding soil's permeability, which delays the consolidation rate. Fifth, the smear zone's permeability (*ks*) often drops due to structural changes and damage to horizontal drainage paths during installation, leading to a significant slowdown in pore pressure dissipation. Finally, an increase in soil layer thickness (H) lengthens the drainage path, which lowers the average rate of consolidation. These results emphasize how crucial it is to optimize soil improvement techniques, column design, and installation methods in order to increase consolidation performance overall.

Kolekar and Dasaka (2014) introduced an innovative gravity loading method using lever arm technology to generate large, uniformly consolidated clay bed samples without the need for placing heavy dead weights directly on the clay surface (as shown in Figure 2.10). In their approach, clay beds were first prepared in a slurry state and then subjected to consolidation through a controlled gravity loading system. Two separate test series, labeled Series A and B**,** were conducted, each comprising seven individual tests**.** Under applied pressures of 18 kPa, 36 kPa, and 72 kPa, respectively, the clay beds in each series were consolidated. The findings demonstrated a high degree of consistency and uniformity in the sample preparation process, which is deemed acceptable for geotechnical testing, as the coefficients of variation (COV) for both the measured shear strength and the recorded water content of the consolidated clay beds remained below 10%.

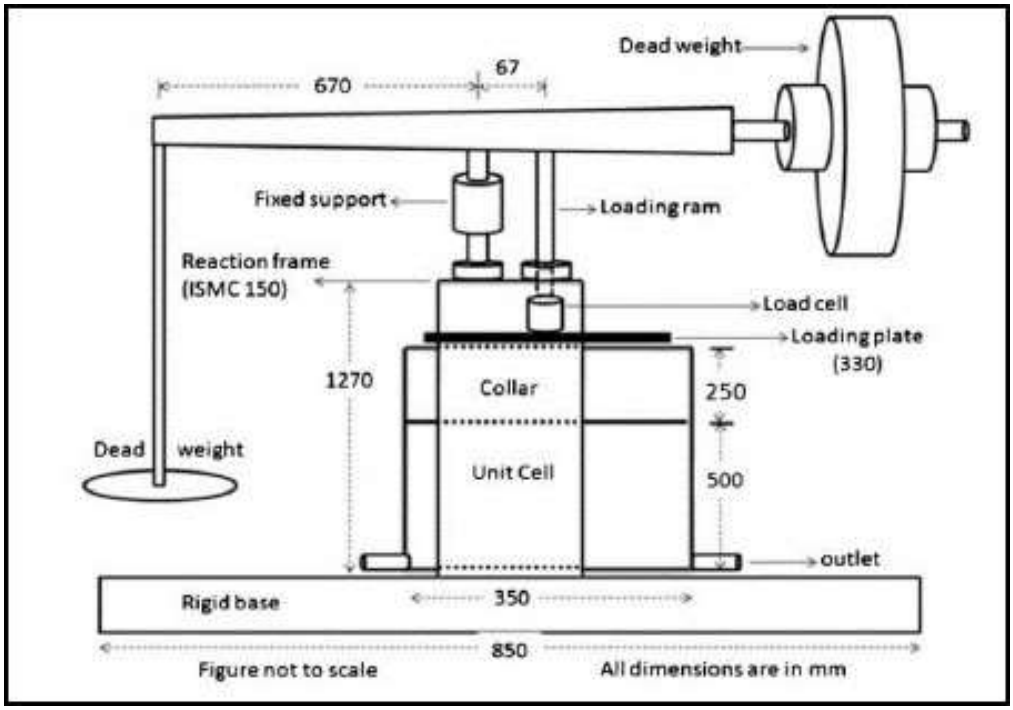


**Figure 2.10.** The response frame's schematic diagram (Kolekar and Dasaka, 2014)

In order to estimate the consolidation rate of soil improved by stone columns, Deb and Shiyamalaa (2015) devised a mathematical model that takes into consideration the blockage caused by particle migration. The model takes into account the possibility of displacement of fluid in the pores as well as tiny particles and contaminants in the soil during consolidation. Clogging occurs in the column material as a result of these fluid-containing particles moving from the earth into the nearby stone column. The concentration of particles in the seepage water determines the degree of blockage, which lowers the stone column's permeability. The rate at which the ground enhanced by stone columns consolidates is slowed down by this decrease in permeability. A single stone column and its sphere of influence—represented as a unit cell—are the subject of the investigation. As seen in Figure 2.11, the unit cell is cylindrical, with a ring of earth encircling the stone column. The dirt zone, smear zone, congested zone, and unclogged zone are the four separate zones that make up the unit cell. The areas impacted by the stone column are represented by these zones, with special attention paid to how blockage affects consolidation behavior.

The findings of the study by Deb and Shiyamalaa (2015) are contrasted with several current models that calculate the consolidation rate for ground improved by stone columns, both with and without the impacts of clogging, as shown in Figure 2.12. Additionally, the study looks into how a number of characteristics affect the model's consolidation rate. Interestingly, it was shown that the diameter ratio and stress concentration ratio both rise with increasing clogging. This suggests that increased clogging alters the geometry of the stone column and the distribution of loads, which impacts the consolidation process.

In a related work, Rangeard et al. (2016) investigated experimentally how clay columns reinforced with sand would settle under constant pressure. This study examined how the hydromechanical behavior of the soil-column system was affected by the construction technique and compaction force utilized during the installation of sand columns. The sand used for the columns had particles ranging from 1 to 1.25 mm, while the kaolin soil (CH), which is a type of clayey soil, was selected as the foundation material. To prepare the soil bed, the wet kaolin bed was subjected to continuous pressure for a specified period, simulating the conditions under which soft soils typically undergo consolidation and improvement through stone or sand columns.

The study investigated how different methods of installing sand columns affect the behavior of kaolin clay. These methods varied depending on whether the clay was displaced and whether the sand was compacted. The approaches included NR-NC (no clay displacement and no sand compaction), NR-WC (no displacement but with sand compaction), and WR-WC (with displacement and compaction). Across all cases, the area replacement ratio was kept between 1% and 6%.

One of the key findings was that the clay surrounding the sand columns experienced localized densification. This densified zone extended about one column radius from the column itself. Consequently, the clay's permeability in this area decreased, and its

coefficient of consolidation increased. However, this localized change did not significantly influence the rapid drainage that occurred during the sand column installation process.

To assess how the reinforcement affected settlement, the study used a parameter called the settlement reduction rate (Tr), calculated using the formula Tr = [(Δhur - Δhr) / Δhr] × 100, where Δhur is the settlement without reinforcement and Δhr is the settlement with reinforcement. Regardless of the construction technique, it was found that Tr rose as the column diameter grew. However, the effectiveness of settlement reduction also depended on the installation approach. The WR-WC method, which involved both displacing the clay and compacting the sand, was found to be the most effective. The NR-WC method also showed improved performance over NR-NC, highlighting the importance of sand compaction even when the clay is not displaced.

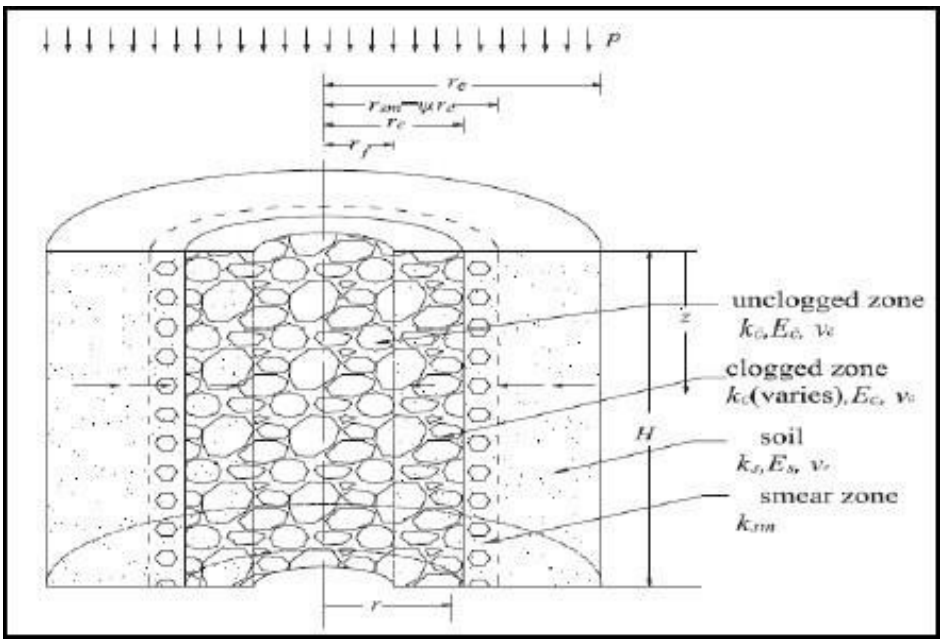


**Figure 2.11** Unit cell cross section (Deb and Shiyamalaa, 2015)

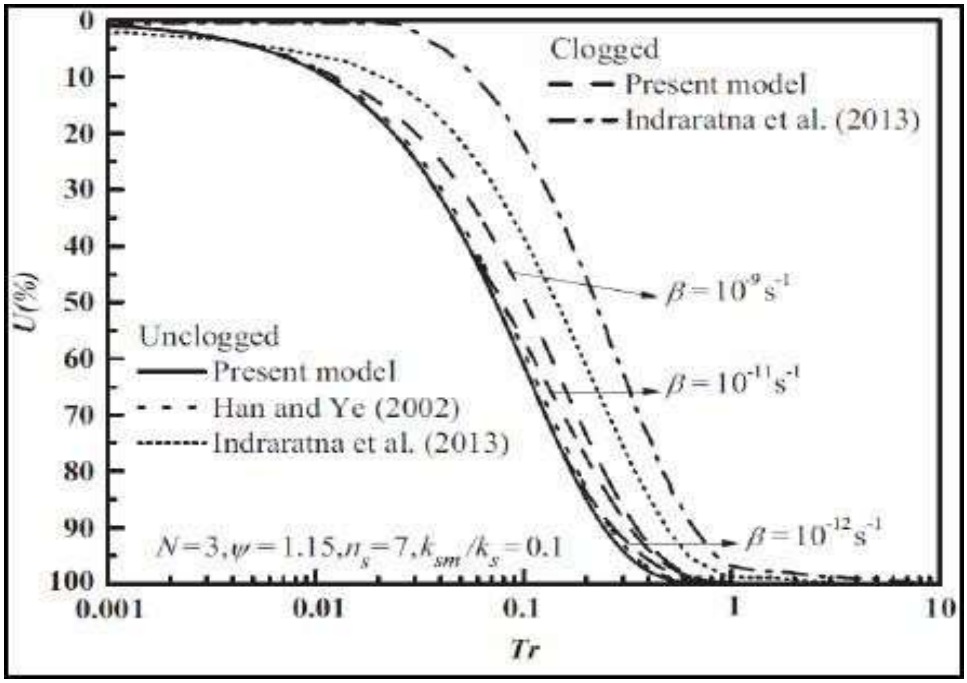


**Figure 2.12** Calculated rate of consolidation compared with various methods (Deb and Shiyamalaa, 2015)

Finally, it was noted that the time required for settlement to begin was nearly the same for all methods and column sizes, indicating that the initiation of settlement is not significantly influenced by the installation technique.

Chardrawanshi (2018) examined the settlement behavior of extremely soft soils, characterized by an undrained shear strength ranging from 2.5 to 7.5 kPa, under sustained loading conditions of 100, 150, and 200 kPa for a minimum duration of thirty hours. Interestingly, IS 15284 (Part 1): 2003 does not offer recommendations for assessing the settlement of soft soils with undrained shear strengths lower than 7 kPa. In order to solve this, Chardrawanshi created design charts (Figure 2.13) that may be used to calculate the projected settlement reduction ratio (SRR) based on certain area replacement ratios seen in the field. Because of the high permeability of the column material, stone columns improve the consolidation of the composite foundation by providing shorter radial drainage paths in addition to the vertical ones. Furthermore, stone columns can absorb a larger portion of the vertical load because of their much higher stiffness than the surrounding earth. This speeds up the consolidation process overall and lessens the strain on the nearby weaker soil.

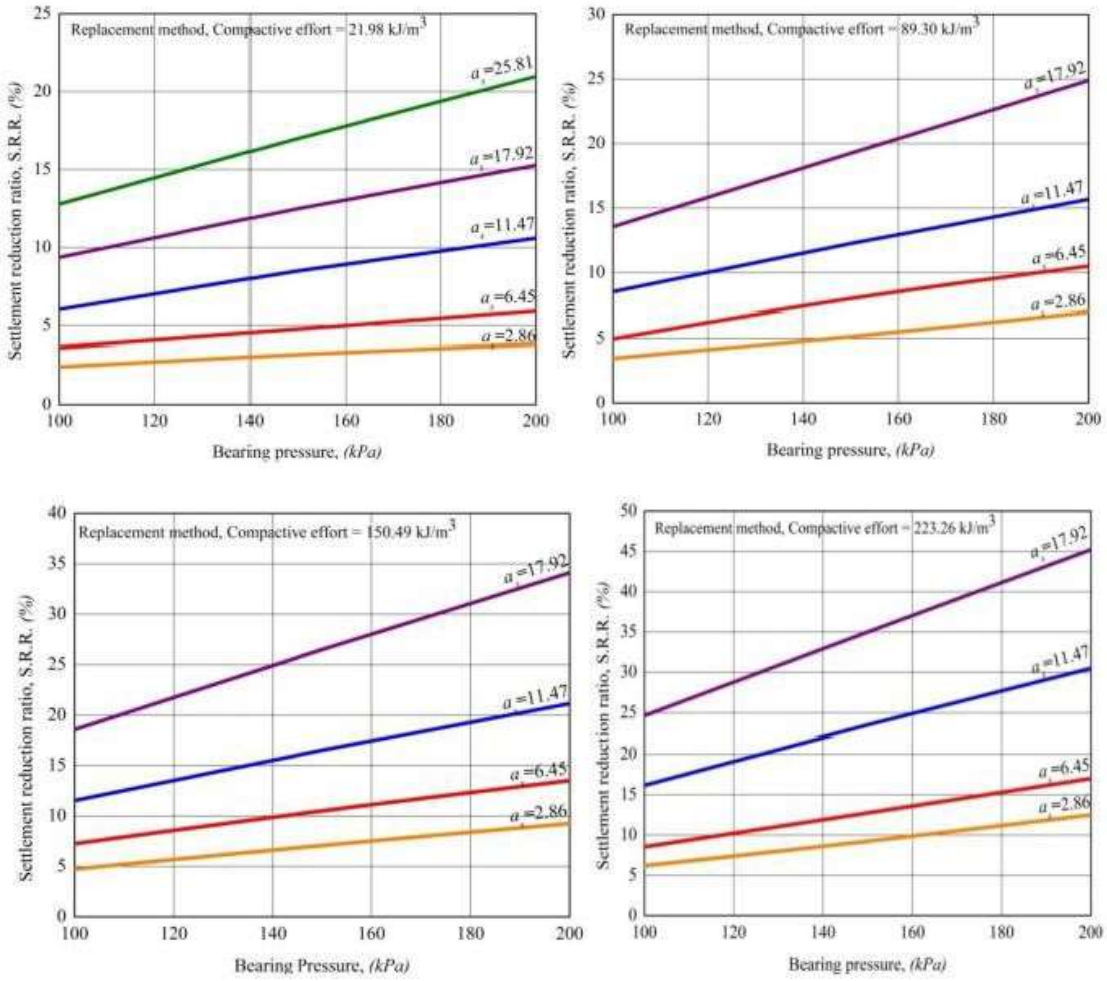


**Figure 2.13.** S.R.R. vs. Bearing pressure for various compactive effort (Chardrawanshi, 2018)

### 2.6.1.3 Limitations of Ordinary Stone Columns

Although the use of stone columns is advantageous in many ground renovation situations, there are some restrictions when it comes to particular soil types. Soils with significant organic content—especially those with peat layers larger than the diameter of the stone column—have one such restriction. According to Waltham (2009), these soils have the capacity to retain moisture up to 10 times their weight, which could result in substantial long-term settlements when the excess pore water pressure gradually dissipates. Additionally, Priebe (2005) stressed that soils with an undrained shear strength (cu) of less than 15 kPa should not be utilized for stone columns since they do not have the strength needed to

support the installation procedure. Finally, McCabe et al. (2009) cautioned that in order to prevent unanticipated failures, long-term settlements must be carefully considered at the design process. Soils such as loose fills and soft clay fills are particularly prone to ongoing settlement, which can undermine the effectiveness of the improvement technique over time.

### 2.6.2 Geosynthetic Encased Stone Column

Stone columns serve multiple functions in ground improvement, including densification of the soil, enhancement of drainage, reinforcement, and material replacement. While most soils and geomaterials possess good strength in compression and shear, they tend to be weak in tension. To address this, geosynthetics—such as geotextiles and geogrids—are often used to provide tensile resistance. These materials also act as separators between incompatible materials, preventing mixing and thereby preserving the integrity of both layers. By reducing the "smear zone" between the column and the surrounding soft soil, this separation improves the stone column's performance (Han and Ye, 2002).

The load-bearing capability of stone columns is greatly increased by the application of geosynthetic encasement, particularly in extremely soft soils. These encasements typically have a tensile stiffness of 1500–6000 kN/m and an ultimate hoop tensile strength of 100–400 kN/m. Conventional (non-encased) stone columns work better in soils with shear strengths more than 15 kPa, while geosynthetic-encased stone columns work best in soils with undrained shear strengths between 5 and 15 kPa (Han, 2015). The typical installation depth for these encased columns is between five and ten meters.

Moreover, geosynthetic-encased stone columns demonstrate high stress concentration ratios, with values reaching up to 8.5, according to Castro et al. (2013). However, one potential failure mode for these systems is the rupture of the geosynthetic encasement under excessive stress. For encased stone columns, Alexiew and Thomson (2013) suggest an area replacement ratio of 0.1 to 0.2 for design purposes.

### 2.6.2.1 Increasing the Bearing Capacity of Stone Columns Encased in Geosynthetic

The load-settlement behavior of stone columns with and without geogrid encasement was investigated experimentally by Malarvizhi and Ilamparuthi (2004). The analysis took into account a number of influencing elements, such as the type of geogrid material utilized and the length-to-diameter (l/d) ratio. Granite stone chips were selected as the column material, while marine clay was used to simulate a soft soil foundation. The study employed three different geogrid types, each with distinct aperture sizes and tensile strengths, to assess their effect on column performance.

Regardless of whether the column was end-bearing or floating, the results showed that the length of the geogrid encasement greatly increased the load-carrying capability of stone columns. The ultimate load capacity attained increases with the stiffness of the encasing material. The ultimate load capacity of geosynthetic-encased stone columns was found to be almost three times higher than the untreated ground in soft clay beds, while traditional stone columns only achieved a twofold gain. Additionally, compared to their non-encased counterparts, encased stone columns were shown to be more successful in reducing settlement.

In order to evaluate the improvements in the load-bearing capability of stone columns when encased with geosynthetics, Murugesan and Rajagopal (2006) carried out a thorough parametric research using finite element analysis. Their study provided both qualitative and quantitative insights, highlighting that encased stone columns significantly outperform conventional stone columns in terms of load capacity. Because of the higher lateral confining pressure the encasement supplied, the enclosed columns showed less lateral bulging and vertical compression under load. According to the analysis, it is only necessary to encase the highest part of the column up to twice its diameter in order to significantly improve its performance. Additionally, the results showed that the encased column's load-bearing capacity gradually increases with the stiffness of the encasing material, highlighting the need of choosing the right geosynthetics for the best reinforcement.

In order to further investigate the improvement in the load-bearing capacity of stone columns as a result of geosynthetic encasement, Murugesan and Rajagopal (2010) expanded on their earlier work by performing a thorough parametric study using finite element analysis. Their findings reaffirmed that encased stone columns outperform conventional stone columns by demonstrating significantly higher load capacities, reduced vertical deformation, and minimized lateral bulging. The increased lateral confining pressure produced by the geosynthetic encasement is responsible for this improvement.

Additionally, their investigation highlighted the positive correlation between the stiffness of the encasing material and the improvement in load-carrying capacity; the more stiff the geosynthetic, the greater the performance gain. They suggested a technique that takes into account the extra confinement offered by the geosynthetic encasement in order to predict the increased bearing capacity. They assumed a bulging length equal to four times the stone column's diameter for computational considerations. This assumption helped in developing a more realistic and practical estimation of bearing capacity, tailored to account for the mechanical interaction between the column and the encasement.

$$q_{ult,c} = (\sigma_{ro} + 4c_u + \sigma_{r,g})K_p$$

Where, $\sigma_{r0}$ = The initial radial stress of the surrounding soil;

Kp = The coefficient of passive earth pressure of the granular material.

The encasement's hoop tensile strength ($T_g$), which may be calculated as follows, is directly proportional to the additional confinement that the geosynthetic ($\sigma_{r,g}$) offers.

:

$$\sigma_{r,g} = 2T_g/d_c$$

The hoop strain ($\varepsilon_g$) and stiffness modulus (J) of the geosynthetic can be used to compute the geosynthetic hoop tensile strength as follows:

$$T_g = J.\varepsilon_g$$

$$\varepsilon_g = \frac{1-\sqrt{1-\varepsilon_a}}{\sqrt{1-\varepsilon_a}}$$

where $\varepsilon_a$ = the compressive strain of the column vertically (vertical compression divided by the bulging length).

Using the granular pile technique, Kumar and Jain (2013) investigated the load-settlement behavior of soft expansive black cotton soil with an unconfined compressive strength (UCS) of 50 kPa. End-bearing piles with diameters of 50 mm, 65 mm, and 80 mm were built using the replacement method using sand as the column material. The cylindrical test tanks in which these piles were placed had matching spacing-to-diameter (s/d) ratios of 3.3, 3.2, and 3.5. The researchers assessed performance by placing a footing on test beds containing both regular granular piles and granular piles encased in geogrid.

Test results revealed significant improvements in load-bearing capacity: regular granular piles supported approximately 300% more load than the untreated clay base, while geogrid-encased granular piles supported up to 470% more. Additionally, encased granular piles were able to support 25% to 50% more load than their non-encased counterparts when comparing the two types of heaps, demonstrating the additional advantage of geosynthetic encasement in improving granular pile performance in soft expanding soils.

Hasan and Samadhiya (2016) used a floating granular pile established in a clay substrate with an undrained shear strength of 5 kPa to conduct a short-term load-settlement research in the lab (Figure 2.14). The granular pile was 375 mm long and 75 mm in diameter, and the experiment was conducted in a model tank that was 200 mm in diameter and 525 mm in height. The replacement approach was used to install the pile. The study investigated the effect of different reinforcement directions, including vertical reinforcement with geotextile, horizontal reinforcement using circular geogrid strips, and a mix of horizontal and vertical reinforcement. Additionally, the spacing of the horizontal reinforcement strips was varied as a study parameter.

The results were compared to untreated soft soil beds and conventional granular pile beds. A plate that matched the granular pile's diameter was used to distribute the applied load. The results showed that the maximum load intensity for the treated clay bed was 195% higher for conventional granular piles, 440% higher for vertically encased piles, and 396% higher for horizontally reinforced piles (with a 50 mm center-to-center strip spacing). The ultimate load intensity for the floating granular pile rose by 485%, 432%, and 428% for horizontal reinforcement spacings of 25 mm, 50 mm, and 75 mm, respectively, when vertical and horizontal reinforcement were combined. These findings show that while horizontal reinforcement spacing has no influence on the combined vertically encased and horizontally reinforced piles, both vertical and horizontal reinforcement greatly increase the granular piles' load-carrying capacity.

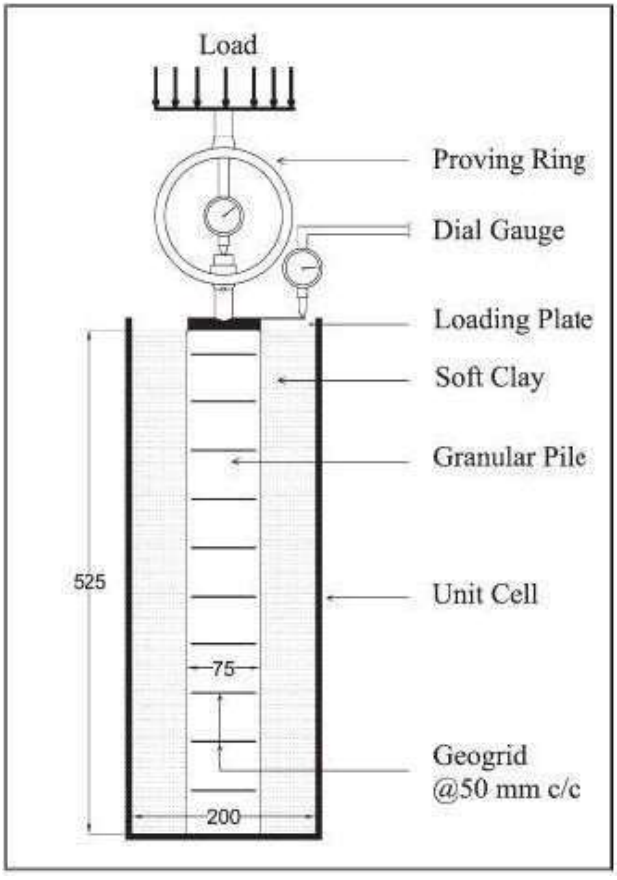


**Figure 2.14** Model test set up (Hasan and Samadhiya, 2016)

### 2.6.2.2 Geogrid Encased Stone Column Settlement Reduction Studies

A number of fundamental presumptions underpin Raithel and Kempfert's (2000) method for estimating the settlement of a granular column-reinforced foundation enclosed in geosynthetic encasement.

:

1. Loading Size and Soil Thickness: The applied load is large enough that the added stress from the load does not diminish with depth, implying that the effects of loading are considered uniform across the depth of the soft soil.
2. Equal Settlement: It is assumed that both the weak soil and the top of the column will settle equally under the applied load, meaning there is no relative displacement between them.
3. No Settlement Below the Column's Toe: The settlement is assumed to occur only above the column's toe, with no settlement expected beneath the column.
4. Active Earth Pressure: The column experiences active earth pressure, which affects the interaction between the soil and the column material.
5. Initial Soil Condition: Before loading, it is assumed that the soil is at rest. The coefficient of earth pressure for the soil in an excavation installation method is given by Ko,s=1−sin ϕsK_o,s = 1 - \sin \phi_sKo,s=1−sinϕs, where ϕs\phi_sϕs is the soil’s friction angle. For displacement installation methods, a higher ground pressure coefficient, Ko,sK_o,sKo,s, should be used.
6. Linear Elastic Behavior of Geosynthetic: The geosynthetic encasement is thought to exhibit linearly elastic behavior when under stress.
7. Constant Volume of Granular Columns: The granular columns are assumed to have constant volumes, as they are considered incompressible.
8. Drained Condition Design: The design assumes a drained condition, meaning that the pore water pressure dissipates quickly enough to prevent significant undrained behavior during loading.

The approach is modeled using the unit cell concept (Figure 2.15), it serves as the foundation for figuring out how a granular column-reinforced foundation with geosynthetic encasement will settle.

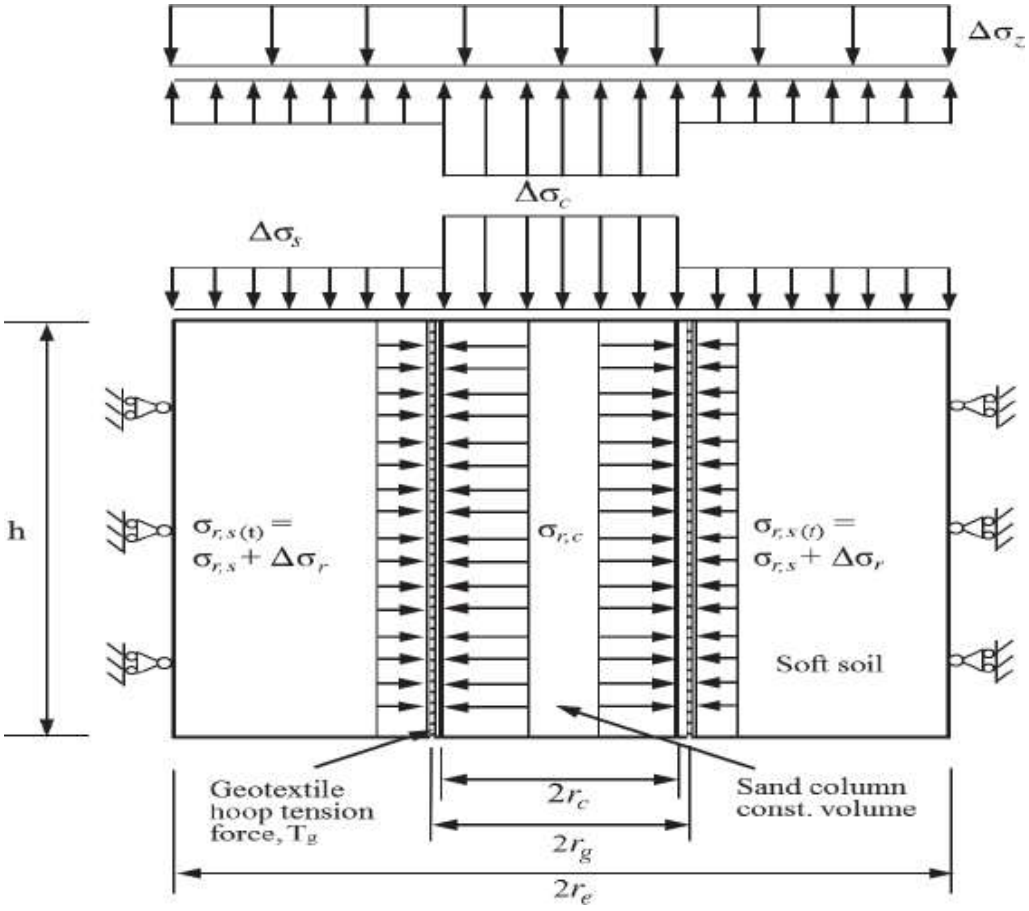


**Figure 2.15.** Geosynthetic encased column – Unit cell model (Raithel and Kempfert, 2000).

The soil and column are stressed by the overburden, as well as the additional stresses on them as follows contribute to the radial stresses in the soil and column:

$$\sigma_{r,c} = \Delta\sigma_c \cdot K_{a,c} + \sigma_{z0,c} \cdot K_{a,c}$$

$$= (1/a_s \Delta\sigma_z - (1 - a_s) / a_s \Delta\sigma_s) K_{a,c} + \sigma_{z0,c}$$

$$K_{a,c}\ \sigma_{r,s} = \Delta\sigma_s K_{0,s} + \sigma_{z0,s} K_{o,s}$$

Where, $\sigma_{z0,c}$= Overburden stress of the column,

$\sigma_{z0,s}$= Overburden stress of the soil,

$\Delta\sigma_c$= Additional vertical stress in the column,

$\Delta\sigma_s$= Additional vertical stress in the soil,

$K_{a,c}$= Active earth pressure coefficient in the column,

$K_{0,s}$= At-rest earth pressure coefficient in the soil, ($K_{0,s}$, should be used if a displacement installation method is used).

17 In order to investigate the behavior of a stone column covered in geogrid inside a soft soil bed, Malarvizhi and Ilamparuthi (2007) performed a finite element analysis using the PLAXIS tool. Their parametric study provided the following key findings:

1. Activation of Hoop Force: The hoop force within the geogrid encasement is activated 80 at the top 1D depth of the column. The hoop force gradually activates along the whole length of the column when pressure is applied, with the largest value of hoop stress happening at the column's 1D depth.
2. 179 Stress Concentration and Load Distribution: The load transferred to the surrounding clay is decreased as a result of the geosynthetic encasement's increased stress concentration on the stone column. This impact improves the column's performance by delaying the composite soil's settlement.
3. Effect of Encapsulation Stiffness: As the geogrid encasement becomes more rigid, the stress concentration factor rises and settlement falls. However, the contribution to the settlement reduction ratio (SRR) becomes negligible when the stiffness exceeds 2000 kN/m, indicating that there is a point of diminishing returns beyond which further increases in stiffness do not provide substantial improvements.
4. Impact of Column Material Shearing Resistance: The shearing resistance of the 174 material inside the column plays a critical role in the settlement reduction ratio (SRR). Compaction of the column material increases the stone column's efficiency, strengthening its resistance to shearing and improving settlement reduction.

19 These results emphasize how crucial the material inside the column and the mechanical characteristics of the geosynthetic encasement are in determining how well stone columns improve soft soil.

A number of small-scale model tests were carried out by Gniel and Bouazza (2009) to examine the behavior of encased stone columns. Their study highlighted the advantages of using geogrid over geotextile as the preferred geosynthetic material for column encasement. The geogrid was found to be more resilient and rigid, offering the necessary compression to achieve the required density in the column material. The research focused on the settlement reduction of both solitary and group columns, comparing encased columns (with both partial and full geogrid encasement) to non-encased columns and untreated soft soil beds.

Clay with a liquid limit (LL) of 62, a plasticity index (PI) of 32, a specific gravity (G) of 2.64, a saturated unit weight ($\gamma sat$) of 16.2 kN/m³, a moisture content of 63%, a compression index of 0.80, and an undrained shear strength (Cu) of 5 kPa made up the soft soil utilized for the testing. These soil properties were consolidated to create homogeneous soil conditions representative of natural deposits. The replacement method, known for its ease of application in soft soils, was used to install the stone columns. Sand with a specific gravity (G) of 2.80, a compacted saturated unit weight of 20.2 kN/m³, and particle sizes ranging from 11 to 4 mm made up the column material.

The influence of varying column encasement percentages (25%, 50%, and 75% of the column length) was examined in the study. The findings demonstrated that when the encasement percentage rose, the vertical strain decreased by 30%, 40%, and 50%, respectively. In fully-encased columns, there was an approximately 80% reduction in vertical strain. Furthermore, fully encased columns had a far higher stress concentration ratio of 10 compared to 2 for non-encased columns. The confinement effect of the geogrid, which increases the column's stiffness and regulates its radial strain, was identified as the cause of this rise in stress concentration. Additionally, the study found that radial expansion below the encasement's level caused isolated columns to break.. The vertical strain of both solitary and group columns decreased progressively as the length of encasement increased. The column capacity for isolated columns improved with increasing encasement length, while the strain at failure remained relatively constant. Fully-encased columns exhibited a marked improvement in capacity. But just below the encasement's base, there was noticeable radial bulging. This bulging was restricted to about two column diameters for solitary columns with partial encasement, but it extended through the non-encased region of group columns.

These results highlight the important role that geogrid encasement plays in improving the performance of stone columns, particularly in terms of lowering vertical strain and increasing load-bearing capacity, with the full encasement offering the most gains.

The impact of geogrid reinforcement positioned beneath a foundation on stone columns in improved soft clay was examined by Deb et al. (2011). The study investigated how the enhanced clay bed's load-settlement behavior was affected by factors such as the diameter of the geogrid layer, the thickness of the sand cushion, and the thickness of the geogrid sand bed. The soft clay used in their studies was categorized as CL with an unconfined compressive strength (UCS) of 19 kPa, and the stone columns were constructed using pebbles that ranged in size from 2 to 6 mm. The diameter of the biaxial geogrid utilized for reinforcement was adjustable between 200 and 500 mm, and it was 1 mm thick.

The researchers performed a short-term load test to determine the optimal thickness for both unreinforced and geogrid-reinforced sand beds. According to their research, the appropriate thickness for a geogrid-reinforced sand bed was 0.3 times the footing diameter, but the perfect thickness for an unreinforced sand bed was 0.5 times the footing diameter. Furthermore, it was discovered that when the sand bed was reinforced with geogrid, the ideal diameter of the reinforcement was three times the diameter of the footing.

This study offers crucial information about how well geogrid reinforcement works to improve the performance of stone columns under footings, especially in terms of load-bearing capacity and settlement management in soft clay conditions.

A thorough experimental and numerical investigation of the consolidation and deformation behavior of stone columns was carried out by Castro et al. (2013). Using a scale factor of 1:10, they conducted small-scale laboratory experiments and contrasted the outcomes with numerical analysis using the finite element method (FEM).The experimental parameters were carefully selected to align with the numerical model to ensure consistency in the comparison.

The investigation discovered that the friction angle and dilatancy angle of the surrounding soil had a substantial impact on the stress concentration factor of the stone columns. These elements were crucial to the soil-column interaction because they affected the column's settlement and the way stress was transferred through the soil. The results showed that a higher rate of consolidation led to an increase in column settlement, which in turn affected how well the stone column reduced settlement.

The fact that the stiffness ratio—that is, the ratio of the stiffness of the stone column to the surrounding soil—had no effect on the decrease in settlement was one of the study's most important findings. This implies that the column's performance was more dependent on variables like stress concentration and consolidation rate. The study also highlighted how crucial extra pore water pressure dissipation is to the consolidation process. The rate at which excess pore pressure dissipates has been demonstrated to be strongly influenced by the modification of the stress concentration factor over time, which is crucial for comprehending the long-term behavior and efficacy of stone columns in soft soil improvement.

By emphasizing the functions of soil mechanics characteristics like friction and dilatancy as well as the intricate relationships between stress concentration and consolidation during the settlement process, these discoveries provide significant knowledge to the design and study of stone columns.

By creating a numerical model and performing a parametric analysis, Hanna et al. (2013) examined the behavior of both single and group stone columns during failure. Their parametric research showed that when the D/B ratio—the ratio of the column diameter to the foundation width—rose, the load ratio rose hyperbolically.. This increase was particularly notable when D/B was less than 0.6, but it became nearly constant when D/B reached 1, which corresponds to the case where the total diameter of all the stone columns in

the group is equal to the foundation width.

The study also showed that for a given D/B ratio, the load ratio increased when the Poisson's ratio of the sand and clay decreased. This suggests that the performance of the stone column is significantly influenced by the elasticity and compressibility of the soil. Additionally, it was discovered that the shear resistance angle of the stone material and the modulus ratio (the ratio of the modulus of elasticity of the column material to the surrounding soil) increased the columns' capacity to support loads.

The kind of failure the columns encountered was one of the main conclusions. According to the study's findings, bulging failure happened when the area replacement ratio was less than 10%, while shear failure happened when stone columns replaced 10–35% of the area beneath the foundation. This emphasizes how crucial column design is to avoiding bulging failure and guaranteeing the best possible load-bearing capability.

These findings contribute to the understanding of how stone columns behave under various loading conditions and the influence of material properties and geometry on their performance, especially when considering different failure modes and their impact on the overall foundation performance.

According to Najjar et al. (2013), the failure of stone columns occurred when they were loaded from the top, with bulging taking place between 0.5 and 3 times the column's diameter. The columns' capacity to support loads rose when exposed to distributed loads, and this was accompanied by a notable decrease in bulging. Shearing, bending, and bulging were among the different ways that the columns failed. Longer columns mostly underwent deformation in the upper part of the column, whereas shorter columns tended to punch and penetrate into the soft soil. The bulging was much diminished and moved from the top to the bottom part of the column's length for encased columns.

Additionally, it was discovered that columns bulged more in soft clays than in stiffer ones, which had an impact on how the columns behaved under load. The composite system's strength and stiffness improved as the area replacement ratio rose. Additionally, raising the length-to-diameter ratio (L/D) increased the ultimate stress and stiffness of the columns for a given area replacement ratio. According to the study, effective load transfer was made possible by columns with an L/D ratio of five to eight times their diameter.

Additionally, it was shown that the stress concentration factor increased up to a particular loading level before declining. By covering the columns with geotextiles or geogrids, the composite ground's stiffness and load-bearing capacity increased while pore pressure was decreased. Additionally, the efficiency of columns with smaller diameters improved more than that of columns with higher diameters.

The study highlighted that loosely packed specimens gained strength more effectively than those in a densely packed state. Additionally, the lateral earth pressures around the columns were significantly influenced by the column spacing. For group loading, the matrix soil was found to be more critical than factors like the installation technique, type of column, and composition.

The implications of column size, encasement, soil conditions, and column spacing are among the key insights these research provide for maximizing the performance of stone columns. The study emphasizes how crucial these elements are to enhancing stone columns' stability and load-bearing ability, particularly in softer soils.

Castro et al. (2014) used numerical calculations to investigate the decrease in composite ground settlement following the installation of stone columns. Their findings revealed that when modest loads were applied and columns were spaced widely apart, poor column installation could actually lead to increased ground settlement, especially in overconsolidated clay. The impact of soil anisotropy — where the soil fabric rotates from cross anisotropy to vertical and back to horizontal when the embankment is loaded — was emphasized in the study. Because the stiffness of the composite ground increases with increased radial stresses, this shift raises the radial stresses, which in turn decreases settlement. Additionally, the study noted that excess pore water pressure reduces effective stress, contributing to increased

settlement. Moreover, the settlement was found to increase as soil plastic stresses rose, particularly with a decrease in the overconsolidation ratio.

In a different study, Kumar et al. (2014) investigated how vacuum application through enclosed stone columns affected soft clay's strength. The model studies demonstrated that the clay soil's undrained shear strength was affected by the amount of vacuum pressure used. It was discovered that applying vacuum pressure greatly increased the columns' rigidity and load-bearing capacity. Furthermore, stone columns subjected to vacuum pre-loading exhibited greater load-bearing capacity compared to those with surcharge loading. The results confirmed that pre-loaded columns had much higher load-carrying capacity than non-pre- loaded columns, especially when vacuum consolidation was employed. The study validated that the use of enclosed columns offers an effective method for applying vacuum pressure, enhancing the stone columns' functionality in areas with soft clay.

Ng and Tan (2014) examined the consolidation and settlement behavior of floating stone columns under spread loading using two-dimensional finite element calculations and the unit cell approach. They found that the enhanced ground's consolidation qualities declined together with the depth ratio, increasing settling. They also found that, at a certain depth ratio, floating columns exhibited similar settling behavior to end-bearing columns, which led to satisfactory consolidation for long-term ground settlement. Additionally, the study showed that settlement was significantly impacted by variables such the area replacement ratio, ground pressure following installation, loading intensity, and the friction angle of the stone column aggregates. The study also found that the behavior of the floating columns was barely affected by the modular ratio, which was impacted by the passive resistance of the surrounding soil.

Hasan and Samadhiya (2016) performed a comparative study on granular piles reinforced with geosynthetics, using laboratory testing and numerical analysis. The study considered short-term loading scenarios and the unit cell approach. The findings demonstrated that the ground's ability to support weight was enhanced by the installation of granular columns, whether they were reinforced or not. Reinforced floating columns outperformed unreinforced ones, especially in terms of reduced bulging. For both unreinforced and vertically encased columns, bulging occurred at depths ranging from approximately 1.0 to 1.6 times the column diameter. However, horizontally reinforced and combined reinforced columns showed

similar bulging behavior. The study also found that longer columns and clay beds with higher undrained shear strength contributed to improved column performance. While the ultimate load-bearing capacity of reinforced columns declined with increasing column diameter that of unreinforced columns stayed constant. Additionally, floating columns demonstrated a higher load-bearing capacity with decreased geogrid strip spacing.

Basack et al. (2017) evaluated the behavior of soft soil reinforced with stone columns using numerical techniques, focusing on lateral deformation. Their study found that the time before column bulging occurred and the zone of bulging were close to the surface of the ground. The restraint coefficients had a significant impact on column deformation, with lateral stress on the columns varying linearly with depth. Vertical stress increased with column depth, reaching a maximum value. When the radial distance from the column increased, so did the vertical stress on the surrounding soft soil. As the soft soil's initial undrained cohesiveness strength increased, bulging expanded deeper but diminished in size. As the column diameter shrank, the bulging's size likewise grew. Additionally, both the final load-carrying capacity and the degree of bulging increased with column spacing. As the stress concentration ratio increased, the bulging depth of columns reduced.

Debnath and Dey (2017) carried out studies on reinforced and unreinforced sand beds on vertical stone columns. According to their findings, the ground's capacity to support weight was greatly enhanced by the installation of stone columns, with the gain being more noticeable for encased columns. The geogrid-reinforced sand bed on encased columns reduced the maximum bulging depth and significantly decreased the amount of bulging. According to the study, the ideal encasement length was three times the column diameter, and the optimal length for encased columns with a geogrid-reinforced sand base was six times the column diameter.

To investigate the effects of geotextile encasement on soft clay reinforced with geotextile-encased stone columns, Miranda et al. (2017) carried out small-scale laboratory tests. According to their findings, encased columns could support a vertical force that was about 1.7 times higher than that of conventional columns. Compared to conventional columns, the reinforced ground's stress concentration factor was around two to four times higher. In comparison to untreated ground, the study also discovered a reduction in settlement when the ground was reinforced with both regular and enclosed stone columns.

Rajesh (2017) carried out a numerical analysis to study the behavior of geosynthetic encased stone columns (GESC) with both complete and partial penetration under time-dependent stress conditions. The study demonstrated that geosynthetic encasement reduced the time required for excess pore water dissipation and decreased lateral distortion or bulging of the columns, thus reducing settlement. The effective stress concentration ratio (ESCR) for encased columns increased significantly compared to regular stone columns, with the ESCR rising consistently during the consolidation period. However, after significant consolidation, the ESCR for regular stone columns increased initially and then declined. As the stiffness of the geosynthetic increased, the study also showed a significant increase in load transfer from the column to the surrounding soft soil.

Das and Deb (2018) investigated the time-dependent behavior of improved ground under embankment stress conditions using model experiments and numerical analysis. The study showed that with increased spacing to diameter ratio, embankment height, and modular ratio, the stress concentration ratio increased, eventually stabilizing over time. However, due to arching effects, the stress concentration ratio decreased after reaching a peak value. The study also found that the maximum stress concentration ratio did not significantly affect the relative densities of the soft soil thickness and embankment material. The results indicated negligible differential settlement when the embankment height was twice the column spacing. Over time, lateral distortion of the columns increased, with the greatest deformation observed at depths approximately 2.5 times the column diameter. Under steady-state conditions, the pore water pressure surrounding the stone columns and the surrounding soil was comparable; however, because of water buildup, the unimproved ground had a higher pore water pressure.

87

These studies provide comprehensive insights into the behavior of stone columns, their interaction with surrounding soils, and the impact of geosynthetic reinforcement on their performance.

# CHAPTER 3
# METHODOLOGY

## 3.1 GENERAL

This chapter uses a number of laboratory model studies to examine how stone columns behave in clayey soil. The study examines both conventional stone columns and those encased with geosynthetics, placed within a soft soil environment. The investigation evaluates the performance of individual columns as well as groups comprising three, four, and six columns arranged in triangular, square, and hexagonal patterns. Important elements including the geosynthetic material's rigidity and the diameter, length, and spacing of the stone columns were taken into account. Two experimental series were carried out: the first focused on individual stone columns with varying reinforcement configurations, while the second examined group behavior under different conditions. Both unencased and geosynthetic-encased columns were tested in each scenario. Numerical modeling utilizing PLAXIS 3D software was used to confirm the experimental data in order to guarantee the validity of the results.

## 3.2 MATERIALS USED

Three main materials were used in this study: a clayey soil sample, a specifically prepared stone column mix, and an encasing polymeric geotextile. To obtain the required qualities, fly ash, stone dust, iron dust, and cement were combined to create the stone column mix. Each of these materials' attributes are described in depth below:

### 3.2.1 Clay

A comprehensive review of existing literature revealed a widespread presence of soft cohesive soils throughout the region, with weak cohesive layers extending to a certain depth below the natural ground level. Given these conditions, a detailed subsurface soil analysis is essential to determine an appropriate ground improvement strategy. Specifically, evaluating the effectiveness of stone columns in cohesive soils, such as clay, is critical for accurately predicting their load-bearing capacity and settlement behavior. To facilitate this, soil samples were collected from various locations in Raisen District, Abdullahganj, Bhopal, Madhya Pradesh, India and brought to the lab for examination. The index properties of the fine-grained soil were assessed using a series of standard procedures, including the hydrometer

test (IS: 2720 Part 4 – 1985), specific gravity test (IS: 2720 Part 3 – 1980), Atterberg limit test (IS: 2720 Part 5 – 1985), the light compaction test (IS: 2720 Part 7 – 1980) and tri axial test (IS: 2720 Part 11 - 1993). The results of these tests, including the determined soil parameters, are summarized in Table 3.1.

**Table 3.1: Properties of expansive soil**

| Parameter | Expansive Soil |
|---|---|
| Differential swell index (%) | 35 |
| Unified Classification System | CH |
| Liquid Limit (%) | 60 |
| Plastic Limit (%) | 27 |
| Specific Gravity | 2.56 |
| Plasticity Index (%) | 33 |
| Shrinkage Limit (%) | 10 |
| Optimum Moisture Content (%) | 19.23 |
| Maximum Dry Density (kN/m$^2$) | 17.16 |
| Cohesion c (kN/m$^3$) | 32.37 |
| Angle of internal friction ($\phi$) | 18.20 |

### 3.2.2 Fly ash, stone dust and iron dust

The India Mart provided the fly ash, iron dust, and stone dust. Fly ash, an industrial waste that has binding qualities similar to cement, is shown in grey. The specific gravity of fly ash was 2.02. One waste product from the crusher plant is stone dust. Sand in concrete was substituted with stone dust. Stone dust has a specific gravity of 1.89. Figure 1 displays the fly ash and stone dust particle size distribution. Tables 3.2, 3.3, and 3.4 display the fundamental characteristics of iron dust, fly ash, and stone dust.

**Table 3.2: Properties of Iron Dust**

| Parameter | Specifications |
|---|---|
| Appearance | Amorphous, lustreless, grey powder |
| Iron Content | 99.8% min |
| Arsenic | <0.001 |
| Lead | <0.001 |

| | |
|---|---|
| Mercury | <0.001 |
| Carbon | 0.04 |
| Sulphur | 0.022 |
| Phosphorus | 0.005 |
| Copper | 0.001 |
| Acid insoluble substance | 0.2% max |
| Sieve analysis | +400 mesh – max 5%<br>-400 mesh – min 95% |

**Table 3.3: Properties of fly ash**

| **Characteristics** | **values** |
|---|---|
| Bulk Density | 1200 kg/m$^3$ |
| Specific Gravity | 2.02 |
| Colour | Grey |
| Particle size distribution<br>Sand (%)<br>Silt (%)<br>Clay (%) | <br>97.47<br>2.53<br>Nil |
| Coefficient of uniformity ($C_u$) | 2.06 |
| Coefficient of Curvature ($C_c$) | 0.432 |

**Table 3.4: Properties of stone dust**

| **Characteristics** | **values** |
|---|---|
| Specific Gravity | 2.72 |
| Coefficient of uniformity ($C_u$) | 1.12 |
| Coefficient of Curvature ($C_c$) | 0.11 |
| Particle size distribution<br>Sand (%)<br>Silt (%)<br>Clay (%) | <br>90.8<br>9.2<br>Nil |

### 3.2.3 Geosynthetics used

Geogrid and geotextile, two kind of geosynthetic encasement, were used in this investigation in both single and group columns. The properties of geosynthetics were given by the

manufacturer. Geogrid is comprised of polypropylene with longitudinal and transverse ribs. By limiting the vertical pressure on granular columns and avoiding additional settlement, these ribs can provide the greatest potential interplay between geogrid, multi-blended granular columns, and expansive soil. This experiment used a woven geotextile. Additionally, it is composed of polypropylene, which has tensile strengths of 34 kN/m in cross-machine direction and 45 kN/m in machine direction.

**Table 3.5: Properties of geosynthetics used**

| Geosynthetics | Properties | Value | Unit | Test method |
|---|---|---|---|---|
| Geogrid | Polymer type | polypropylene | - | - |
| | Structure | Bi-oriented geogrids | - | - |
| | Carbon black content | 2 | % | ASTM D4218 |
| | Cross machine direction | 350 | kN/m | ISO 10319 |
| | Stiffness at 0.5% strain machine direction | 550 | kN/m | ISO 10319 |
| | Installation damage factor | 1 | - | ASTM D5818 |
| | Aperture size<br>Machine direction<br>Cross Machine direction | <br>30<br>30 | <br>mm<br>mm | <br>-<br>- |
| | Residual resistance to chemical degradation | 100 | % | EN 14030 |
| | Residual resistance to weathering | 100 | % | EN 12224 |
| | Apparent coefficient of friction soil/ Geosynthetics at 10 kPa soil/ | 1.78<br>1.14 | - | EN 13738 |

| | | | | |
|---|---|---|---|---|
| | geosynthetics at 20 kPa | | | |
| **Geotextile** | Polymer type | polypropylene | - | - |
| | Weight of fabric | 200 | $g/m^2$ | ASTM D5261 |
| | Tensile strength<br>Machine direction<br>Cross Machine direction | <br>45<br>34 | <br>kN/m<br>kN/m | IS 1969 |
| | Elongation at break<br>Machine direction<br>Cross Machine direction | <br>30<br>28 | <br>kN/m<br>kN/m | IS 1969 |
| | Apparent opening size | 0.075 | mm | ASTM D4751 |
| | Puncture resistance | 700 | N | ASTM D4833 |

## 3.3 EQUIPMENTS & APPARATUS

### 3.3.1 Tank

To simulate the behavior of a clay bed reinforced with stone columns, a model tank measuring 1500 mm in length, 900 mm in width, and 600 mm in height was constructed. Figure 3.1 depicts the tank's dimensions and design. In order to withstand any potential lateral displacement during the filling operation, the tank walls were built with sufficient thickness. The inside surfaces of the tank were coated with a thin layer of grease to lessen friction between the clay and the tank walls.

**Fig 3.1:** Model Test Tank with Loading Frame

### 3.3.2 Loading and Measurement System

As shown in Figure 3.1, the model tank had a single loading system and a strong loading frame that applied loads to both the stone column materials and the soft soil. For usage with both single and numerous columns, a circular iron foundation plate measuring 300 mm in diameter, 10 mm in thickness, and 7200 grams in weight was recommended. A hydraulic jack (Figure 3.2) with a maximum force of 50 kN was used to apply the load, and the loading system functioned under a stress-controlled mechanism. In order to assess the load-displacement behavior of the soft clay, a vertical monotonic load was applied to the clay reinforced with stone columns during testing. Settlement measurements were taken using three dial gauges positioned 120º apart, and the final settlement value was calculated as the average of the readings from these three gauges.

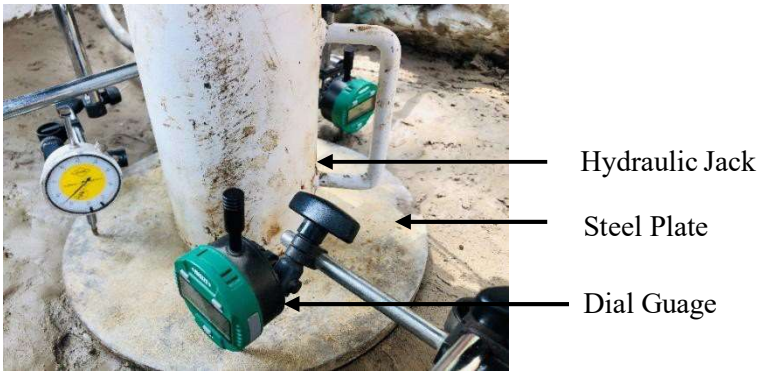


**Figure 3.2.** Test setup showing various components

### 3.3.3. Pipes for construction of Stone Column

The replacement approach was employed to build the columns using steel pipes whose internal diameter matched that of the stone columns. In order to maintain the area replacement ratio within the suggested range of 5% to 35%, the pipe sizes were selected. In order to lay stone column material, these hollow pipes were used to create voids in the soft earth bed. Each pipe was 600 mm long, 2 mm thick, and had one beveled end to lessen

disruption when inserted into the soft clay bed. Figure 3.3 shows the pipe utilized in the investigation.

**Figure 3.3.** Pipes used for making stone column

### 3.3.4 Compaction Tools

The clay layer was compacted by dropping it from a height of 250 mm using a specially made tamper unit that measured 200 × 200 mm in plan. A 1.5 kilogram steel rod with a diameter of 20 mm and a length of 100 mm was used to compact the stone fill inside the stone columns.

## 3.4 MODELLING CONSIDERATIONS

Boundary effects, the L/D ratio, and the geometric similitude ratio were taken into consideration when modeling the stone column and test tank parameters (length, L, and diameter, D). The smallest complete column diameter is approximately 13 mm (Shahu and Reddy, 2011), while prototype stone column diameters normally range between 0.6 m and 1 m (Wood et al., 2000). Prototypes often have an L/D ratio of 5 to 20 (Shahu and Reddy, 2011). The current study used column diameters of 50 mm and 70 mm, with L/D ratios kept between 5 and 10, in accordance with these recommendations. It was discovered that the relevant similitude ratio (Dmodel/Dprototype) fell between 0.05 and 0.1.

A key consideration in designing the model tank was ensuring that boundary effects remained minimal, meaning the tank walls were placed far enough from the test zone to avoid stress constraints that could lead to overestimation of results. Accordingly, the overall testing box depth was set at 0.4 m for end-bearing columns and 0.25 m for floating columns. Similar cylindrical tank model setups for single and multiple reinforced stone columns were also reported by Ali et al. (2011).

### 3.5 CLAY BED PREPARATION

A model tank with dimensions of 1500 x 900 mm and a height of 600 mm was used to prepare clay beds. To stop water loss and friction between the tank and wall, a thick plastic cover was installed within the tank. The steel tank was filled with 400 mm of soft, expansive dirt that had been remolded. The soil was placed using the rainfall method. The clay pieces were extracted from the paddy field, ground cleaned of grass, soil biota, gravel, pebbles, and other unwanted objects, and then left in the daylight to dry To get a soft consistency, the fine clayey soil was thoroughly mixed with the necessary amount of water. Using a 25 kg rammer, the soil is compacted into four 100 mm layers and left for seven days to ensure that the moisture content is evenly distributed throughout the soil. Each layer's bulk density was kept at 18 kN/m³ to guarantee uniformity, and it was routinely monitored during the filling process using a mold with a known volume at three separate locations within the layer. To provide an even surface and consistent thickness, the top surface of the clay bed was leveled and cut in every experiment. For every test, the same process was used to prepare the clay layer. To guarantee even water distribution throughout the whole model tank, the moisture content was tested using an oven distribution method at 10 cm intervals across the clay layers. The moisture content of the clay bed varied by less than 1.5% in each instance. To stop evaporation, iron and plastic sheets were placed over the tank.

**Figure 3.4:** (a) Testing Tank (b) clay bed prepared

## 3.6 Forming of stone column mix

After seven days of curing, various cube samples were cast and tested in a compression testing machine to determine the ideal combination of stone dust, fly ash, iron dust, and OPC. The area of the cube was 4900 $mm^2$. The 1:3 mix was prepared with 3 samples each to opt for the average strength value. The sample was mixed thoroughly by a mixer and compacted by a vibrating machine in the cube sampler. The only ratio of cement, fly ash, and iron dust mixed with three parts of stone dust and water. Water added = $\frac{P}{4} + 3$, where P is the cement consistency (Verma Pallavi, Sahu A. K. (2019)). The multi-blended column was cast using the combination with the highest strength.

In this study, sample 4 was used to cast the multi blended column because this gave optimum compressive strength of the cube, and less percentage use of cement as a binder material was shown from an economic point of view. Fly ash and cement worked as binder materials.

The specific gravity of the multi blended column mix was calculated as 2.61.

**Table 3.6: Column mix selection**

| Sample | Proportion (cement + fly ash + iron dust) | Compressive Strength ($kN/mm^2$) |
|---|---|---|
| 1 | 45% cement + 50% fly ash + 5% iron dust | 9.61 |
| 2 | 50% cement + 45% fly ash + 5% iron dust | 9.03 |
| 3 | 45% cement + 45% fly ash + 10% iron dust | 9.19 |
| 4 | 40% cement + 50% fly ash + 10% iron dust | 10.2 |
| 5 | 50% cement + 40% fly ash + 10% iron dust | 9.65 |
| 6 | 45% cement + 40% fly ash + 15% iron dust | 9.51 |
| 7 | 40% cement + 45% fly ash + 15% iron dust | 8.61 |

**Figure 3.5:** a) Failed sample in CTM loading b) Cubes for testing

## 3.7 STONE COLUMNS CONSTRUCTION FOR UNENCASED COLUMNS

Boundary effects and the geometric similitude ratio (L/D) were considered when developing the stone column parameters. These factors led to the choice of column diameters of 50 mm and 70 mm in the current investigation, with L/D ratios kept between 5 and 10. The stone columns were built from steel pipes with internal diameters of 50 and 70 mm and walls that were around 2 mm thick. For each sample, a small layer of oil was applied to the inner and outer surfaces of the pipes to reduce disturbance of the surrounding soil during installation.

### 3.7.1 Single Stone Column

After marking the exact center of the tank, a pipe with the necessary diameter was placed vertically in the clay bed and its alignment was carefully maintained. In contrast to the force penetration and soil displacement methods that are frequently employed in the field, the stone columns were built utilizing the soil replacement approach, which is appropriate for small-scale modeling. The stone columns were formed by steel casings that were put into the test soil and had internal diameters of 50 mm and 70 mm and a wall thickness of 2 mm. The main reason for using the top-down construction approach was to keep the soil from collapsing while the borehole was being formed. The cavity was prepared by scraping out any leftover dirt after the clay inside the casing was removed using a screw auger with a diameter of 38 mm. To minimize the smearing effect, the pipe had a thin coating of oil both inside and out. The floating column and end bearing were cast in the soil bed. After the soil was removed from the pipe, the column's length was measured using a scale of the required length. The mixture was then added to the column in five layers, compressed with a 20 mm diameter rod weighing 1.5 kg, and left for a full day to reach its maximum strength. To reach a target relative density of 68% (equal to 15.8 kN/m$^3$), a trial-and-error method was used to calculate the required drop height and total number of strikes. Given the impermeable nature of the surrounding soil, this level of compaction is considered effective for ensuring successful load transfer. Literature indicates that relative densities ranging from 50% to 80% have been used in clayey soils. This method involved discharging aggregates into a container, compacting them, and then removing the case all at once. The resulting relative density of the placed aggregate showed a variation within the range of 68±2%. Figure 3.4 represents a constructed hole by a pipe for d= 70 mm.

**Figure 3.6:** (a) Unit cell column (b) Column mix filled column

### 3.7.2 Group of Stone Columns

The first phase of the procedure looked like a solitary, unreinforced stone column. A critical step involved selecting the appropriate spacing and arrangement pattern for the stone columns before forming the hollow pipe. Spacing-to-diameter (S/D) ratios of 2, 2, and 3 were used to construct stone columns in triangular, square, and hexagonal patterns. For the triangular, square, and hexagonal patterns, groups of three, four, and six stone columns were formed utilizing the soil replacement method. The same auger mentioned earlier was employed to remove soil from the pipes. Figure 3.7 illustrates the triangular and hexagonal arrangements for a typical column diameter of 50 mm with an S/D ratio of 2 and 3. Similar arrangements were also prepared for other S/D ratios, as required for testing purposes.

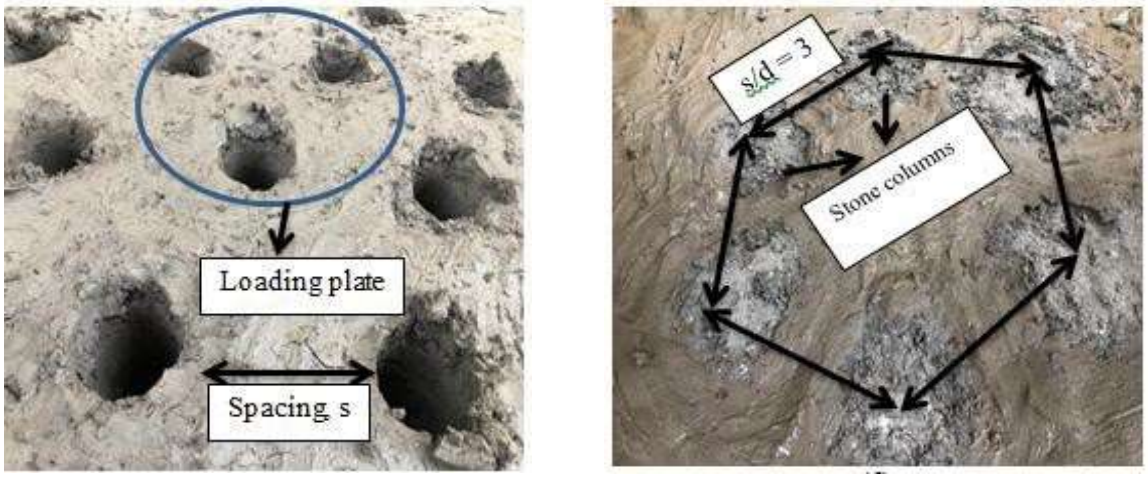


**Figure 3.7:** Typical arrangement of triangular and hexagonal pattern of stone column in groups for D = 50mm and S/D = 2 & 3

## 3.8 CONSTRUCTION OF STONE COLUMNS FOR VERTICALLY ENCASED STONE COLUMNS

Geosynthetics was shaped into the necessary diameter tube and inserted with the casing for the encased stone columns. To ensure that the final diameter of the encased stone column is identical to the diameter of the stone column, the casing pipe's diameter was slightly less than the stone column's formation diameter. Initially, the column (Lr=L) had a length of geotextile reinforcement, and the pipe's entire length was wrapped in geosynthetics. The pipe was completely encased by the geosynthetics and was lowered into the desired position. The column mix were put into the geotextile-wrapped tube and compacted similarly to that done during ordinary stone column case.

For stone column in groups, again triangular, square and hexagonal pattern of columns were arranged for s/d ratio of 2, 2 and 3. The required pipes as per the desired pattern were encased around it and lowered into the soil as the designated position. The pipes are subsequently filled with the amount of column mix calculated and compacted as it was done in the previous case.

## 3.9 TEST PROCEDURE

In stone column research and design, the area replacement ratio ($A_r$) is a key parameter influencing load distribution and settlement behaviour. According to the literature, Ar is defined as the ratio of the stone columns' cross-sectional area to the foundation's overall size; practical values usually fall between 5% and 35%. A 300 mm diameter loading plate was used in the current study to evaluate individual stone columns with diameters of 70 mm for single columns and 50 mm for groups of columns, resulting in Ar values of 7.09% and 6.25%, respectively. To guarantee minimal deformation under loading, an iterative procedure of repeated testing and analysis was used to determine the loading plate thickness. After testing, a plate thickness of 10 mm was finally chosen since it showed very little distortion. A hydraulic jack with a 50 kN capacity was used to apply load at a controlled pace in the stress-controlled loading system. Through the plate placed centrally above the column, a monotonic vertical force was supplied to the treated clay; the load application was stopped when the settlement reached 50 mm. Twenty-five stone column tests were conducted in all. A minimum length-to-diameter (L/D) ratio of 5 was maintained for every test, surpassing the crucial value of 4 suggested in the literature to avoid bulging failure. The full details of the experimental program are summarized in Table 3.7.

## 3.10 DETAILS OF EXPERIMENTAL PROGRAM

To accomplish the required goals, the laboratory research is basically separated into various test series. The test series were divided into two portions. First series was done for single stone column for unencased and encased case. Two types of columns are designed i.e. end bearing columns and floating columns for unencased and encased case. The encasement was provided up to the length of the column. Also two types of encasement was tested i.e. geotextile and geogrid.

Second series of tests was done for group of columns for end bearing and floating columns arranged in triangle, square and hexagonal pattern for varying S/D ratio of 2, 2 and 3. Both type of encasement were used to study the encasement effect similar to that done in the analysis of a single stone column.

**Table 3.7: Brief description of an experimental test**

| S.No. | Type of Reinforcement | Specific characteristics | | No of tests |
|---|---|---|---|---|
| | | Single column | Group of columns | |
| 1 | Natural expansive soil | - | - | 1 |
| 2 | Expansive Soil + stone column (end bearing and floating) | l = 400mm (end bearing)<br>l = 250 mm (floating)<br>Dia 70 mm<br>No of experiment = 2 | l = 400 mm (end bearing)<br>l = 250 mm (floating)<br>Dia 50 mm, s/d = 2 (triangle & square) and 3 (hexagonal).<br>No of experiment = 6 | 8 |
| 3 | Expansive soil + stone column (end bearing and floating) with geosynthetic encasement | l = 400mm (end bearing)<br>l = 250 mm (floating)<br>Dia 70 mm<br>No of experiment = 4 | l = 400 mm (end bearing with encasement)<br>l = 250 mm (floating with encasement)<br>Dia 50 mm, s/d = 2 (triangle & square), 3 (hexagonal).<br>No of experiment = 12 | 16 |

## 3.11 COLUMN EXHUMATION

In order to evaluate the in-situ geometry, continuity, and material quality of ground improvement columns—such as stone, sand, or cement/lime-treated columns—column exhumation is a post-construction investigative process. The process involves the careful excavation of a constructed column, typically in a trial or test section, to expose its full or partial length without significantly disturbing its structure. During excavation, measurements of diameter, depth, and shape are recorded at various levels, and any variations such as bulging, necking, or voids are noted. Representative material samples are collected for laboratory testing to determine gradation, density, and other relevant properties.

This method provides direct visual and physical verification of construction quality and enables comparison between the as-built column and design specifications, making it valuable for both research studies and quality assurance in ground improvement projects.

In this study after the test done, the column mix from the column was carefully removed, and to address the column's misaligned shape, a thin plaster of Paris paste was put to the hole. By scraping away the surrounding earth, the cured plaster of Paris was extracted for further investigation. Following the test, measurements were taken of the deformed columns' length and the column's bottom penetration.

## 3.12 NUMERICAL MODELLING

### 3.12.1 General

For a geotechnical problem to have an exact solution, the conditions of compatibility, equilibrium, material efficiency, and boundary constraints for both forces and displacements must be content. It has been discovered in recent years that numerical analysis techniques fully meet these requirements. This discovery has driven significant progress in numerical methods, supported by the widespread use of advanced technologies and software capable of performing complex computations within a reasonable time. Commonly used numerical approaches include the finite difference method (FD), discrete element method (DE), finite element method (FE), and boundary element method (BE).

In this analysis, the finite element method (FEM) is employed. FEM studies the behaviour of an infinite system by representing it with a finite number of elements, expressed through ordinary or partial differential equations. This method allows the modelling of any shape through flexible arrangements of elements, removing the need for various analytical solutions when dealing with non-linear equations or complex geometries. FEM effectively handles continuum behaviour, composite equations, and irregular boundary conditions. The capacity to adapt to changes in material stiffness, even at the element level, is its main benefit. Furthermore, it enables the application of multiple boundary conditions, making it possible to produce universally acceptable approximate solutions to physical problems.

### 3.12.2. Plaxis 3D

Owing to its theoretical foundation, which relies on the concept of virtual work to estimate stress and pressure distribution within a continuum for solving challenging engineering issues, the Finite Element Method (FEM) has shown itself to be a useful technique.. PLAXIS 3D, a three-dimensional FEM software specifically developed for geotechnical engineering,

is particularly effective in simulating the intricate behaviour of small groups of granular columns. This software was therefore employed for the finite element analysis in the present study. It incorporates advanced constitutive models—described in detail in a later chapter—to represent the properties of both soil and stone. To guarantee the accuracy of the numerical outcomes, preliminary investigations such as mesh sensitivity analysis and assessment of the influence of boundary distance were conducted.

The numerical analysis involved comparing the load–settlement responses obtained from experimental investigations with those derived from the PLAXIS 3D model. The boundary conditions for the earth and stone columns were established using the Mohr–Coulomb model. For the clay and column materials, a drained behavior was anticipated. For meshing, 15-node triangular elements were employed. In order to assess the stone column's performance within the soil matrix, common deformation patterns, and column meshing, boundary conditions were established to limit medium deformation. Aggregates, surrounding soil, and geotextiles were modelled using various constitutive options available in PLAXIS 3D.

### 3.12.3 Material Properties

A popular and simple method for depicting the behavior of soils that are linearly elastic until yielding and then totally plastic is the Mohr–Coulomb model. The model's plastic component adheres to the Mohr–Coulomb failure criterion, which was developed within a non-associated plasticity framework, while its elastic component is based on Hooke's equation for isotropic elasticity. The yield surface of a totally plastic constitutive model, like Mohr-Coulomb, is completely determined by its parameters and is not impacted by plastic straining. All strains are reversible and the soil reaction is completely elastic for stress levels that fall within this yield surface. The yield surface does not change in size or shape once the stress state reaches it; instead, plastic deformation takes place.

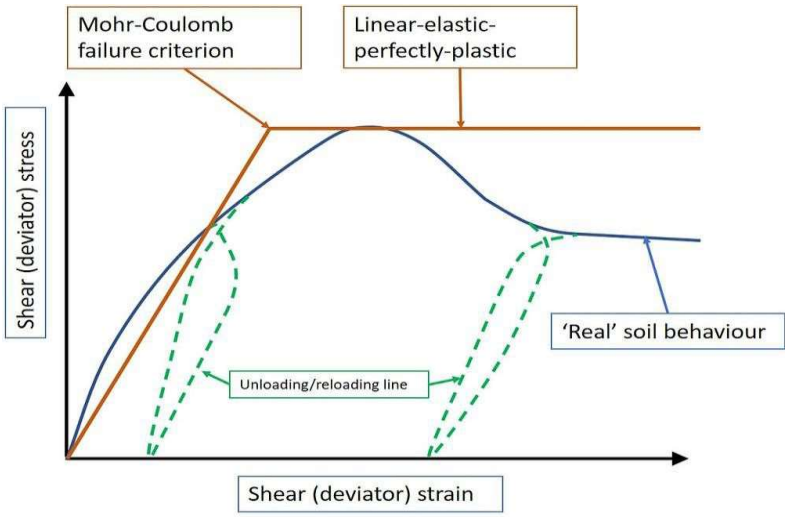


**Figure 3.8.** Real soil behaviour by Mohr - Coulomb model

The Mohr–Coulomb model was used in this study to simulate the behavior of the soft clay. Geotechnical engineers are commonly familiar with the five parameters needed for the linear elastic, completely plastic Mohr–Coulomb formulation, all of which may be derived from simple laboratory measurements on soil materials. The following is a list of these parameters and their standard units:

E: Young's modulus [kN/m$^2$]

$\phi$: Friction angle [º]

$\nu$: Poisson's ratio [-]

$\psi$: Dilatancy angle [º]

c: Cohesion [kN/m$^2$]

Young's modulus is the main indicator of stiffness in PLAXIS's Elastic and Mohr-Coulomb models, however other stiffness moduli are also included. Since many geomaterials exhibit nonlinear behavior from the very beginning of loading, careful parameter value selection is crucial since stiffness has the dimensions of stress. In triaxial testing, the beginning slope of the stress-strain curve is called the tangent modulus, or E0, and the secant modulus that corresponds to 50% of the material's peak strength is called E50. E0 can be utilized for materials with a wide linear elastic range, however E50 is recommended for the majority of soil-loading situations. The unload–reload modulus, Eur, should be used in place of E50

when unloading and reloading take place.

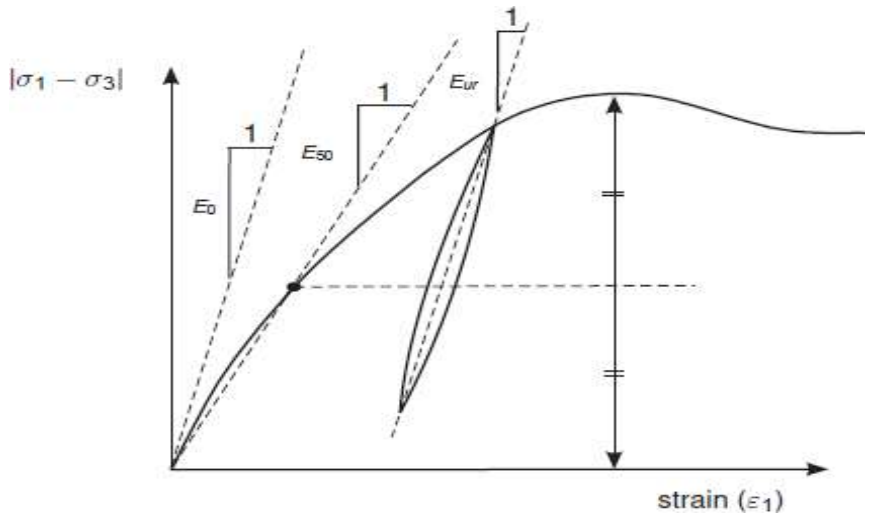


**Figure 3.9.** $E_0$, $E_{50}$ and $E_{ur}$ of a soil sample from triaxial test results

In the Mohr–Coulomb model, one-dimensional compression under gravity loading is used to determine realistic $K_0 = \sigma_h' / \sigma_v'$ ratios. For this loading condition, PLAXIS produces $\{\sigma_h' / \sigma_v'\} = \{\nu/ (1 - \nu)\}$ making it straightforward to select a Poisson's ratio that matches the desired $K_0$. This approach typically yields $\nu$ values between 0.3 and 0.4, which extends beyond one-dimensional compression to loading circumstances.

Similar to stiffness, cohesiveness has stress-related characteristics. The Mohr–Coulomb model defines a realistic effective friction angle $\phi'$ and the soil's effective cohesiveness $c'$. While dense sands may exhibit high friction angles, excessively large values increase computational effort in plastic analyses and may lead to unrealistic behaviour due to strain-softening—where very high friction cannot be maintained under large strains. The dilatancy angle $\psi$ (in degrees) defines volumetric expansion during shear; for clays, except for heavily over-consolidated layers, $\psi$ is generally close to zero.

A popular critical state soil model for simulating the stress-strain behavior of typically consolidated and slightly overconsolidated clays is the Modified Cam Clay (MCC) model. The MCC model, which is based on the ideas of critical state soil mechanics, takes into consideration both plastic and elastic volumetric strains, with stiffness being stress-dependent rather than constant. The yield surface in this model extends or contracts in response to the preconsolidation pressure and is circular in the q–p′ plane. Poisson's ratio (v), the initial preconsolidation pressure (p′c0), the slope of the critical state line (M) in the deviatoric

stress–mean effective stress space, and the slopes of the normal compression line (λ) and swelling line (κ) in the void ratio–logarithmic mean effective stress space are the main input parameters. In Plaxis, the elastic bulk modulus and shear modulus are calculated internally from these parameters and the current stress state, with the bulk modulus expressed as

$$K = \frac{(1+\nu)p'}{\kappa}$$

and the shear modulus as

$$G = \frac{3(1-2\nu)}{2(1+\nu)}K$$

Consequently, the instantaneous Young's modulus can be obtained from

$$E=2G(1+\nu),$$

but it varies throughout the analysis as the mean effective stress changes. The MCC model is particularly suitable for simulating embankment loading, consolidation, and undrained shear behaviour of clays, although it is less applicable to sands or heavily overconsolidated soils. In present study value of $\nu = 0.3$ and $\lambda = 0.05$.

The main limitation of simulating column mix in PLAXIS is the inability to explicitly define column mix sizes. As presented in Table 3.6, the shear strength parameters and unit weights for both the modelled aggregates and the surrounding soil were obtained from laboratory testing.

**Table 3.8.** Properties of soil and aggregate

| Properties | Soil | Stone Column mix | Geogrid | Geotextile |
|---|---|---|---|---|
| Soil | Clay | - | - | - |
| Cohesion (c) | 32.37 kN/m$^2$ | 1 kN/m$^2$ | - | - |
| Material Model | Mohr Coulomb | Cam Clay | Elastic | Elastic |
| Friction angle (ϕ) | 18.2º | 40º | - | - |
| Bulk Unit Weight ($\gamma_{unsat}$) | 17.16 kN/m$^3$ | 15.8 kN/m$^3$ | - | - |
| Modulus of Elasticity | 20,000 kN/m$^2$ | 80000 kN/m$^2$ | 100000 kN/m$^2$ | 120000 kN/m$^2$ |

| | | | | |
|---|---|---|---|---|
| Saturated Unit Weight ($\gamma_{sat}$) | 18.75 kN/m$^3$ | 17.1 kN/m$^3$ | - | - |
| Poisson ratio | 0.33 | 0.34 | - | - |

Geogrids are elastic, flexible sheet-like elements that resemble a grid or fabric and are incapable of carrying compressive forces. In PLAXIS 3D, each geogrid dataset corresponds to a specific material type and can be assigned to the relevant geogrid element or group within the geometry model. For elastoplastic behaviour, geogrid properties are defined in terms of stiffness and strength.

The axial stiffness EA needs to be given for elastic behavior. Orthotropic and anisotropic material qualities are supported by PLAXIS and are described as:

EA1: The standard elastic stiffness in one direction (in-plane).

EA2: The typical two-dimensional elastic stiffness.

GA stands for anisotropic behavior, or in-plane shear stiffness.

Force-elongation diagrams can be used to determine axial stiffness, which is usually supplied by the manufacturer. It is calculated as:

$$EA = \frac{F}{\Delta l / l}$$

Where F is the axial force per unit width, $\Delta l$ is the elongation, and l is the actual length. For isotropic behaviour, only $EA_1$ is required, EA2 = EA1 and GA = EA1/2.

For elastoplastic modelling, two strength parameters are needed:

Np,1 - The maximum force in 1-direction.

Np,2 - The maximum force in 2-direction.

Here, Np is the maximum axial tension per unit width. Exceeding Np causes stress redistribution according to plasticity theory, resulting in irreversible deformations. Since output axial forces are calculated at element nodes, extrapolation from stress points may lead to nodal values slightly exceeding Np. In isotropic mode, only Np1 is required, with Np,2 = Np,1

### 3.12.4 Model Generation/ Geometry Modelling Process

The various model setups created for the experimental analysis of single stone columns and stone columns in groups were replicated in the numerical modelling. Figure 3.10 represents modelling a clay bed inside the tank of the same dimension used for the experimental analysis. A 70 mm column diameter for single column and 50 mm column diameter for group of columns was taken to show the generated model of an ordinary stone column, vertically encased stone columns for end bearing and floating columns. For different S/D ratios, the model setup has been depicted for both individual and groups of stone columns arranged in triangle, square, and hexagonal designs. The model configuration of a single regular type stone column is shown in Figure 3.11. Figure 3.12 represents model of encased stone column. The images gave in 3.11 and 3.12 are the reference images of end bearing column. Similar modeling is done for the floating columns.

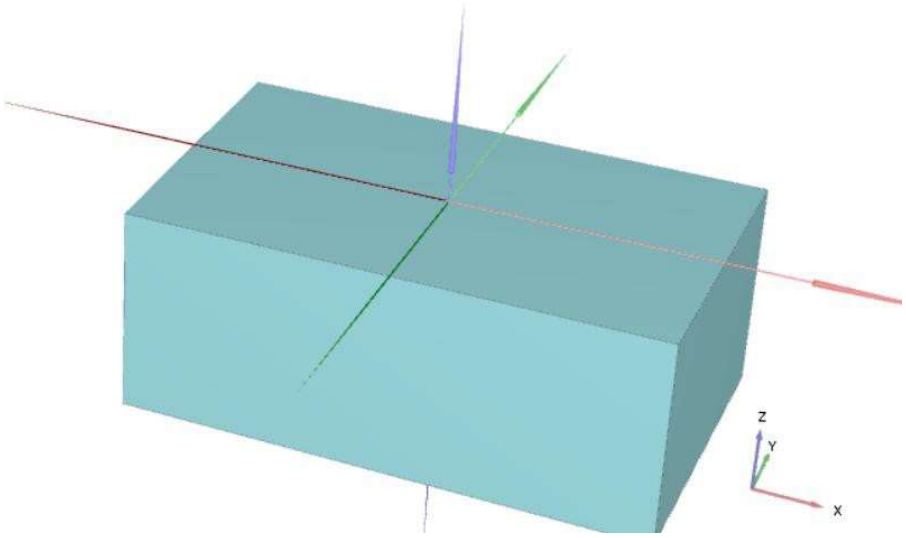


**Figure 3.10.** Model setup of soft clay

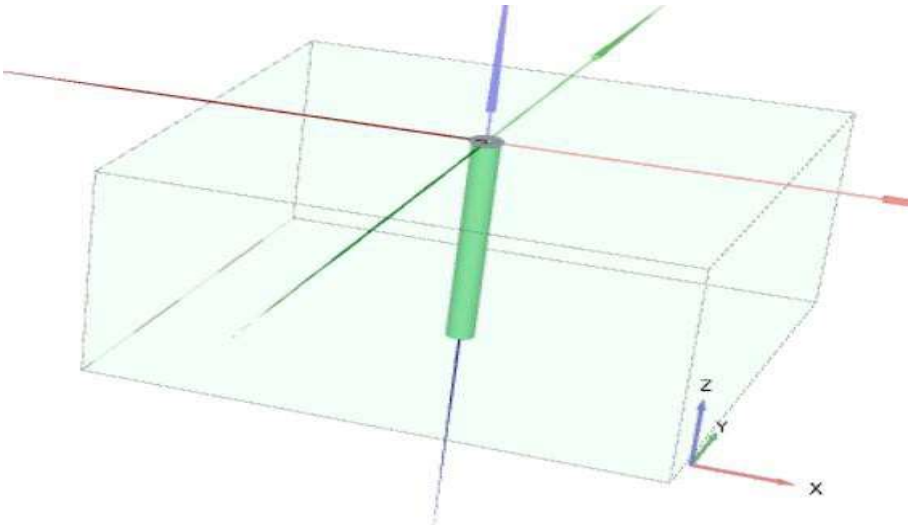


**Figure 3.11.** Model setup of an ordinary stone column for diameter of 70 mm

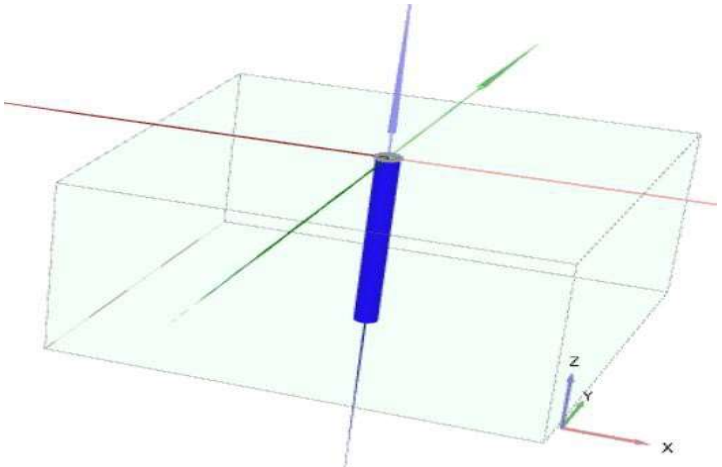


**Figure 3.12.** Model setup of encased stone column

For analysis of group, Figure 3.13, represents ordinary stone column arranged in triangular pattern with S/D=2, respectively. Figure 3.14, represents ordinary stone column arranged in square pattern with S/D=2 respectively. Figure 3.15 represents encasement for end bearing column arranged in triangular pattern with S/D = 2 respectively. Figure 3.16 represents encasement for end bearing column arranged in square pattern with S/D=2 respectively. The images gave in 3.13, 3.14, 3.15 and 3.16 are the reference images of end bearing column. Similar modeling is done for the floating columns and for hexagonal pattern too.

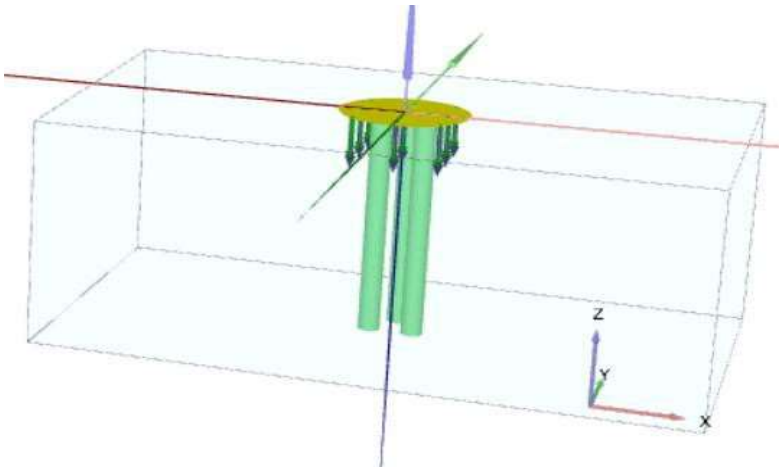


**Figure 3.13.** Model setup of ordinary stone column arranged in a triangular pattern for S/D = 2 for D=50mm

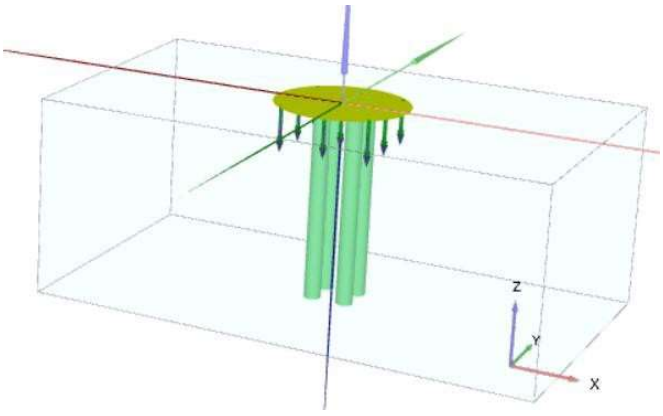


**Figure 3.14.** Model setup of ordinary stone column arranged in a square pattern for S/D = 2 for D = 50mm

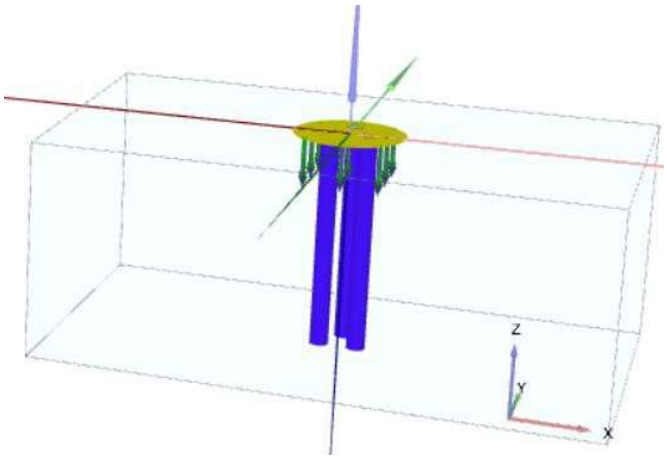


28

**Figure 3.15.** Model setup of encasement for end bearing column arranged in a triangular pattern with S/D = 2 for D=50mm

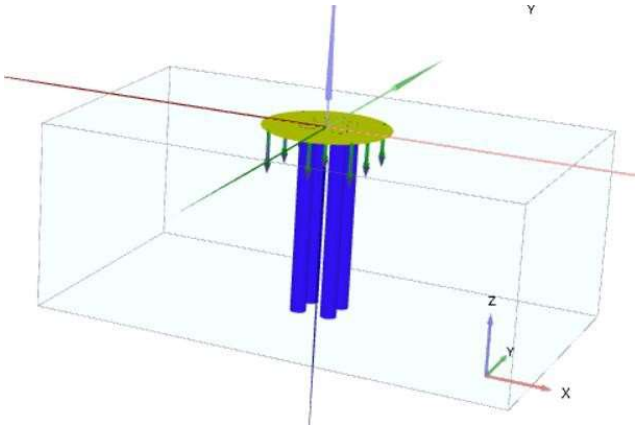


**Figure 3.16.** Model setup of encasement for end bearing column arranged in a square pattern with S/D=2 for D=50mm

### 3.12.5 Mesh Generation

46

In order to define the geometry and set up staged construction, it is essential to generate an adequate finite element mesh. To facilitate the numerical analysis, the geometry must be divided into finite elements after it has been thoroughly described. To guarantee precise and seamless computations, the mesh—an arrangement of these finite elements—must satisfy specific requirements.

A high-quality mesh avoids excessively elongated or distorted elements, which could cause numerical instability. Element sizes should be sufficiently small in regions where significant stress or strain changes are expected, but not unnecessarily fine throughout the entire model, as this would lead to excessive computation times. The goal is to strike an optimal balance between accuracy and efficiency.

The mesh in PLAXIS 3D is automatically created while accounting for loads, boundary conditions, structural components, and soil stratigraphy. Ten-node tetrahedral elements make up the majority of the 3D finite element mesh for soil (Figure 3.9).

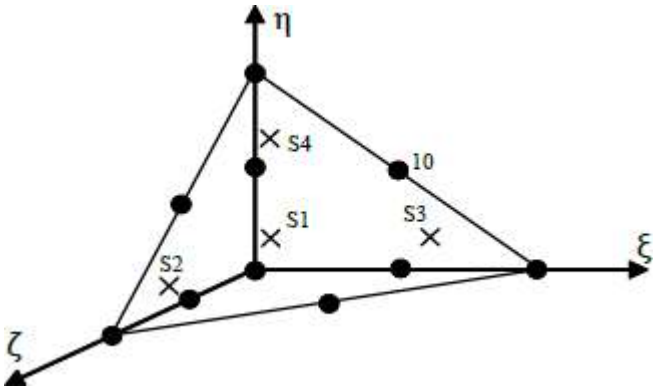


**Figure 3.17.** 10 - noded tetrahedral 3D soil element

The mesh generator requires the desired element dimension, which is given by the global meshing parameter le. This parameter is calculated using the outer geometry dimensions ($x_{min}$, $x_{max}$, $y_{min}$, $y_{max}$, $z_{min}$, $z_{max}$). The following formula is used to determine the desired element dimension..

$$l_e = r_e \times 0.05 \times \sqrt{(x_{max} - x_{min})^2 + (y_{max} - y_{min})^2 + (z_{max} - z_{min})^2} \quad (3.1)$$

where $r_e$ = relative element size factor; which is being determined from the element distribution. Element distribution has five global levels as represented in table 3.7.

**Table 3.9.** Predefined value of $r_e$ (element distribution)

| **Element distribution** | **$r_e$** |
|---|---|
| Very Fine | 0.5 |
| Fine | 0.7 |

| | |
|---|---|
| Medium | 1.0 |
| Coarse | 1.5 |
| Very coarse | 2.0 |

The precise number of finite elements in the mesh depends on the geometry's shape and the local refinement parameters chosen. While other parts might not need such precision, places where significant stress concentrations or steep deformation gradients are anticipated should use a finer mesh. This scenario frequently occurs in models with edges, corners, or structural elements.

PLAXIS 3D allows each geometric object to be assigned a local coarseness factor, which governs element size relative to a target size defined by the element distribution parameter. For most objects, this factor defaults to 1.0; for structural elements and loads, it is set to 0.5, which halves the element size. Acceptable values range from 0.0625 (very fine) to 8.0 (very coarse). Values above 1.0 produce locally coarser meshes, while smaller values refine the mesh. The software automatically performs additional refinements around structural elements, loads, and prescribed displacements to ensure high mesh quality.

In the present analysis, fine meshing is applied near the soil–stone column interface to accurately capture stress and deformation behaviour. This refinement enables the detection of bulging failures under load. The mesh is progressively coarser toward the lateral boundaries and finer near the interface region.

### 3.12.6 Staged Construction and Calculations

After discretizing the composite ground, the initial groundwater level and equilibrium stresses are defined. This is usually done by positioning the phreatic line at the specified location. Since PLAXIS operates primarily with effective stress, this parameter is particularly important for undrained soil conditions. In geotechnical analysis, specifying initial stresses is essential, as they are influenced by both the soil's self-weight and its stress history. Usually, the coefficient of lateral earth pressure connects the initial vertical effective stress ($\sigma'_{v,0}$) to the initial horizontal effective stress ($\sigma'_{h,0}$):

$$\sigma'_{h,0} = K_0 \times \sigma'_{v,0}$$

Initial stresses can be created in PLAXIS 3D using the $K_0$ method, Gravity Loading, or the Field Stress option. The $K_0$ method was employed in this investigation because it takes the soil's loading history into consideration. Jaky's empirical formula is frequently used to estimate $K_0$ for regularly cemented soils:

$$K_0 = 1 - \sin\phi$$

By default, PLAXIS employs this formula. On the other hand, stresses that do not meet the Mohr-Coulomb failure criterion may result from very high or low $K_0$ values. In these situations, PLAXIS marks these stress locations as plastic by automatically reducing lateral stresses to meet the failure condition. The $K_0$ method uses the established $K_0$ value to compute horizontal stresses and the soil's self-weight to determine vertical stresses. Because this method does not generate shear stresses, it cannot ensure full stress equilibrium except for cases with horizontal surfaces, parallel soil layers, and a parallel phreatic level. For non-horizontal geometries, where shear stresses are needed for equilibrium, the $K_0$ procedure is not advised.

After establishing the initial stresses with the $K_0$ method, another phase was introduced where all model components—soil, stone columns, and geogrid—were activated. In the subsequent phase, the prescribed displacements and corresponding boundary conditions were applied, and the analysis was performed. Both unreinforced and reinforced stone columns were evaluated for deformation and failure using plastic analysis. Plastic analysis was chosen because it develops the stiffness matrix from the original, undeformed state of the reinforced ground and is well-suited for simulating elastic–plastic deformation without considering the dissipation of excess pore water pressure. The same modelling and analysis procedure was applied for a group of stone columns.

### 3.13 XRD and SEM Analyses

#### 3.13.1 General

By analyzing the diffraction patterns created when a powdered sample is subjected to X-rays, X-ray diffraction (XRD) is an analytical method used to ascertain the mineralogical content and crystalline structure of soils. The method is based on Bragg's Law, which connects the angle of diffraction and the incident X-ray wavelength to the distance between crystal lattice planes. Each mineral exhibits a characteristic set of diffraction peaks at specific angles, allowing precise identification and, in some cases, estimation of relative abundance.

In geotechnical studies, XRD is widely used for identifying clay minerals such as kaolinite, illite, and smectite, which influence the soil's plasticity, swelling potential, and engineering behaviour. The method is non-destructive, requires only a small quantity of material, and provides high accuracy for crystalline phases, although it is less effective for amorphous materials. XRD analysis in this study was employed to characterise the clay fraction and assess its potential impact on the mechanical behaviour of the tested soils.

By scanning a concentrated electron beam across a sample's surface, scanning electron microscopy (SEM), a high-resolution imaging method, can analyze the surface morphology and microstructure of materials, including soils. A variety of signals, including secondary electrons, backscattered electrons, and distinctive X-rays, are produced when the electrons interact with the specimen's atoms. These signals are then recognized and transformed into finely detailed images. SEM provides magnifications much higher than optical microscopes, enabling observation of particle shapes, sizes, arrangements, and fabric, as well as microcracks or cementation bonds. In geotechnical engineering, SEM is particularly valuable for studying clay particle orientation, pore structure, and the effects of soil treatment or stabilization at the microscale. SEM can also offer elemental composition information to supplement mineral identification from methods like X-ray diffraction (XRD) when paired with Energy Dispersive X-ray Spectroscopy (EDS). In this study, SEM was utilised to visualise the soil's microstructure and correlate observed features with its mechanical behaviour.

### 3.13.2 Process Used

In order to determine the crystalline minerals in the soil and those used to form columns, such as fly ash, stone dust, and iron dust, as well as the mix design of the granular column, an X-ray diffraction test was conducted using Bragg-Brentano in Bruker D8 advanced machines. A Jeol JSM-6610 LV operating in a very high vacuum was used for the SEM investigation. Both normal plane and cross-section view modes were used to gather the SEM pictures. In accordance with the resolution criteria, the SEM's operating voltage was 5 kV.

# CHAPTER 4

# RESULTS AND DISCUSSION

## 4.1 GENERAL

The main objective of this chapter is to compare the performance of encased stone columns with that of conventional (ordinary) stone columns. Both types of columns were installed in weak cohesive soil beds of identical properties. To assess their behaviour, single stone columns as well as column groups arranged in triangular, square, and hexagonal patterns were constructed and tested, with and without encasement. The study examined load–settlement responses for unreinforced columns and for those vertically encased with geosynthetics, both as individual units and in groups. Experimental results were analysed to determine variations in soil bearing capacity, and numerical analyses were carried out to validate these findings. In addition, to further understand the structural and mineralogical characteristics of the soil and reinforcing materials, tests using X-ray diffraction (XRD) and scanning electron microscopy (SEM) were performed.

## 4.2 EXPERIMENTAL RESULTS: FINDINGS FROM MODEL TESTS FOR SINGLE STONE COLUMN AND GROUP OF COLUMNS

### 4.2.1 Analysis of the load-settlement behaviour of a clay bed

To assess the load-settlement behavior of untreated clay without any reinforcement, a load test was first carried out. A hydraulic jack was used to apply the load, and a 50 mm settlement was used to calculate the ultimate load-carrying capability. For this reason, a load-settlement curve was plotted, as shown in Figure 4.1. According to the findings, under an applied load of 5.9 kN, the clay bed without a stone column showed a maximum settlement of 50 mm.

### 4.2.2 A single stone column used to strengthen a clay bed

The diameter D = 70 mm was used in the present investigation. A 300 mm diameter loading plate was utilized. The area of the stone column in relation to the surrounding soil is known as the area replacement ratio. In the current study, the percentage of Ar found in columns with 70 mm diameters was 7.09%. The load-settlement behavior of the floating stone column and ordinary end bearing is shown in Figures 4.2 and 4.3. The figure showed that the composite clay bed's load carrying capacity is increased when the soft clay bed is reinforced with regular stone columns.

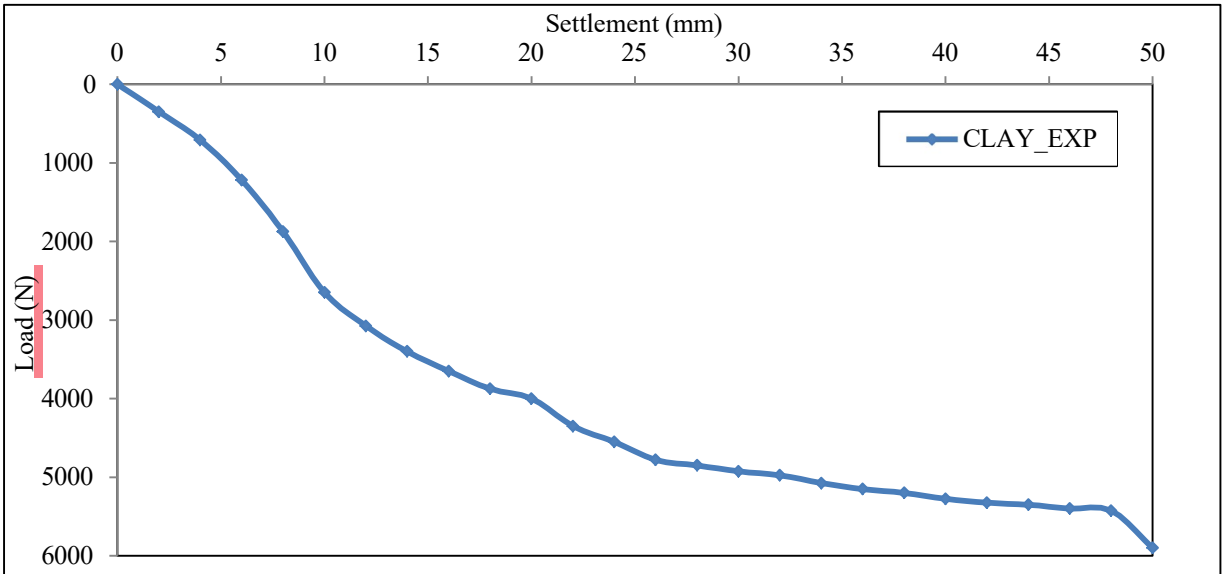


**Figure 4.1** Load-Settlement variation of clay bed without any reinforcement

For the unreinforced clay bed, the load at an ultimate settlement of 50 mm was 5.9 kN, which was increased to 7.2 kN for D = 70 mm for end bearing column and 6.5 kN for D = 70 mm for floating column when it comes to regular stone columns. Replacing a portion of soil with a column made up of column mix results in creating a stiff composite soil mass, which further increases the load carrying capacity. For D = 70 mm, the load capacity rises by using an OSC in soft clay. 22.03% for end bearing column and 10.77% for floating column, respectively.

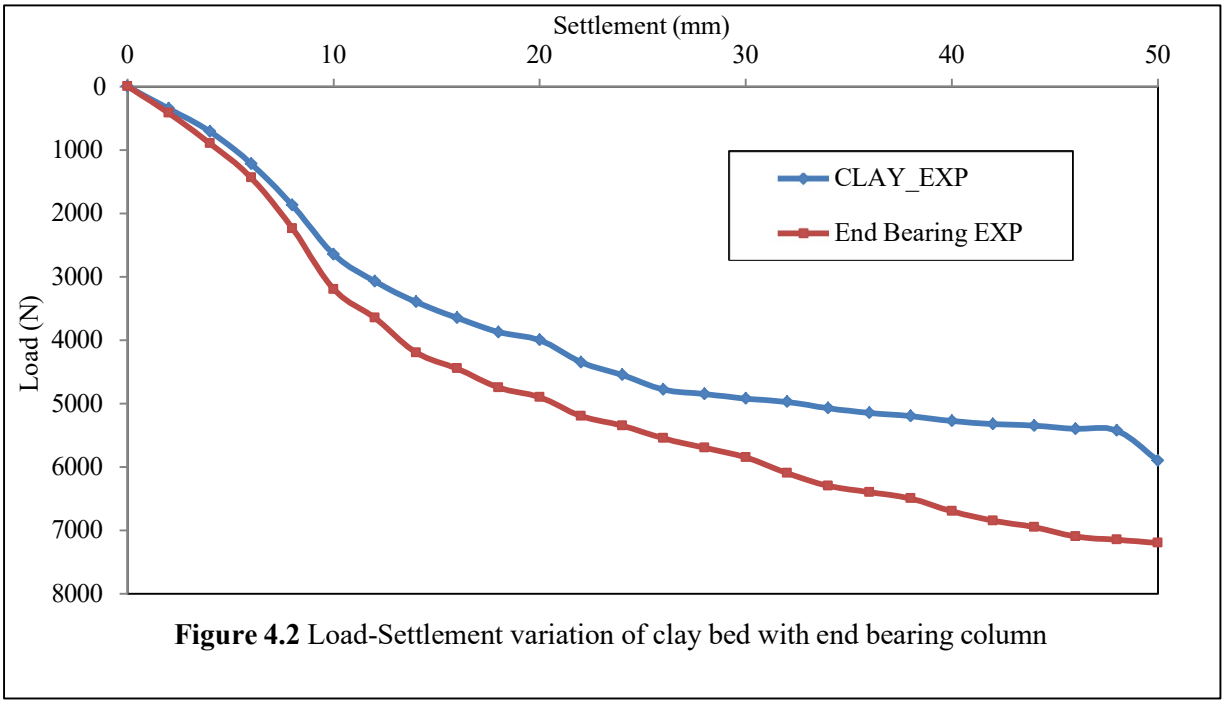


**Figure 4.2** Load-Settlement variation of clay bed with end bearing column

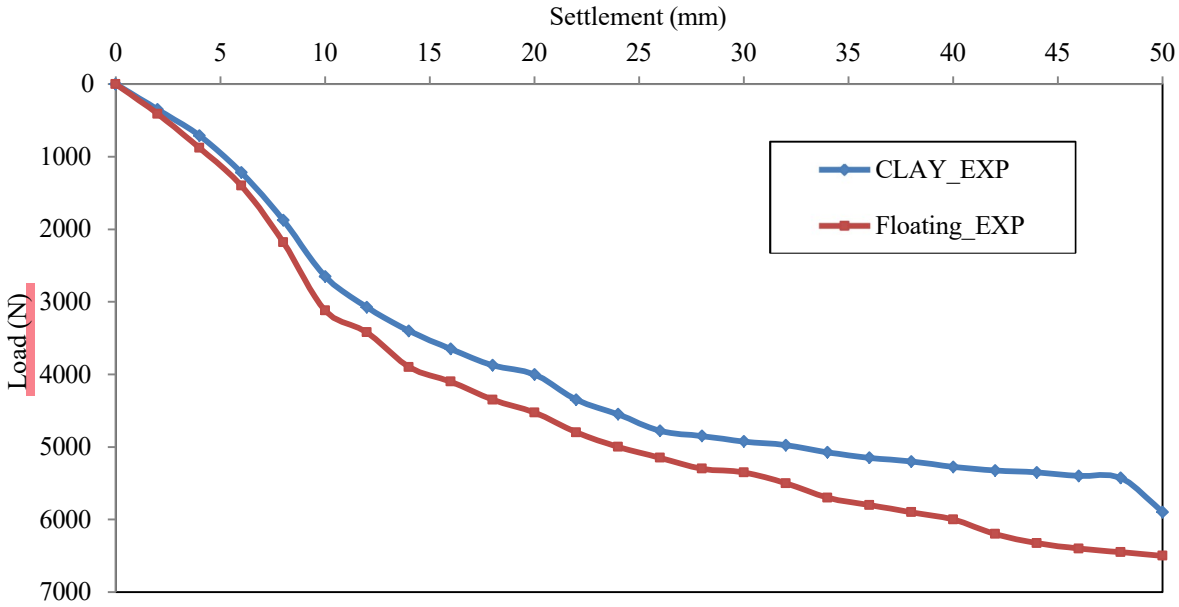


**Figure 4.3** Load-Settlement variation of clay bed with Floating column

### 4.2.3 Encased stone column for clay bed reinforcement: Single Stone Columnn

In very weak soil, ordinary stone columns mainly offer vertical load-bearing capacity but contribute little to lateral support, which can be problematic. To overcome this limitation, stone columns are enclosed with geosynthetic materials to provide lateral confinement. In this study, to investigate the impact of the stiffness of the encasement material for both end bearing and floating columns, two types of encasements (geotextile and geogrid) were applied to the column length.

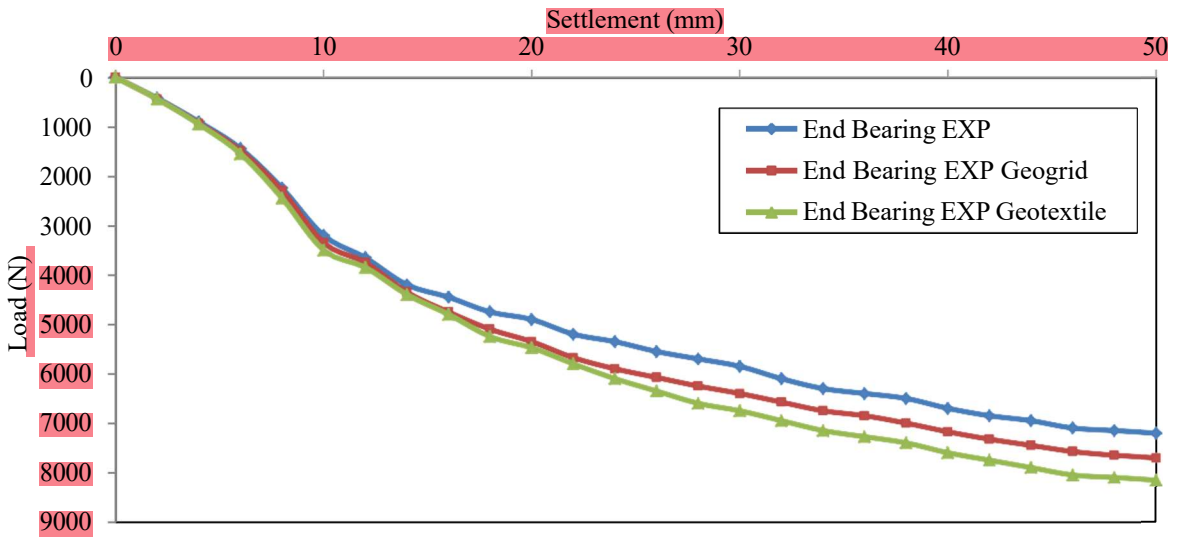


**Figure 4.4** Load-settlement variation of the end bearing stone column with varying encasement

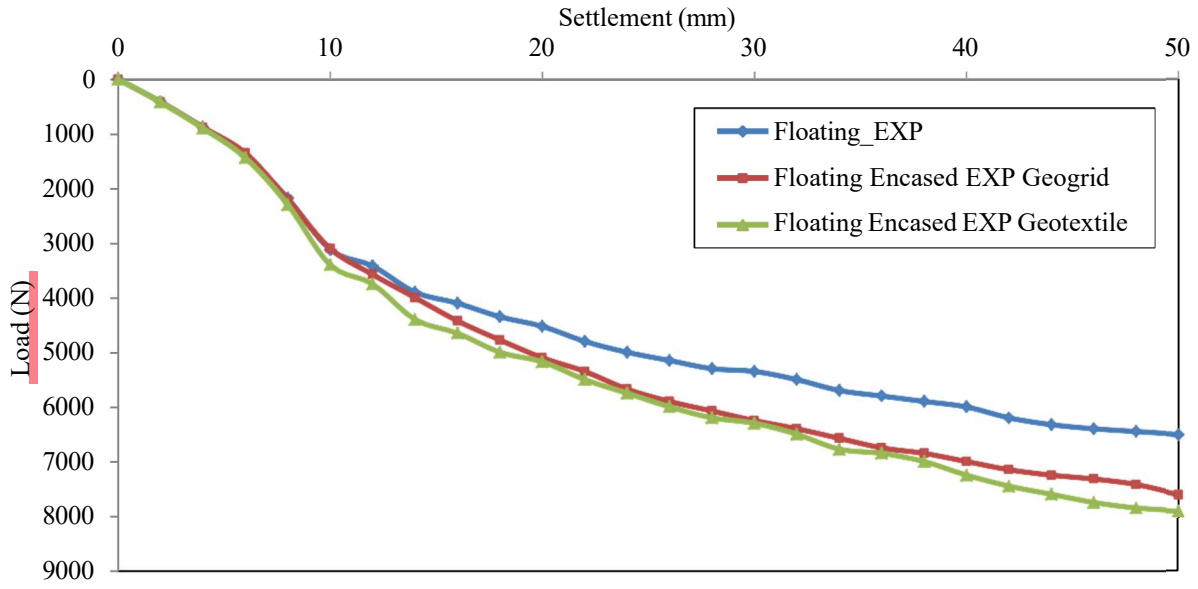


**Figure 4.5** Load-settlement variation of the floating stone column with varying encasement

27

Figure 4.4 and 4.5 shows the load-settlement behavior of enclosed stone columns for floating and end-bearing columns with D = 70 mm for both types of geosynthetics. For D = 70 mm, the load carrying capacity for end bearing column, end bearing column encased with geogrid and end bearing column encased with geotextile was 7.2, 7.7 and 8.15 kN respectively. Similarly for floating columns, floating columns encased with geogrid and floating columns encased with geotextile was 6.5, 7.6 and 7.9 kN respectively. The outcome showed that the soil mass's capacity to support loads increases when encasement is provided. Further the load capacity increases by 22%, 30% and 38% for end bearing columns and 10%, 28.81% and 33.90% respectively. The advantage of geosynthetic encasing is that it can improve granular column confinement. The encasement induces hoop stresses within the column material, which remain mobilised during loading and are not dissipated with time. This sustained confinement prevents excessive lateral deformation of the column and counteracts the expanding clay's propensity to push outward. As a result, the characteristic bulging failure commonly observed in unreinforced stone columns is significantly reduced. By controlling bulging, the encasement not only improves the overall stability of the column but also enables more efficient transfer of stress from the footing to the foundation stratum via the column. A comparison between the two types of encasement used in this study further revealed that geotextile performed better for single columns, primarily due to its finer pore size, which restricted the loss of fines during loading.

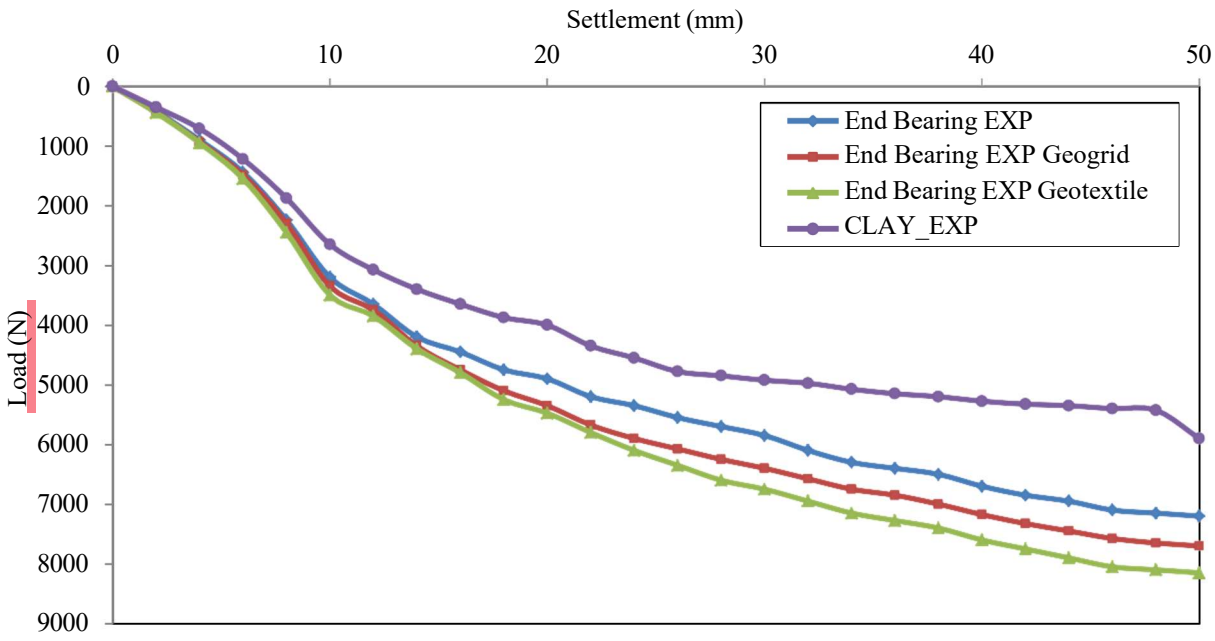


**Figure 4.6** Comparison graph of end bearing column with unreinforced soil and encasement provided.

The load–settlement response in figure 4.6 highlights the significant improvement achieved through the installation of end-bearing columns and their subsequent encasement with geosynthetics. The untreated expansive clay exhibited the lowest load capacity, sustaining only about 5.9 kN at an ultimate settlement of 50 mm. With the inclusion of an end-bearing granular column, the capacity increased to 7.2 kN, representing an improvement of approximately 22% over the virgin clay bed. Further enhancement was noticed when the column was covered in geogrid, where the load capacity rose to 7.7 kN, corresponding to a 31% increase compared to the unreinforced clay. The maximum improvement was recorded for the geotextile-encased column, which sustained 8.15 kN at 50 mm settlement, nearly 38% higher than the virgin soil and around 6% greater than the geogrid-encased counterpart. These results clearly demonstrate that geosynthetic encasement effectively increases lateral confinement, reduces bulging, and enhances load transfer, with geotextile proving to be more effective than geogrid for single end-bearing column configurations.

Figure 4.7, showed the floating column configuration demonstrated a considerable enhancement over the untreated expanding clay bed in terms of load-bearing performance. At an ultimate settlement of 50 mm, the virgin clay sustained only about 5.9 kN, whereas the installation of a floating column increased the capacity to 6.5 kN, representing a 10% improvement. Encasement further enhanced the behaviour, with the geogrid-encased floating

column carrying 7.6 kN, which is approximately 29% higher than the clay bed and 17% greater than the unencased floating column. Similarly, the geotextile-encased floating column achieved 7.9 kN, corresponding to a 34% improvement over the virgin soil and a 22% increase relative to the unencased floating column. These results highlight the effectiveness of geosynthetic encasement in mitigating bulging and enhancing confinement even for floating configurations. Moreover, the geotextile again outperformed the geogrid, owing to its superior fines retention capacity, thereby sustaining higher hoop stresses and enabling more efficient load transfer to the neighbouring soil.

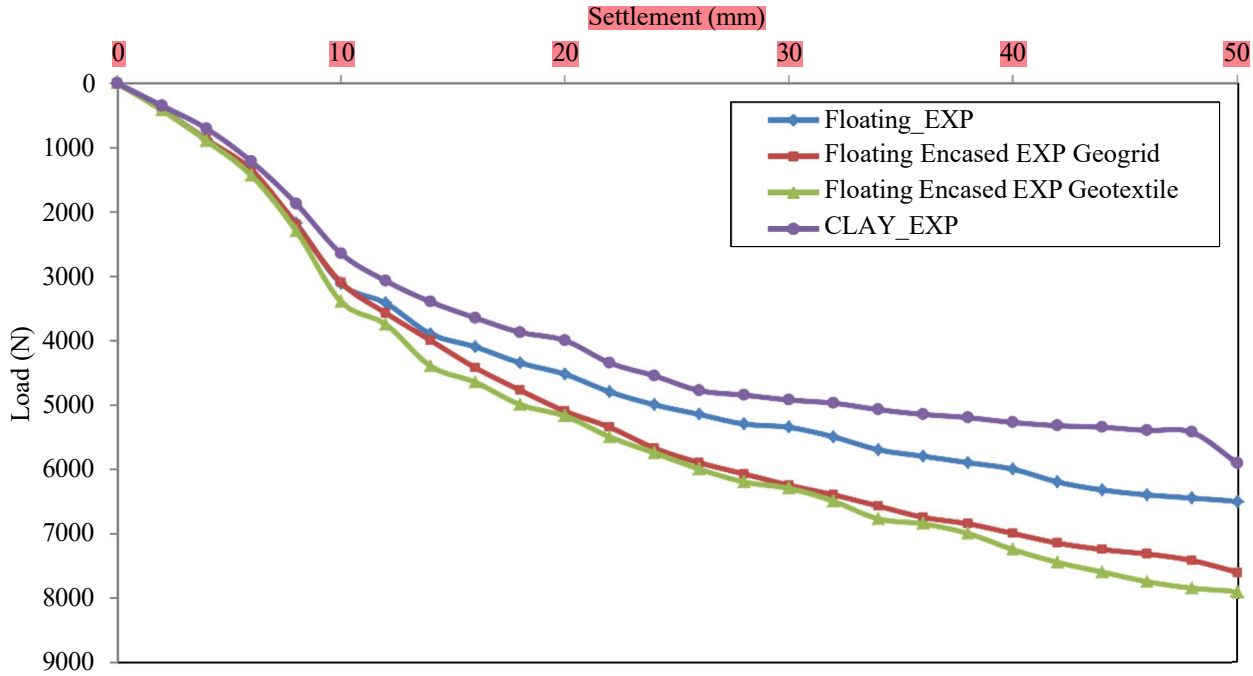


**Figure 4.7** Comparison graph of floating column with unreinforced soil and encasement provided.

### 4.2.4 Clay bed reinforced with ordinary stone column- Group of stone columns

Triangular pattern (3 stone columns), square pattern (4 stone columns) and hexagonal pattern (6 stone columns) were used for the group analysis with varying spacing(S)/diameter(D) ratio. The S/D ratio for triangle and square pattern was 2, 2 and for hexagonal pattern 3 was used for the analysis. Figure 4.8 and 4.9 depict the load-settlement behavior of a collection of stone columns constructed in square, triangle, and hexagonal patterns for varying S/D ratios for D = 50 mm, respectively. For a triangular pattern with a 50 mm settlement and S/D = 2, the ultimate load bearing capacity was determined to be 9.10 kN for end bearing columns and 9.6 kN for floating columns, respectively. For a square pattern with a 50 mm settlement and S/D = 2, the ultimate load bearing capability was determined to be 9.6 kN for end bearing columns and 8.10 kN for floating columns, respectively.

Similarly, for D = 50 mm, the ultimate load bearing capacity of hexagonal pattern for S/D = 3 was found as 7.9 kN for end bearing column and 7.3 for floating column respectively.

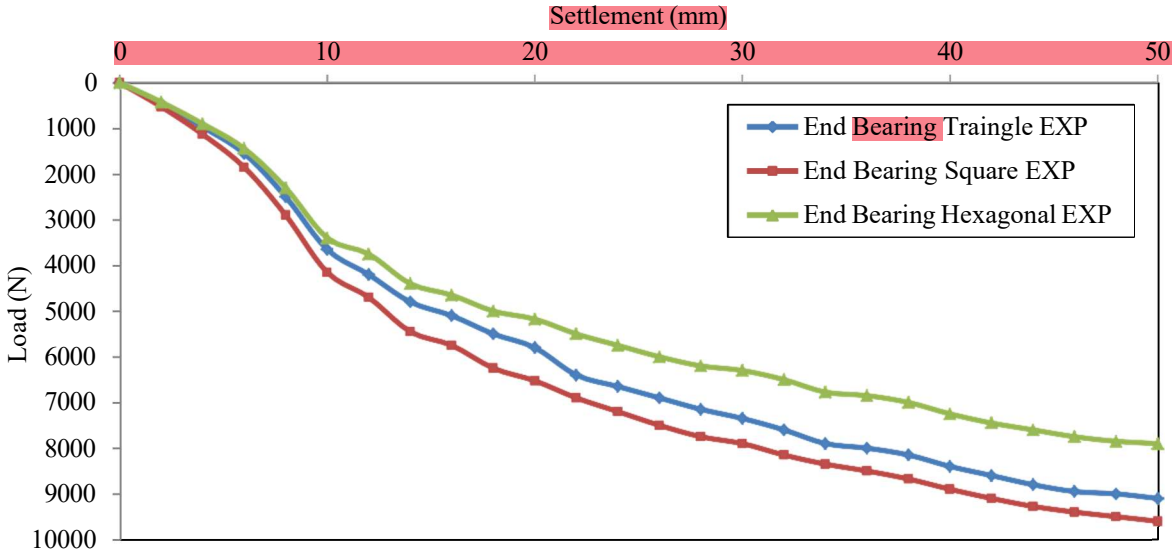


**Figure 4.8** Load settlement variations of different patterns for unencased end bearing columns

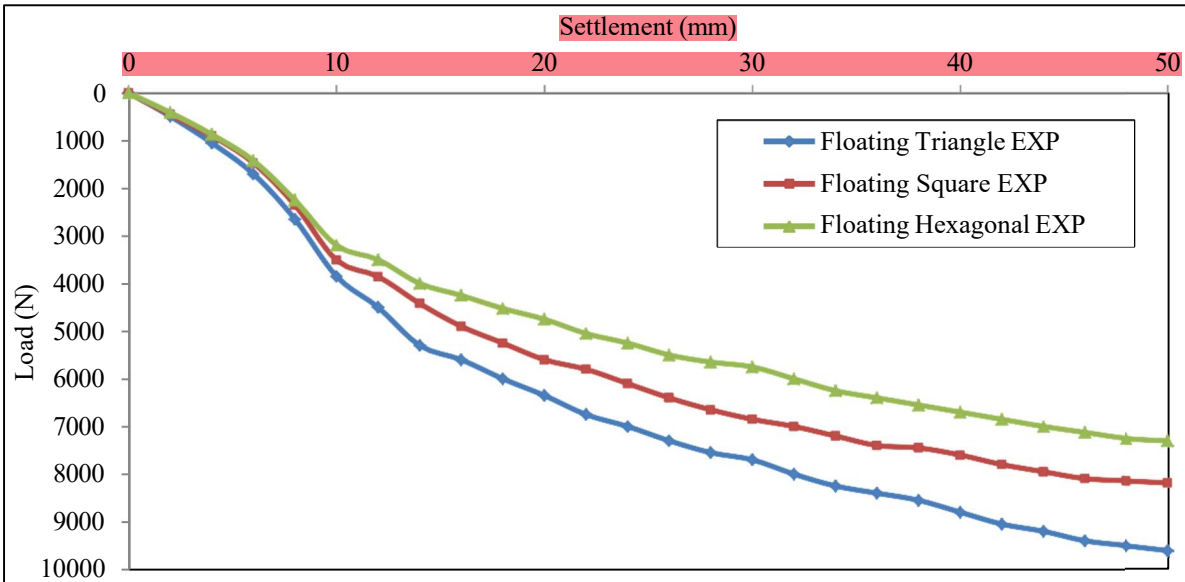


**Figure 4.9** Load settlement variations of different patterns for unencased floating columns

As shown in figure 4.8 and 4.9, Column arrangement's impact on load-settlement behaviour was evident from the group tests. For both end-bearing and floating conditions, the Triangular arrangement consistently demonstrated the highest load-carrying capacity, followed by the square arrangement, while the Hexagonal arrangement showed the least improvement. In end-bearing groups, the triangular configuration sustained greater loads due to its closer spacing and enhanced confinement, which allowed more efficient stress transfer to the rigid base. A similar trend was observed in floating groups, although their overall capacity was slightly lower than that of end-bearing groups because of the absence of a firm stratum. Nevertheless, the relative improvement achieved by adopting the triangular arrangement was more pronounced in floating columns, as the efficient stress distribution helped to offset the lack of end restraint. These results clearly emphasise the importance of optimising group geometry, with the triangular configuration offering the most effective arrangement for reducing settlement and enhancing stability in both end-bearing and floating column systems.

### 4.2.5 Clay bed reinforced with encased stone column- Stone Columns in Group

Similar to the single stone column analysis, for encased stone columns, group analysis was also carried out. Additionally, encasement was applied across the whole length of the column for both end bearing and floating columns in the group analysis. Additionally, for the analysis, both types of geosynthetics were employed and contrasted.

**1. Triangular**

The load-settlement behavior of end-bearing encased stone columns organized in a triangle pattern for S/D = 2 for D = 50 mm is shown in Figure 4.10. The load-settlement behavior of floating encased columns arranged in a triangle for S/D = 2 and D = 50 mm is similarly depicted in Figures 4.11. The maximum load bearing capability for end bearing encased stone columns with a triangular pattern for S/D = 2 was determined to be 9.2 kN for geogrid and 9.8 kN for geotextile, respectively, for D = 50 mm. For floating encased stone columns with a triangular design and S/D = 2, the ultimate load bearing capacity was determined to be 8.8 kN for geogrid and 9.2 kN for geotextile, respectively.

The results indicate that for D = 50 mm and S/D = 2 in triangular pattern, both end bearing and floating encased stone columns exhibit improved load–settlement performance with encasement. Among the end bearing columns, the ultimate load carrying capacity was higher for geotextile encasement (9.8 kN) compared to geogrid (9.2 kN), showing a 6.52% increase.

Similarly, for floating columns, geotextile also outperformed geogrid, providing a capacity of 9.2 kN against 8.8 kN, which corresponds to a 4.55% increase. Overall, geotextile encasement proved more effective than geogrid, and end bearing columns showed slightly higher load resistance compared to floating columns under identical conditions.

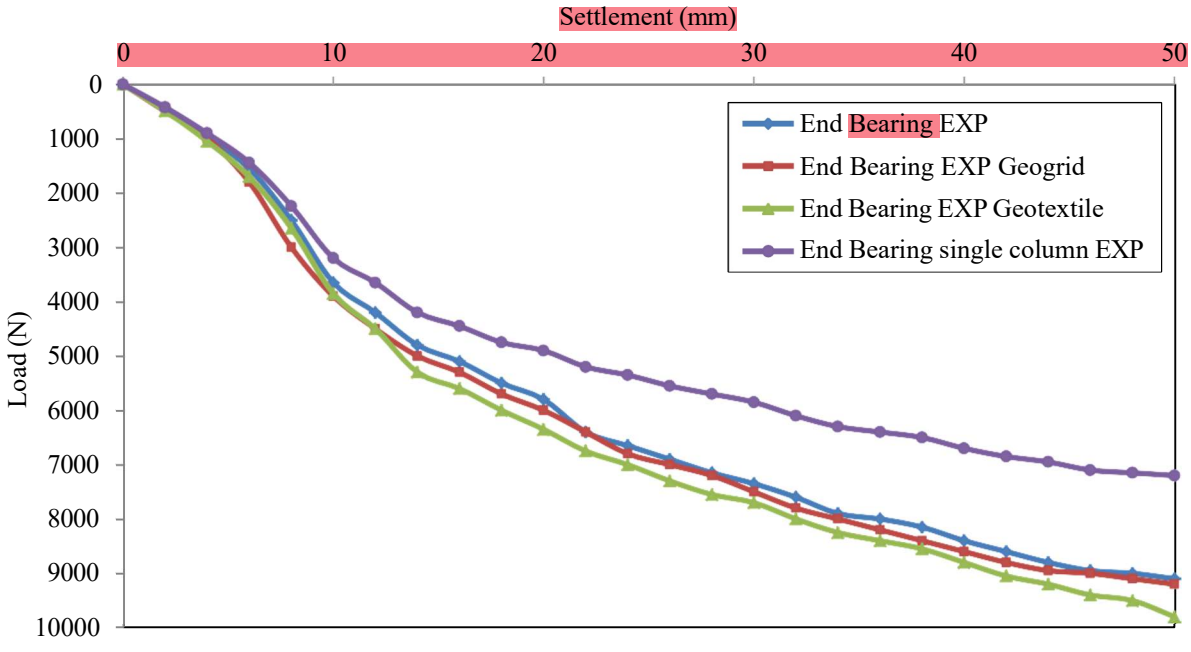


**Figure 4.10** Load settlement variations of triangular patterns for end bearing columns

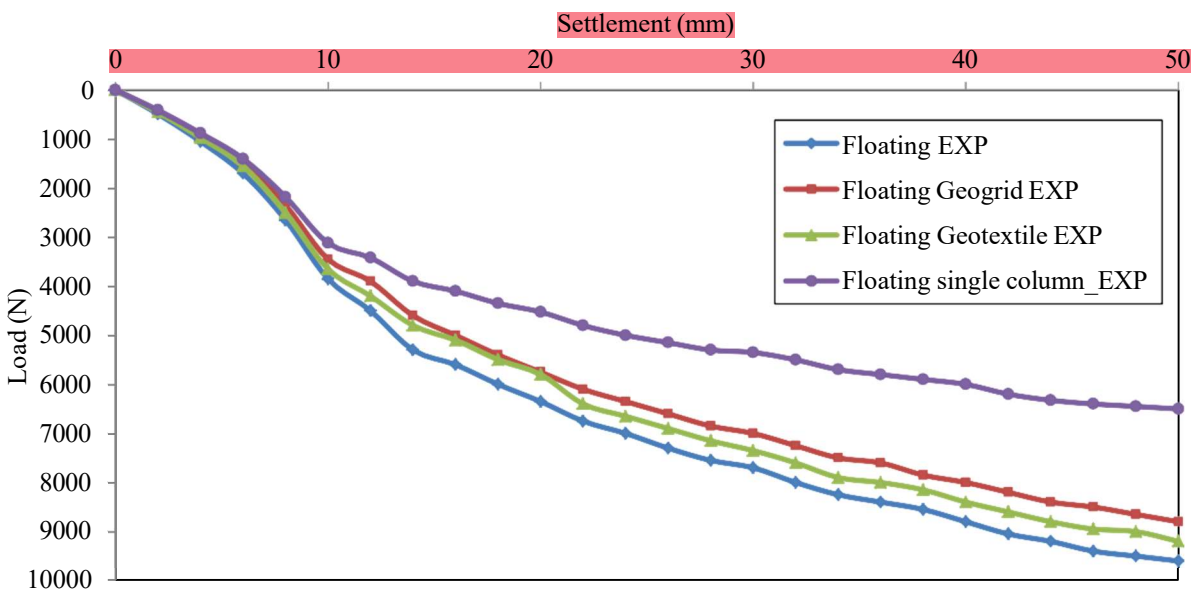


**Figure 4.11** Load settlement variations of triangular patterns for floating columns

**2. Square**

The load-settlement behavior of end bearing encased stone columns is shown in Figure 4.12, arranged in square pattern for S/D = 2 for D = 50 mm. Similarly, Figures 4.13 show the load-settlement behaviour of floating encased columns arranged in square pattern for S/D = 2 for D = 50 mm, respectively. The maximum load bearing capability for end bearing enclosed square-patterned stone columns with D = 50 mm and S/D = 2 was determined to be 8.60 kN for geogrid and 9.10 kN for geotextile, respectively. In a similar vein, floating encased stone columns' maximum load-bearing capacity of square pattern for S/D = 2 was found as 8.60 kN for geogrid and 8.70 kN for geotextile respectively.

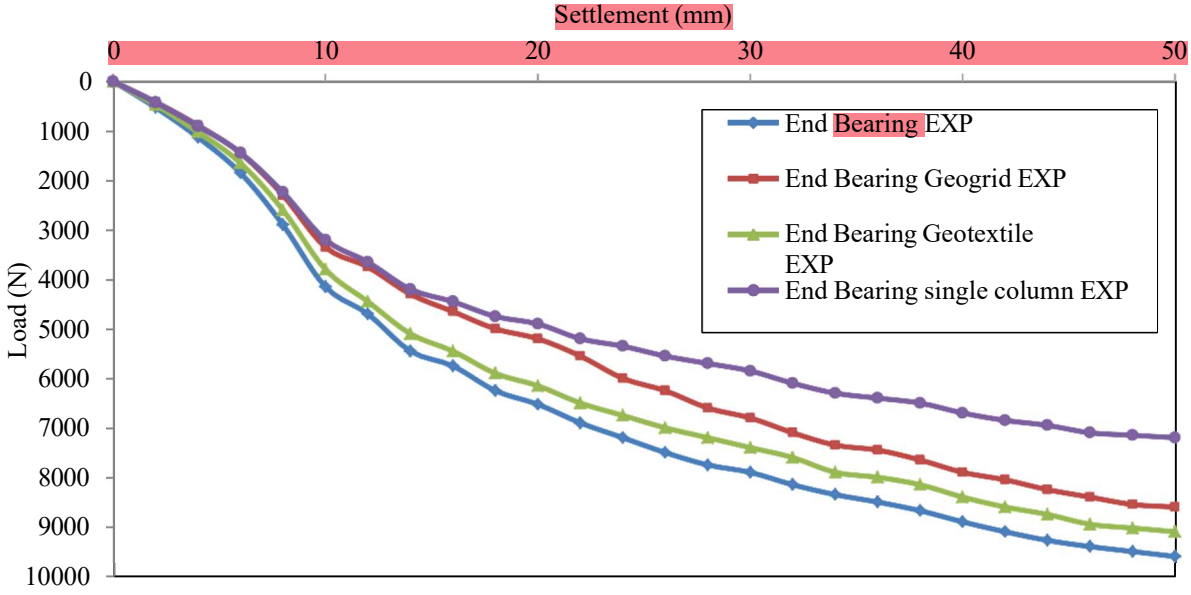


**Figure 4.12** Load settlement variations of square patterns for end bearing columns

The results for D = 50 mm and S/D = 2 in square pattern show that both end bearing and floating encased stone columns improved their load–settlement behaviour with geotextile compared to geogrid. For the end bearing arrangement, The final load carrying capacity was 5.81% higher with geotextile (9.10 kN) than with geogrid (8.60 kN). The final load capacity for floating columns was 8.70 kN with geotextile and 8.60 kN with geogrid, indicating a mere 1.16% improvement. Therefore, geotextile encasement worked better, especially for end-bearing columns, although it only slightly improved floating columns in a square design.

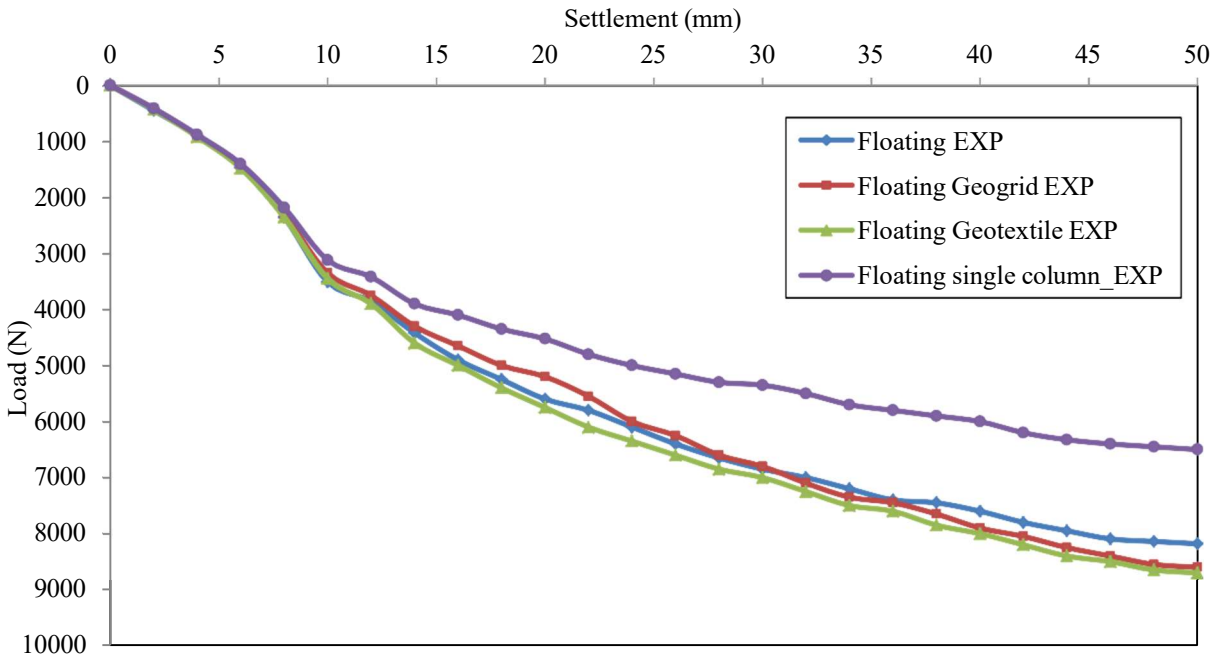


**Figure 4.13** Load settlement variations of square patterns for floating columns

### 3. Hexagonal

The load-settlement behavior of end bearing enclosed stone columns is shown in Figure 4.14. arranged in hexagonal pattern for S/D = 3 for D = 50 mm. Similarly, Figures 4.15 show the load-settlement behaviour of floating encased columns arranged in hexagonal pattern for S/D = 3 for D = 50 mm, correspondingly. The maximum load bearing capability for end bearing encased stone columns with a hexagonal pattern for S/D = 3 was determined to be 7.9 kN for geogrid and 8.5 kN for geotextile, respectively, for D = 50 mm. Similarly, for floating encased stone columns with a hexagonal design and S/D = 3, the ultimate load bearing capability was determined to be 7.9 kN for geogrid and 9.1 kN for geotextile.

The results for D = 50 mm and S/D = 3 in hexagonal pattern indicate that both end bearing and floating encased stone columns exhibited higher load–settlement performance with geotextile compared to geogrid. For the end bearing arrangement, the ultimate load carrying capacity was 8.5 kN with geotextile and 7.9 kN with geogrid, showing a 7.59% increase. When floating columns are included, the maximum load capacity was 9.1 kN with geotextile against 7.9 kN with geogrid, corresponding to a 15.19% increase. Hence, geotextile encasement provided notable improvement in both cases, with the effect being more pronounced in floating stone columns.

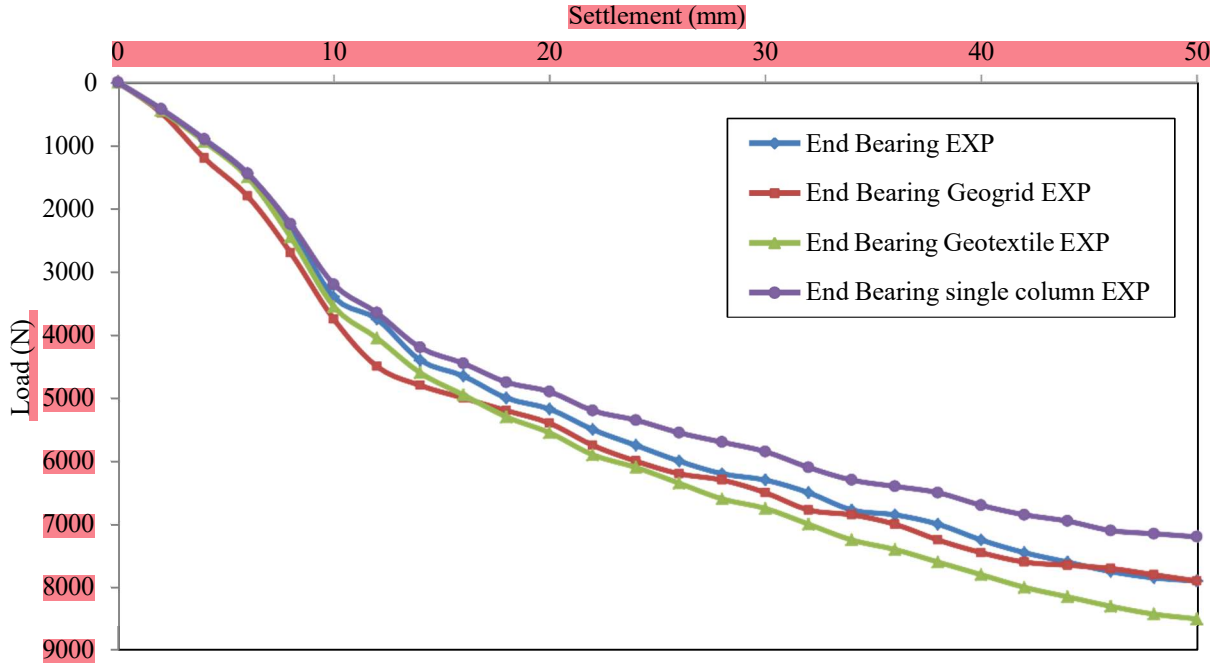


**Figure 4.14** Load settlement variations of hexagonal patterns for end bearing columns

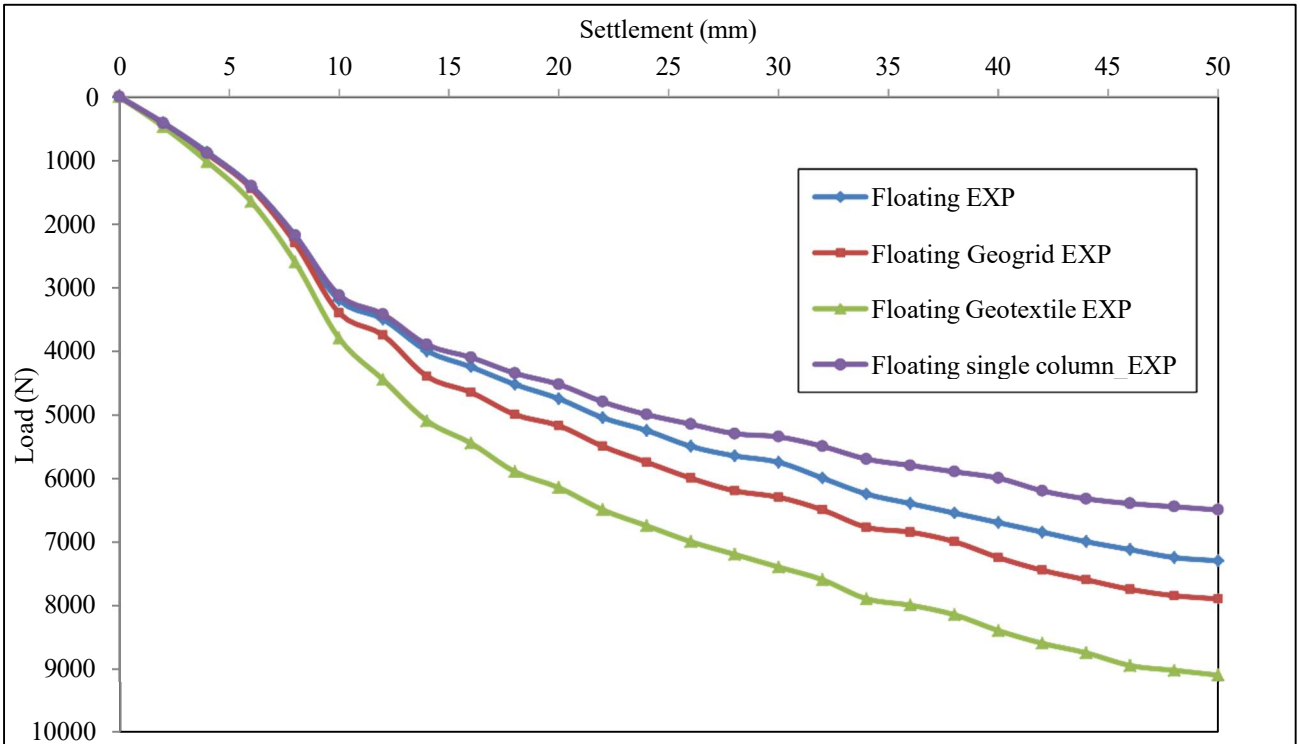


**Figure 4.15** Load settlement variations of hexagonal patterns for floating columns

The comparison of group arrangements with single columns clearly demonstrates the advantage of pattern configuration and encasement. For single columns, the load carrying capacity was limited, and failure was governed mainly by bulging in end bearing columns and punching in short floating columns. In group arrangements, however, the ultimate load carrying capacity improved due to mutual confinement between adjacent columns, which restricted excessive lateral deformation. The comparative study of triangular, square, and hexagonal patterns for D = 50 mm revealed that geotextile encasement consistently outperformed geogrid in enhancing the behavior of end-bearing and floating stone columns under stress. When arranged in a triangle, geotextile outperformed geogrid by 6.52% for end-bearing columns and 4.55% for floating columns. The improvement in the square pattern was 5.81%. for end bearing columns and only 1.16% for floating columns, indicating a relatively marginal effect. In contrast, the hexagonal arrangement showed the improvement, with 7.59% for end bearing and a pronounced 15.19% for floating columns. Among the patterns, triangular and hexagonal arrangements showed superior performance compared to the square pattern, with geotextile encasement consistently enhancing the load capacity beyond that of geogrid. Overall, group encased columns, particularly in triangular and hexagonal configurations, not only outperformed their geogrid counterparts but also exhibited substantial gains over single columns, highlighting the combined benefits of encasement and group action.

### 4.3 Column exhumation

After stress tests were finished, column exhumation was done to gain a better understanding of the stone columns' failure process. The surrounding soil was carefully removed to expose the stone column, which allowed direct observation of its deformation pattern. The exhumation revealed noticeable bulging of the column, confirming it as the predominant mode of failure under vertical stress because the surrounding clay's lateral confinement is insufficient. This visual evidence complemented the load–settlement response obtained during testing and provided a clearer understanding of the stress redistribution and interaction between the neighboring soil and the column.

Two experimental findings about the failure mechanism of stone columns under load are displayed in figure 4.16. The image on the left figure 4.16 (a) depicts an extracted stone column after load testing, where bulging of the column can be clearly seen. The sketched outline highlights this bulging, which is a common failure mode of stone columns under vertical loading. It shows lateral expansion of the column as it deforms outward as a result of applied pressure, reflecting the mobilization of lateral stresses within the surrounding clay

soil. The image on the right figure 4.16 (b) presents the surface cracks in the surrounding clay bed during loading. The arrows point to the formation and propagation of cracks radiating outward from the loaded area, which highlight the redistribution of stresses and the progressive failure of the clay matrix around the column. These observations confirm that, apart from bulging, surface cracking is also a visible manifestation of failure. Overall, Figure (a) illustrates the stone column's bulging failure, and Figure (b) depicts the surrounding soil's surface cracking, both of which clearly highlight the stress response and failure processes during the load-settlement tests.


**Figure 4.16** (a) Exhumed single column showed bulging failure; (b) failure cracks developed on the bed.

The failure mechanism of stone columns that experience punching failure is shown in Figure 4.17. As shown in Figure 4.17 (a), a distinct bulb formation is observed at the base of the column after exhumation, which is a characteristic sign of punching failure where the column penetrates into the underlying soil mass instead of undergoing bulging. Figure 4.17 (b) shows the surface condition during loading, where visible cracks have developed around the loaded area as a result of the punching action. These cracks indicate the gradual breakdown of the clay bed and the transfer of forces to the surrounding soil. Together, these observations confirm punching as the governing failure mechanism in this case, characterized by bulb development at the column base and surface cracking in the clay.

The exhumation studies revealed that the way stone columns fail is dependent on their type. For end bearing columns, bulging was identified as the predominant failure mechanism.


**Figure 4.17** (a) Bulb is developed at the base of the column due to punching failure; (b) cracks developed at the surface due to punching.

In this instance, the column's outward displacement and the corresponding surface fissures demonstrated lateral expansion along its length as a result of inadequate confinement from the surrounding clay. In contrast, floating columns primarily failed by punching, as indicated by the formation of a bulb because of downward penetration into the underlying soil at the column's base. This was accompanied by the development of cracks concentrated around the loaded area. Hence, bulging is characteristic of end bearing columns, while punching is more common in floating columns, highlighting the variation in load transfer and soil–column interaction mechanisms.

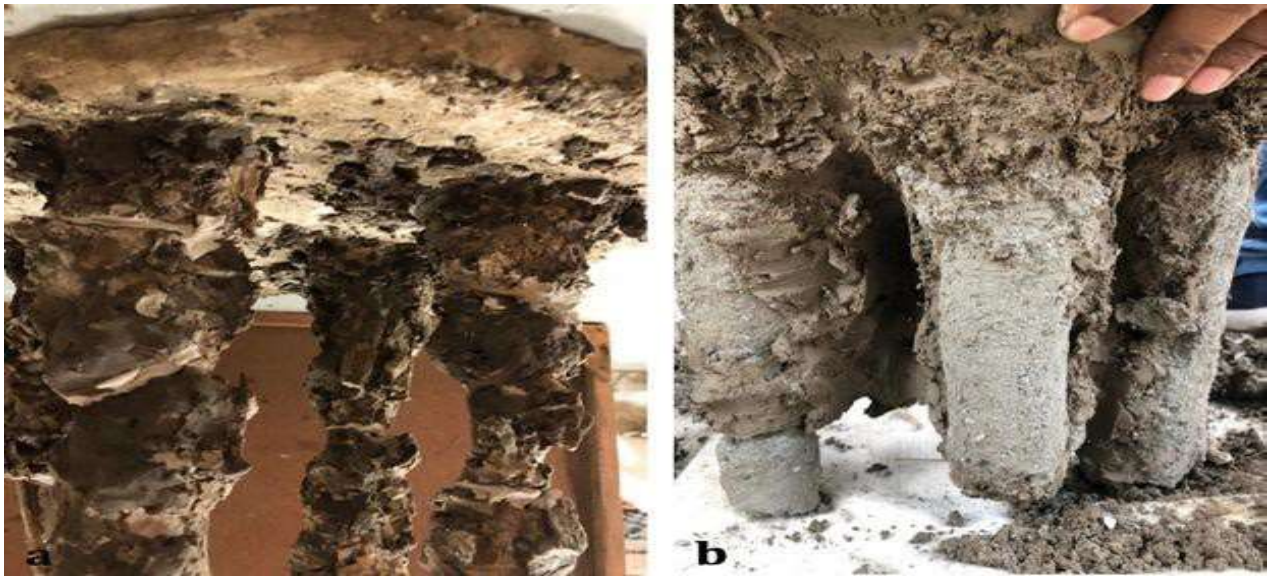


**Figure. 4.18**: (a) Exhumed square pattern column; (b) exhumed hexagonal column.

Figure 4.18 shows the exhumation of group stone columns after load testing. In Figure 4.18 (a), the columns are observed after removal of the overlying soil, clearly showing the way adjacent columns interact with one another. The protrusion of individual columns along their length can be noticed, which indicates lateral deformation due to the applied vertical loading. In Figure 4.18 (b), a closer view of the group of columns is presented, highlighting the reduced lateral expansion as a result of group confinement. The presence of surrounding columns restricts excessive bulging of individual columns consequently; the group system performs better and is more stable than single columns. These observations confirm that stone columns in group arrangement not only experience bulging but also benefit from mutual confinement, which enhances their overall load carrying capacity.

The overall results highlight that the arrangement pattern of stone columns is crucial in controlling their load-settlement behavior and failure mechanism. For the triangular pattern, higher load carrying capacities were recorded, particularly with geotextile encasement, and exhumation revealed pronounced bulging controlled by mutual confinement among columns. In the square pattern, the load capacity was slightly lower compared to the triangular pattern, with exhumed columns showing noticeable bulging due to relatively less confinement. The hexagonal pattern exhibited comparatively better confinement and interaction among columns, as observed during exhumation, resulting in more uniform deformation and improved stability. Overall, the triangular and hexagonal arrangements performed better than the square pattern, with geotextile encasement consistently enhancing performance across all configurations.

The comparison between individual and collective stone columns clearly demonstrates the beneficial effect of group action on load–settlement performance. In single column tests, failure was primarily governed by bulging or punching, depending on the column type, and lateral deformation was more pronounced due to limited confinement from the surrounding soil. In contrast, exhumation of group columns, revealed reduced bulging and more uniform deformation. This improvement is explained by the mutual confinement that neighboring columns provide, which limits excessive lateral expansion and more efficiently distributes the applied stress. As a result, group columns are more stable than single columns and increase the overall load carrying capability.

## 4.4 NUMERICAL RESULTS: INDIVIDUAL STONE COLUMN and COLLECTIVE STONE COLUMNS

### 4.4.1 Validation

The load-settlement response seen in Murtaza and Samadhiya's model testing was simulated in order to validate the numerical models [35]. They examined the behavior of individual stone columns immersed in soft clay through laboratory experiments based on the unit cell idea. Columns with diameters of 75 mm and 90 mm were tested under two different loading scenarios: (a) stress applied solely to the column and (b) loading applied throughout the full unit cell area. Conditions for both end-bearing and floating columns were investigated.

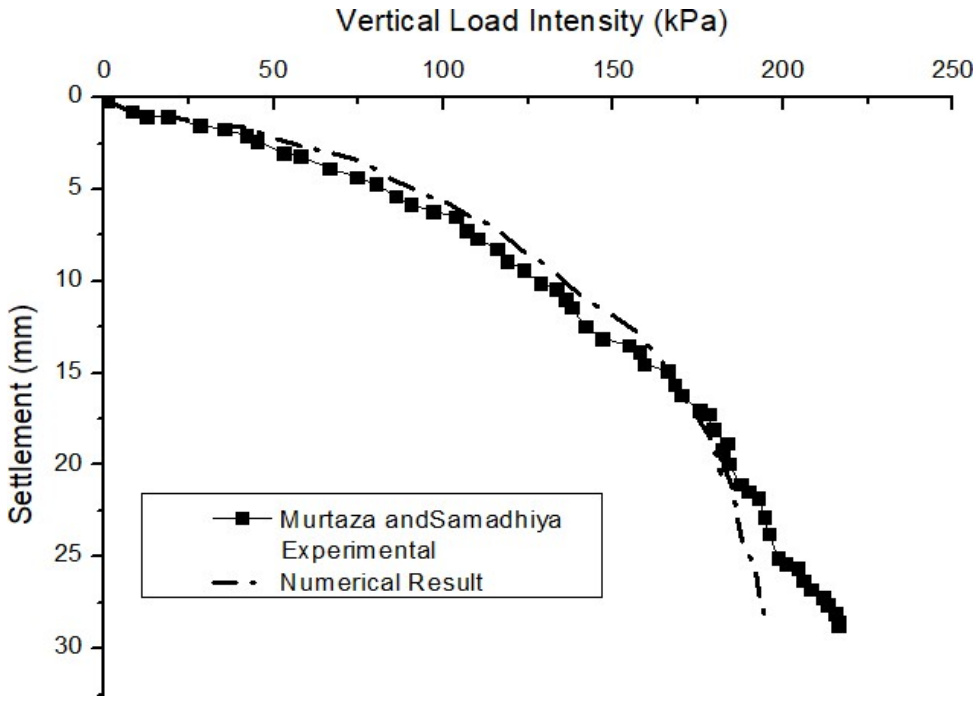


**Figure 4.19**. Comparing the end bearing column's vertical load intensity settlement behavior

The situation of column area loading for both end-bearing and floating conditions was the special focus of validation in the current study. One column measuring 525 mm in length and 75 mm in diameter was taken into consideration. A geotextile with a tensile strength of 4.4 kN/m was used to cover the column. The material properties used in the numerical model were in line with what Murtaza and Samadhiya [35] had reported. The vertical load–settlement response of end-bearing granular piles from the current work is contrasted with the experimental findings in Figure 4.19.

The comparison shows that settlement differed by less than 3% in most cases, with a maximum variation of about 15% occurring at settlements between 20–30 mm. These findings show that the suggested model closely matches experimental results, demonstrating the modeling approach's applicability for approximating the behavior of soft clay reinforced with enclosed stone columns.

### 4.4.2 Examination of a clay bed's load-settlement behavior

The load-settlement behavior of an unreinforced clay bed was assessed numerically. The load–settlement response of untreated soft clay is presented in Figure 4.35. At an ultimate settlement of 50 mm, the clay bed exhibited a load-carrying capacity of 5.4 kN.

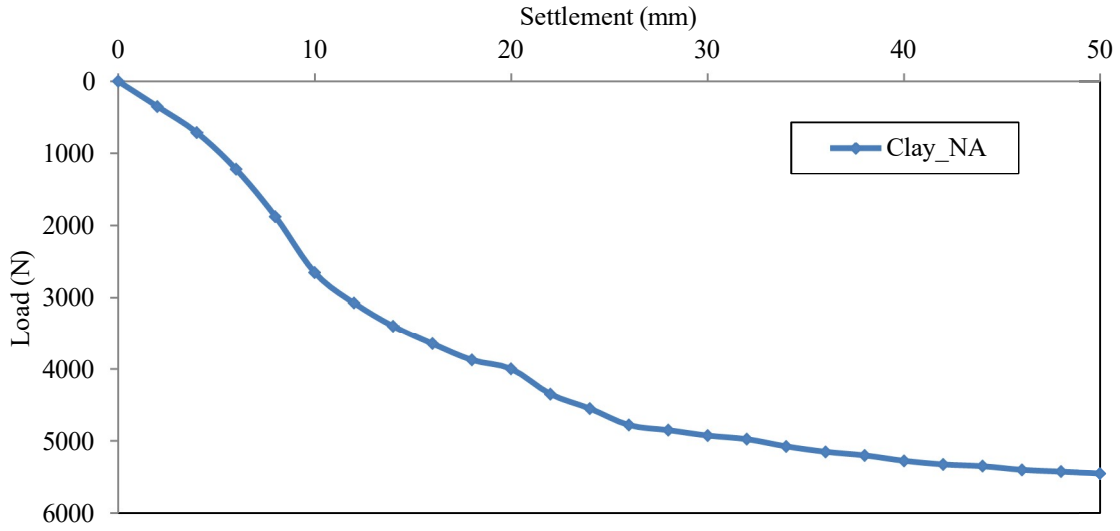


**Figure 4.20** Load-Settlement variation of clay bed without any reinforcement

### 4.4.3 Clay bed reinforced with ordinary stone column- Single Stone Column

The numerical analysis was conducted using a stone column with a diameter of 70 mm, much like in the experimental inquiry. A 300 mm diameter loading plate was utilized. In the current study, the proportion of Ar found in columns with a diameter of 70 mm was 7.09%. The load-settlement behavior of the floating column and regular end bearing stone column is shown in Figures 4.21 and 4.22. For the unreinforced clay bed, the load at an ultimate settlement of 50 mm was 5.4 kN, which was increased to 7.15 kN for end bearing column, corresponding to an increase of approximately 32.41% compared to the unreinforced

bed and 6.30 kN in the case of floating stone column analysed numerically which represents an enhancement of about 16.67%. The load carrying capacity of the composite clay bed is increased when the soft clay bed is reinforced with regular stone columns, a tendency that is similar to that shown in the experimental results.

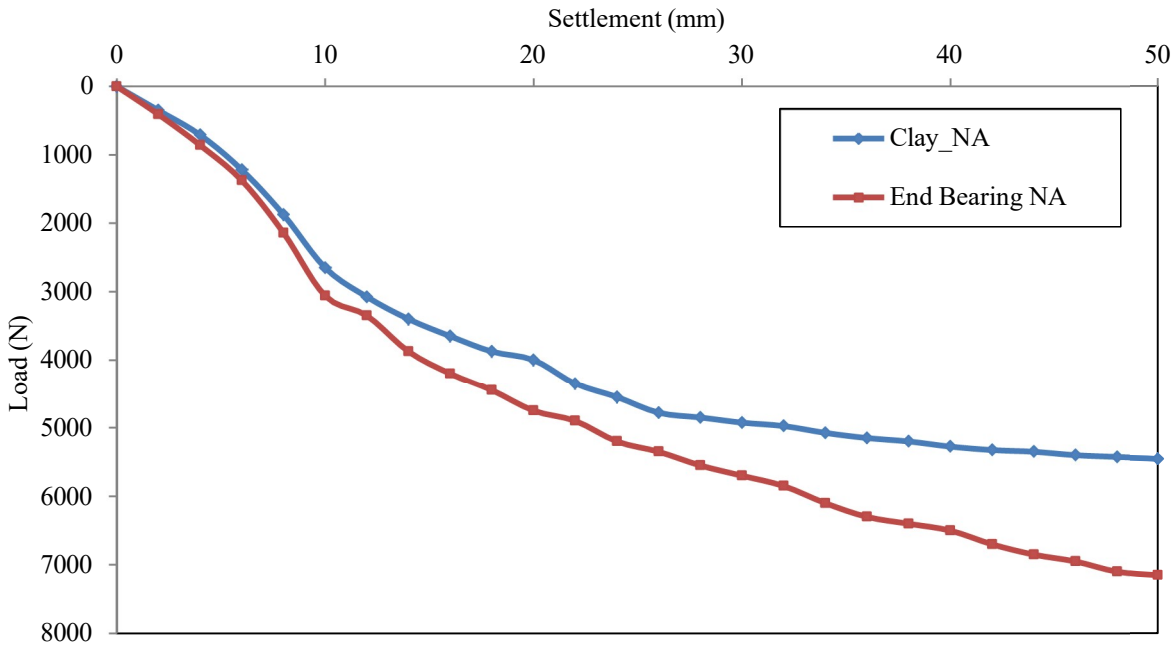


**Figure 4.21** Load-Settlement variation of clay bed with end bearing stone column

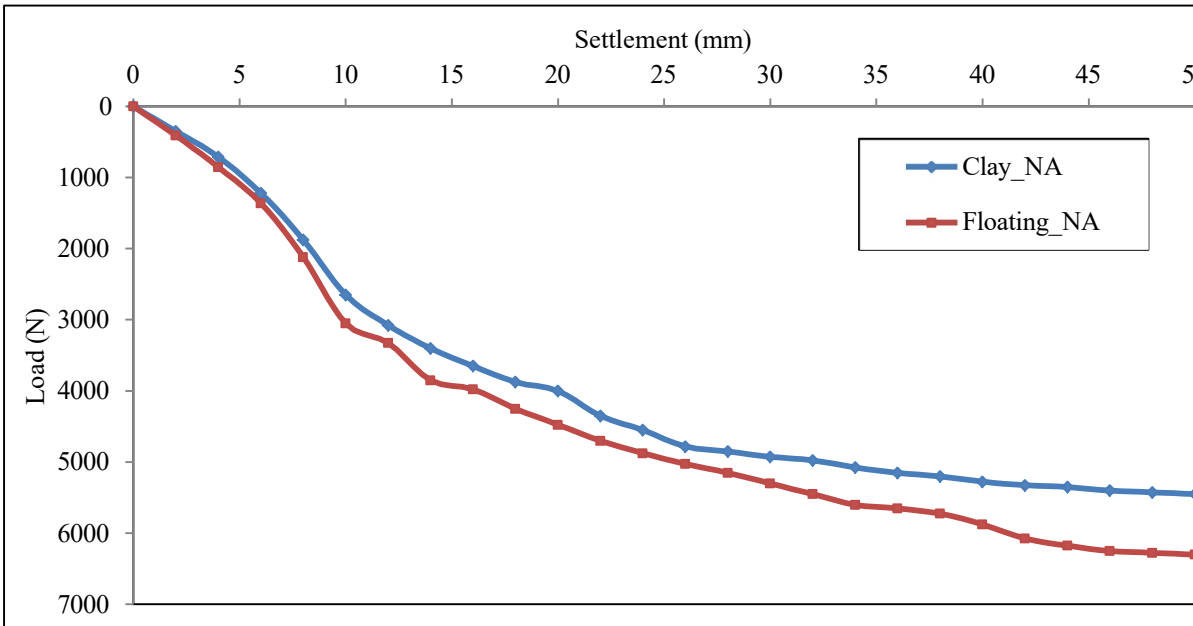


**Figure 4.22** Load-Settlement variation of clay bed with floating stone column

The results show that the addition of stone columns significantly increased the composite clay bed's load-carrying capacity, with the end bearing column outperforming the floating column. The trend found is in line with the experimental study, confirming that stone columns are useful for enhancing the strength and settlement response of soft clay soils.

### 4.4.4 Clay bed reinforced with encased stone column- individual Stone Column

Similar to the experimental analysis that employed two types of geosynthetics to understand the behavior of the encased stone column, the numerical analysis also employed geogrid and geotextile to ascertain the behavior of the composite soil bed. Both end bearing and floating columns were subjected to the analysis.

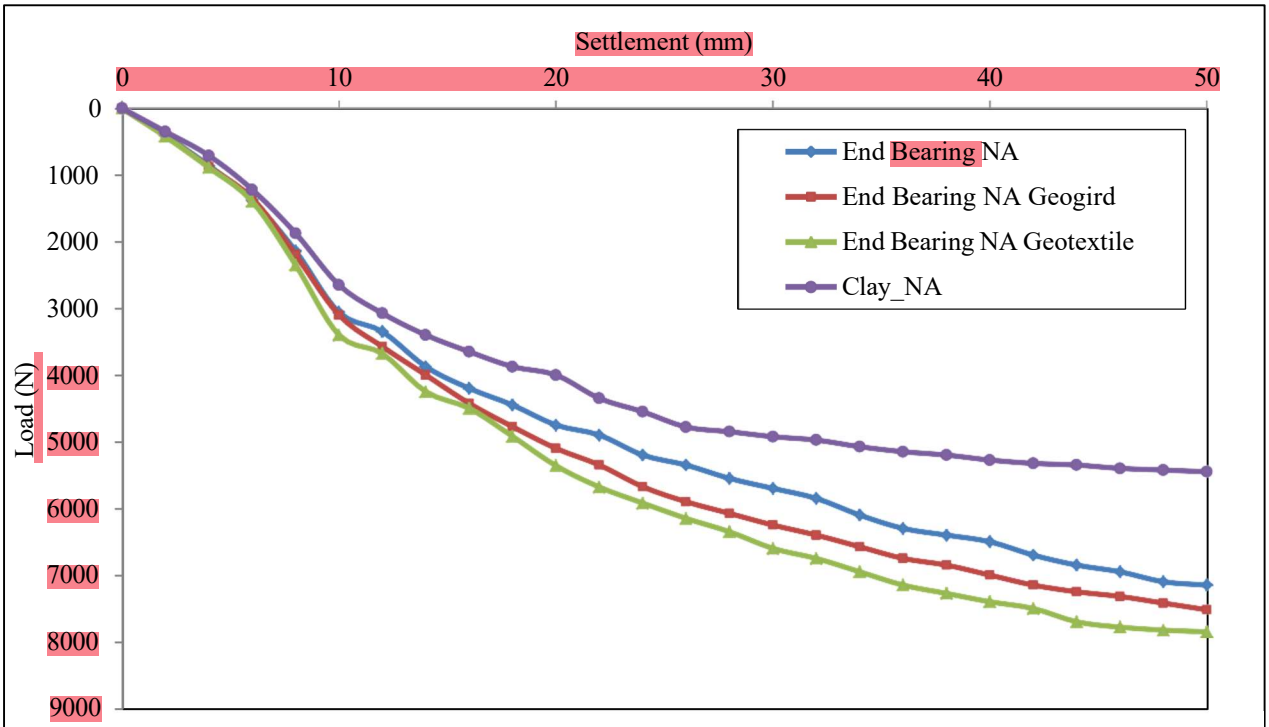


**Figure 4.23** Load-settlement variation of the end bearing stone column with varying encasement

The load-settlement behavior of enclosed stone columns for end bearing and floating columns with D = 70 mm for both geosynthetics is shown in Figures 4.23 and 4.24. The load carrying capability for the unreinforced clay bed was found to be 5.4 kN at an eventual settlement of 50 mm. The strength of the composite ground was greatly increased by the addition of stone columns. For end bearing columns, the load carrying capacity increased to 7.15 kN, representing an improvement of 32.41% over the unreinforced bed. Further enhancement

was achieved by encasement, where end bearing columns reinforced with geogrid and geotextile exhibited capacities of 7.52 kN and 7.85 kN, corresponding to 39.26% and 45.37% improvements, respectively. Similarly, floating columns also improved the capacity to 6.30 kN (16.67% increase), while geogrid and geotextile encasement raised the values to 7.25 kN and 7.45 kN, giving 34.26% and 37.96% improvements. These results highlight that column encasement with geosynthetics, particularly geotextile, provides substantial gains in load carrying performance, with end bearing columns showing superior improvement compared to floating columns.

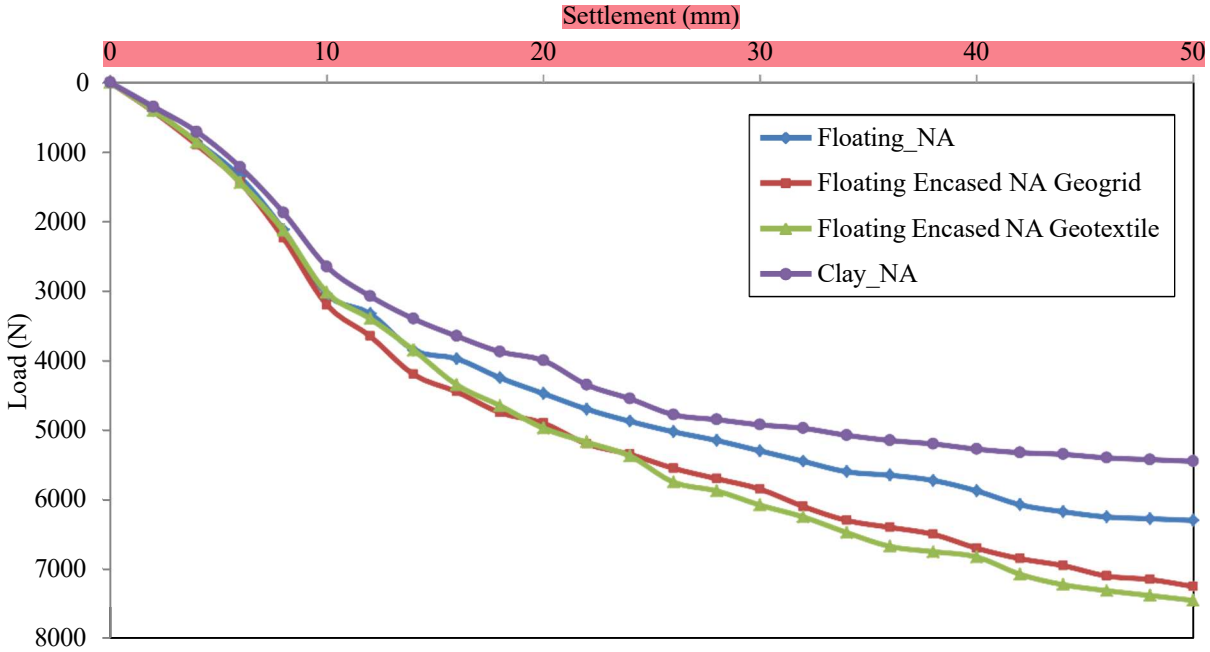


**Figure 4.24** Load-settlement variation of the floating stone column with varying encasement

The untreated clay bed demonstrated the lowest load carrying capacity and the highest settlement, indicating its poor performance under applied loads, according to the load–settlement response of both end bearing and floating stone columns. Because of the direct load transfer to the firm stratum, end-bearing columns outperformed floating ones, and the addition of stone columns greatly improved the behavior. Further enhancement was observed with geosynthetic encasement, where both geogrid and geotextile provided additional confinement, leading to higher load resistance and reduced settlement. Between the two, geotextile encasement consistently outperformed geogrid, demonstrating greater efficiency in restricting lateral bulging of the column. The greatest load carrying capacity was generally demonstrated by end-bearing stone columns with geotextile encasement, while floating stone

columns with geogrid encasement offered comparatively lower but still notable improvement over untreated clay. This confirms that reinforcement not only increases the stiffness of the composite ground system but also ensures more reliable and durable performance under loading conditions.

The displacement contours of different stone column configurations highlight the distinct deformation patterns under loading. Regarding the Ordinary Stone Column (OSC) (Figure 4.25 a), the displacement is uniformly distributed along the column, with the magnitude being the least among all configurations. This indicates better confinement and lower lateral bulging, thereby ensuring improved stability of the column within the clay bed.

39 For the End Bearing Column (Figure 4.25 b), The column's center zone is where the bulging phenomena is most noticeable. Effective load transfer to the underlying firm stratum is achieved by the column; however, due to the soft clay surrounding it, a significant lateral displacement occurs in the bulging zone. This behavior confirms that end bearing columns are more effective in enhancing load capacity but remain vulnerable to bulging unless encased with reinforcement.

In contrast, the Floating Column (Figure 4.25 c) shows pronounced settlement and displacement near the bottom portion of the column. Since it does not rest on a firm stratum, the column depends primarily on skin friction for load transfer. This leads to a concentration of stresses near the tip and results in higher deformation compared to the other two cases. Consequently, floating columns are less efficient in reducing settlement and require reinforcement or group installation for improved performance.

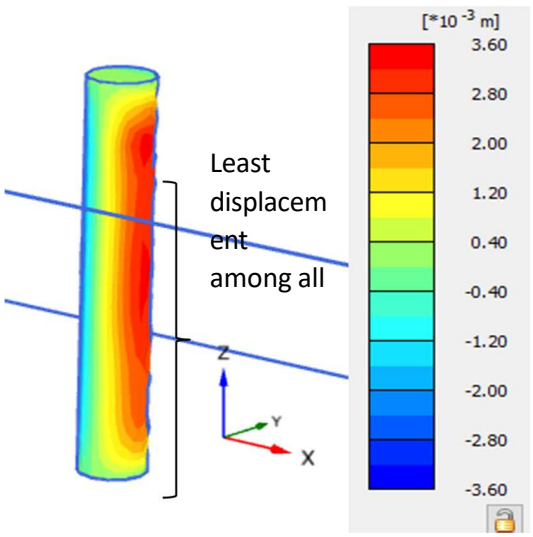


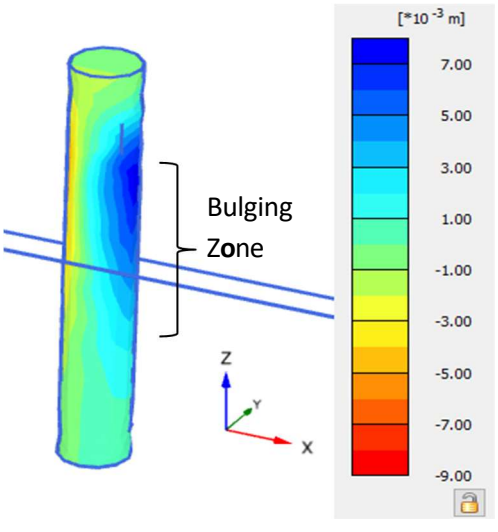


**Figure 4.25**. (a) OSC (b) End bearing column

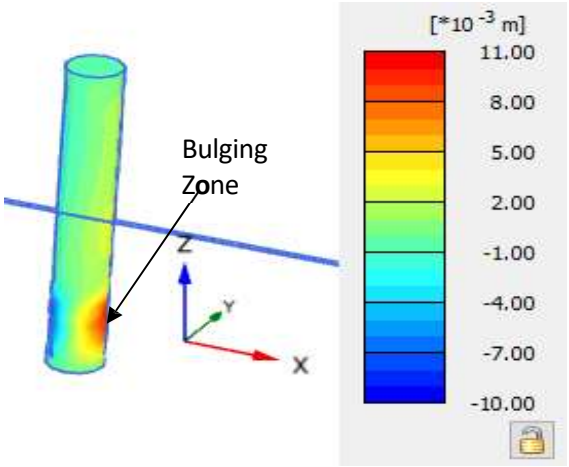


(c) Floating column

### 4.4.5 Clay bed reinforced with ordinary stone column- Group of stone columns

The load carrying ability of the composite ground was significantly improved, according to the group analysis of stone columns organized in triangular, square, and hexagonal designs with different S/D ratios displayed in figures 4.26 and 4.27. The maximum load at 50 mm settlement for the triangle arrangement (S/D = 2) was 8.75 kN for end bearing columns and 9.10 kN for floating columns, representing improvements of 61.94% and 68.52% over the unreinforced clay bed, respectively. End bearing columns demonstrated the maximum capacity of 9.15 kN in the square pattern (S/D = 2), which is 69.44% more than the unreinforced bed, while the floating columns carried 7.45 kN, a 37.96% increase. For the hexagonal configuration (S/D = 3), the capacities reduced to 7.65 kN and 6.45 kN for end bearing and floating columns, yielding 41.67% and 19.44% improvements, respectively. These results indicate that the square pattern provides the maximum improvement in load carrying capacity for end bearing columns, whereas the triangular pattern favours floating columns, while the hexagonal arrangement shows comparatively lower efficiency due to the larger spacing between columns.

Therefore, it can be said that while wider spacing, like in the hexagonal pattern, produces relatively less improvement, closer spacing and compact arrangements, like triangular and square patterns, are more effective in enhancing the load carrying performance of stone column-reinforced ground. Moreover, end bearing columns perform better in square arrangements, while floating columns benefit more from triangular configurations.

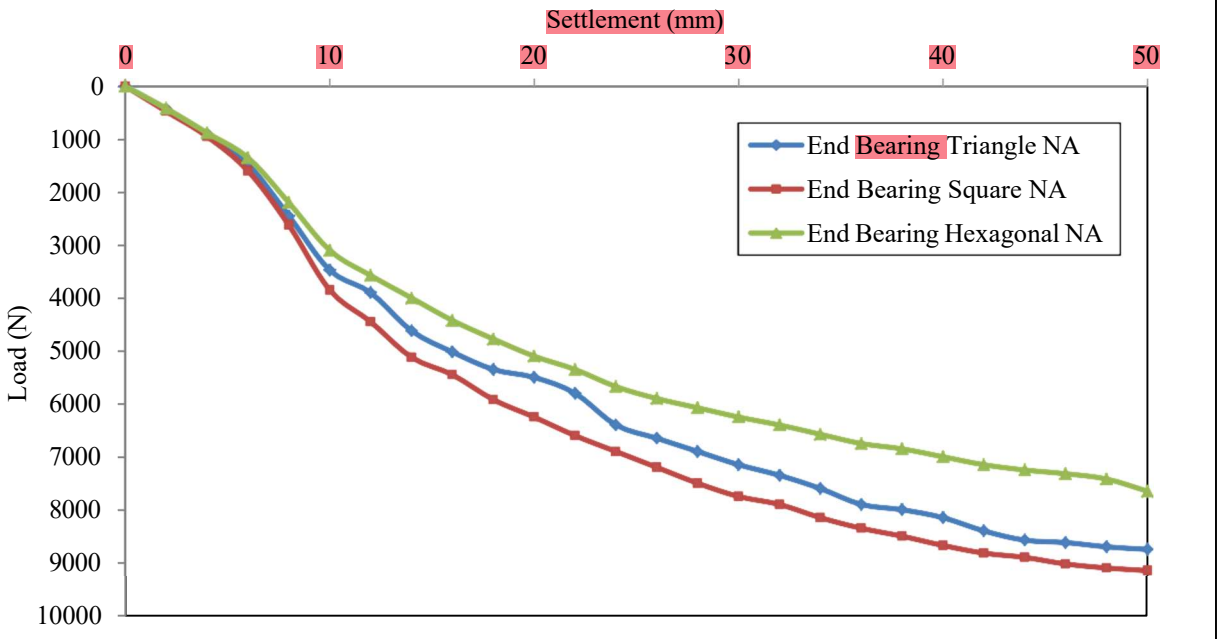


**Figure 4.26** Load settlement variations of different patterns for unencased end bearing columns

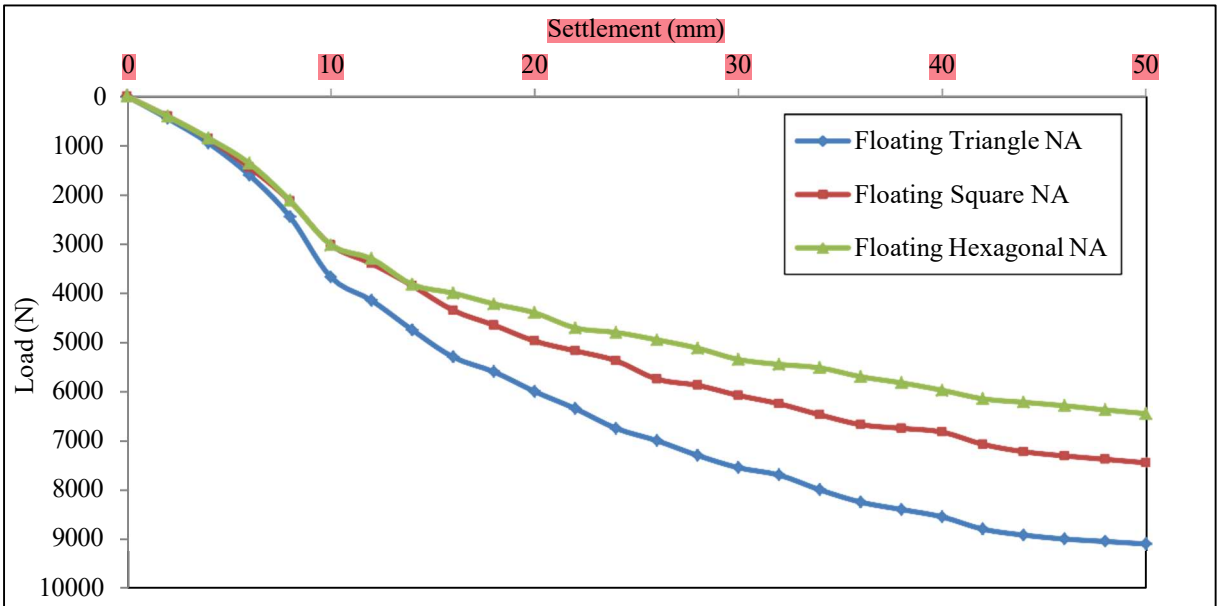


**Figure 4.27** Load settlement variations of different patterns for unencased floating columns

### 4.4.6 Reinforcing clay bed with encased stone column- Group of Stone Columns

Group analysis was performed for encased stone columns in a manner similar to that of the single stone column study. Additionally, encasement was applied across the whole length of the column for both end bearing and floating columns in the group analysis. Additionally, for the analysis, both types of geosynthetics were employed and contrasted.

### 1 Triangular

The load-settlement behavior of end-bearing encased stone columns arranged in a triangle for S/D = 2 for D = 50 mm is shown in Figure 4.28. Similarly, Figures 4.29 show the load-settlement behaviour of floating encased columns arranged in triangular pattern for S/D = 2 for D = 50 mm, respectively. The ultimate load bearing capacity for end bearing encased stone columns with a triangular pattern for S/D = 2 was determined to be 8.75 kN for geogrid and 9.3 kN for geotextile, respectively, for D = 50 mm. This suggests that geotextile offers better confinement and increases the overall stiffness of the composite system. Similarly, the ultimate load bearing capacity for floating encased stone columns with a triangular pattern for S/D = 2 was determined to be 8.65 kN for geogrid and 8.75 kN for geotextile, respectively, demonstrating comparable performance, however geotextile once more offered a little greater improvement. Overall, the findings show that encasing improves the efficiency of stone columns, with geotextile outperforming geogrid and the triangular configuration providing a good load-settlement response for both floating and end-bearing columns.

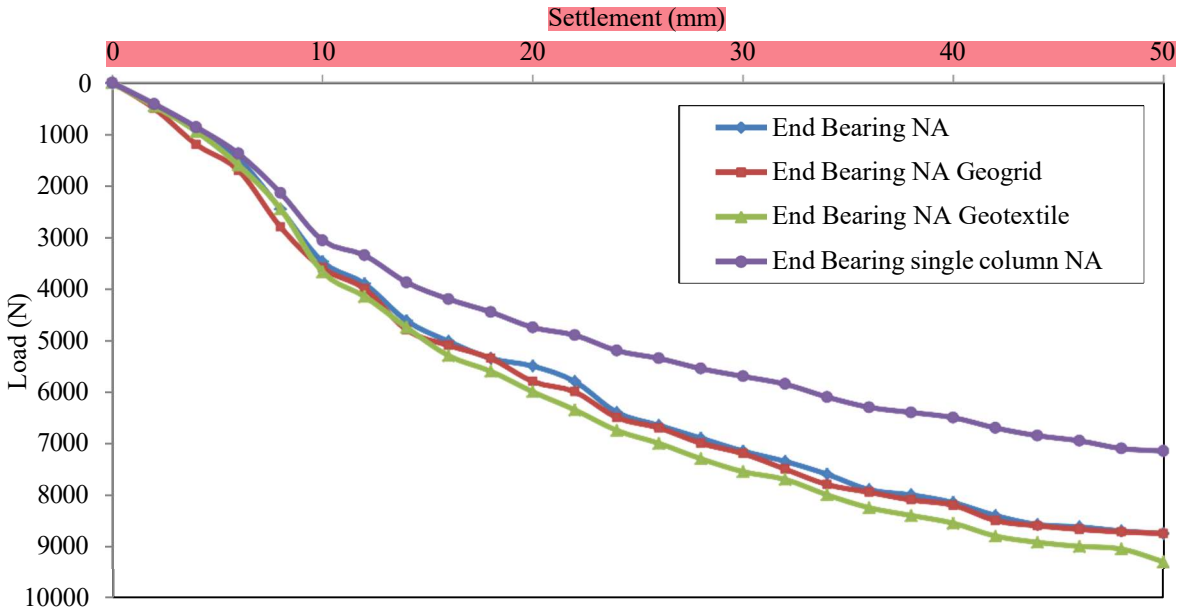


**Figure 4.28** Load settlement variations of triangular patterns for end bearing columns

The study clearly demonstrates that encasement significantly enhances the performance of stone columns in triangular arrangements (S/D = 2, D = 50 mm). With geogrid and geotextile encasement boosting the load carrying capability by 62.04% and 72.22%, respectively, end bearing columns demonstrated the greatest improvement, over the unreinforced clay bed. Floating columns also benefitted, with improvements of 60.19% for geogrid and 62.04% for

geotextile encasement. These observations confirm that geotextile performs better than geogrid, providing superior confinement and higher load resistance. Furthermore, the results highlight that end bearing columns gain more advantage from encasement than floating columns, making them the most efficient configuration for improving ground strength.

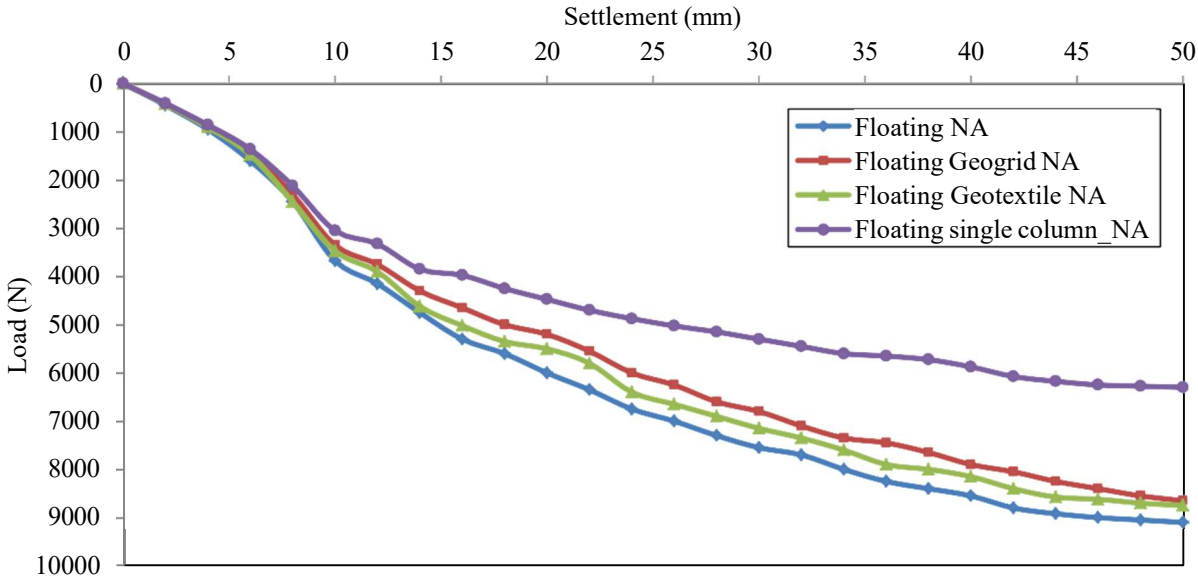


**Figure 4.29** Load settlement variations of triangular patterns for floating columns

**2. Square**

The load-settlement behavior of end bearing encased stone columns placed in a square pattern for S/D = 2 for D = 50 mm is shown in Figure 4.30. The load-settlement behavior of floating encased columns placed in a square pattern for S/D = 2 and D = 50 mm is similarly depicted in Figures 4.31. The maximum load bearing capability for end bearing enclosed square-patterned stone columns with D = 50 mm and S/D = 2 was determined to be 8.15 kN for geogrid and 8.70 kN for geotextile, respectively. Similarly, for floating encased square-patterned stone columns with S/D = 2, the ultimate load bearing capability was determined to be 7.35 kN for geogrid and 8.4 kN for geotextile.

When compared to the unreinforced clay bed, the findings of the square pattern arrangement (S/D = 2, D = 50 mm) demonstrate that encasement significantly increases the load carrying capacity of stone columns. For end bearing columns, the capacity increased to 8.15 kN with geogrid (50.93% improvement) and further to 8.70 kN with geotextile (61.11% improvement), indicating that geotextile provides superior confinement. Floating columns also benefitted, with capacities of 7.35 kN for geogrid (36.11% increase) and 8.40 kN for

geotextile (55.56% increase). These observations confirm that geotextile performs better than geogrid in enhancing load resistance, and that end bearing columns derive greater benefit from encasement than floating columns in square arrangements.

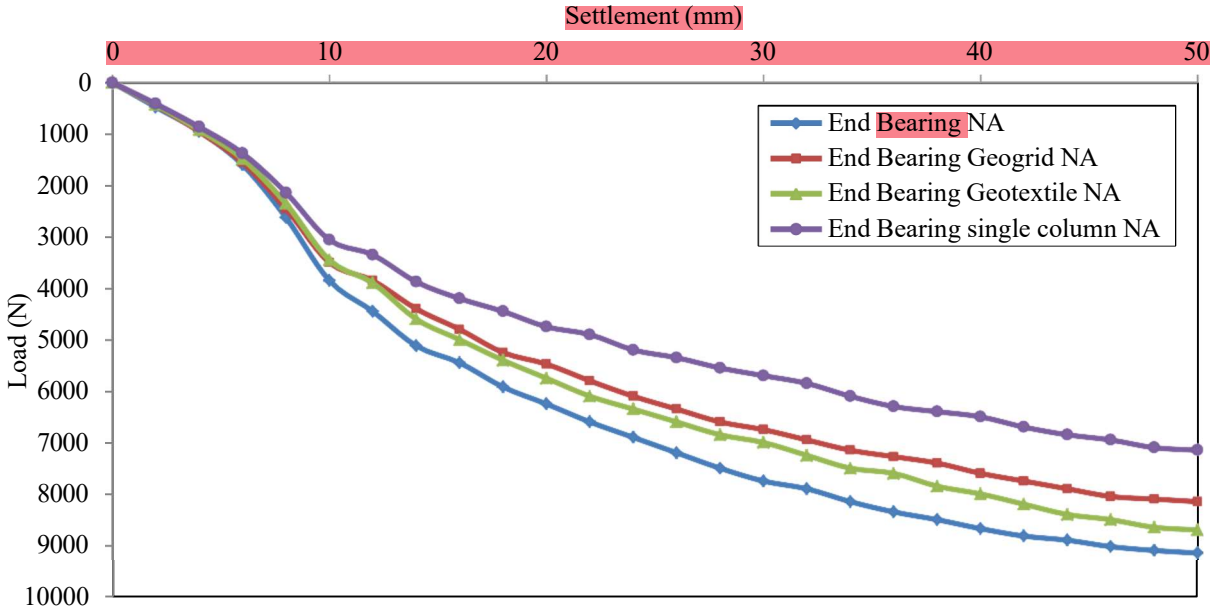


**Figure 4.30** Load settlement variations of square patterns for end bearing columns

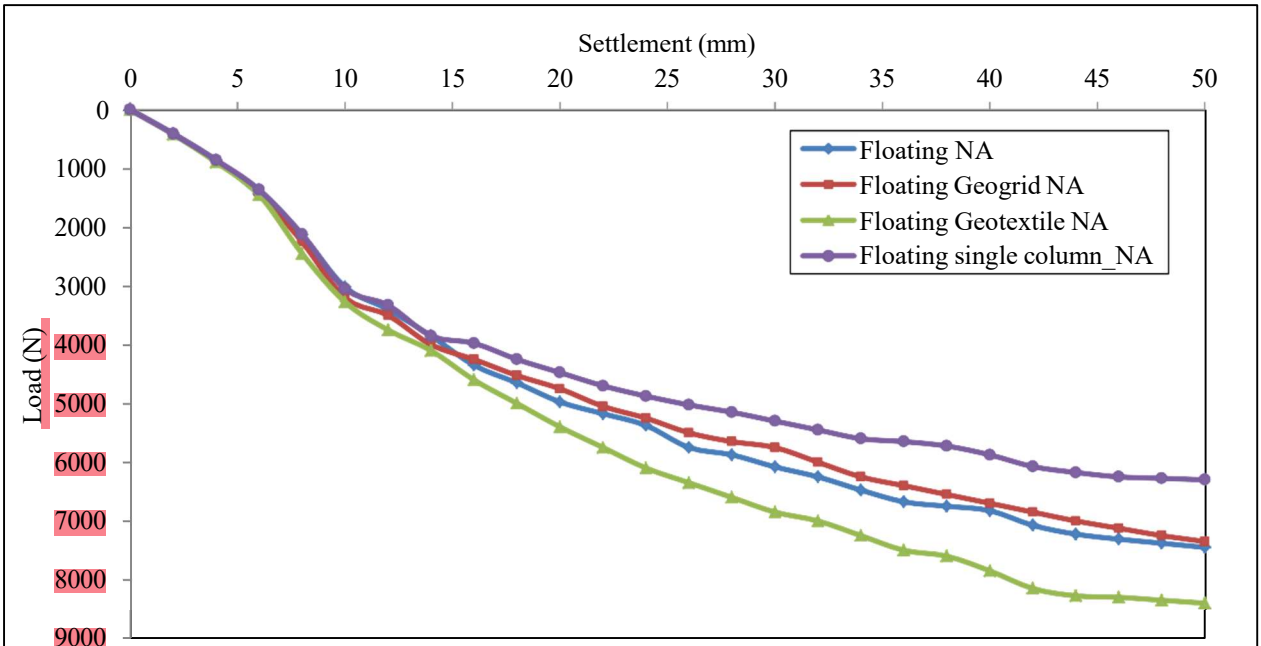


**Figure 4.31** Load settlement variations of square patterns for floating columns

The observations indicate that encasement of stone columns in square arrangements with S/D = 2 significantly improves the load carrying capacity compared to the unreinforced clay bed.

End bearing columns showed greater improvement than floating columns, with geotextile encasement proving more effective than geogrid in both cases. This confirms that geotextile provides better confinement and strength enhancement, while end bearing encased columns are the most efficient configuration for improving ground performance in square patterns.

### 3. Hexagonal

3 The load-settlement behavior of end bearing encased stone columns placed in a hexagonal configuration for S/D = 3 for D = 50 mm is shown in Figure 4.32.Similarly, Figures 4.33 show the load-settlement behaviour of floating encased columns arranged in hexagonal pattern for S/D = 3 for D = 50 mm, respectively. The ultimate load bearing capability for end bearing encased stone columns with a hexagonal pattern for S/D = 3 was determined to be 7.45 kN for geogrid and 8.22 kN for geotextile, respectively, for D = 50 mm. Similarly, for floating encased stone columns with a hexagonal design and S/D = 3, the ultimate load bearing capability was determined to be 8.42 kN for geogrid and 7.45 kN for geotextile.

137

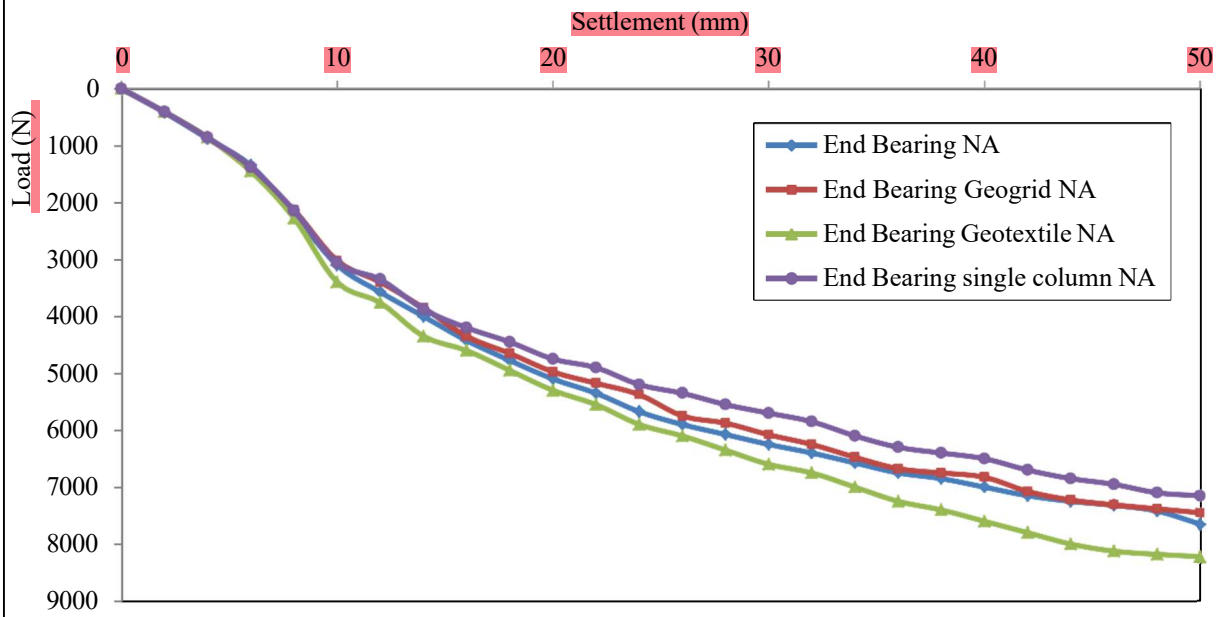


**Figure 4.32** Load settlement variations of hexagonal patterns for end bearing columns

The results of the hexagonal pattern arrangement with S/D = 3 and D = 50 mm show that encasement improves the stone columns' ability to support loads, albeit the improvement is not as noticeable as in square and triangle layouts. For end bearing columns, geogrid and geotextile encasement increased the capacity to 7.45 kN (37.96% improvement) and 8.22 kN (52.22% improvement), respectively, with geotextile again showing better confinement. For

floating columns, the behaviour was less consistent, with geogrid providing the highest improvement of 55.93%, while geotextile resulted in only a 37.96% increase. Overall, geotextile is more effective for end bearing columns, while geogrid provides better results for floating columns in the hexagonal arrangement. The larger spacing in the hexagonal pattern reduces group efficiency, making it less effective than triangular or square configurations.

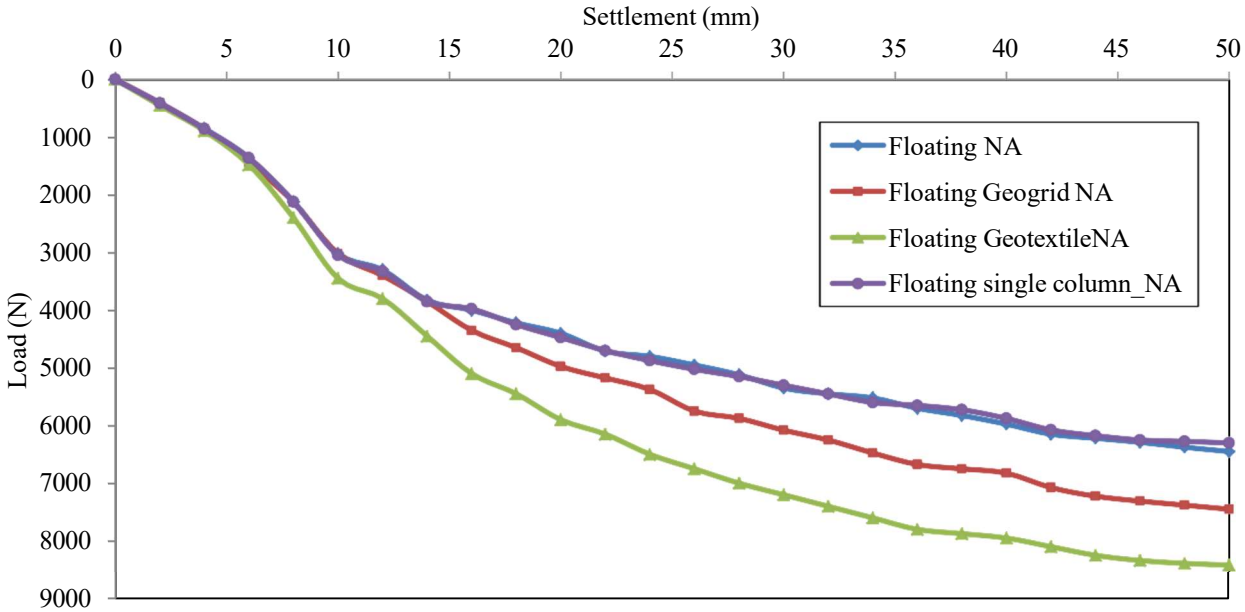


**Figure 4.33** Load settlement variations of hexagonal patterns for floating columns

The comparative study of encased stone-column groups shows a clear pattern: closer, more compact arrangements (S/D = 2) and geotextile encasement produce the largest gains in load carrying capacity, while wider spacing (S/D = 3) reduces group efficiency. Overall, the triangular and square patterns outperform the hexagonal pattern. The best result in the tested cases is the triangular pattern with geotextile encasement for end bearing columns (9.30 kN; 72.22% increase over the unreinforced clay bed), followed by triangular geogrid and geotextile encasements for floating columns (60–62% increases). Square patterns also give large improvements, particularly for end bearing columns with geotextile (8.70 kN; 61.11% increase) and for floating columns with geotextile (8.40 kN; 55.56% increase). The hexagonal pattern (S/D = 3) is the least effective overall because the larger spacing reduces interaction between columns; although some encasement cases (for example, floating with geogrid at 8.42 kN, 55.93%) still show moderate gains, they do not match the top performances of triangular or square layouts.

Two consistent findings emerge: (1) encasement materially increases capacity for floating columns as well as end bearings, and (2) geotextile generally provides superior confinement and higher increases than geogrid—particularly for end bearing columns—while geogrid occasionally gives competitive results for some floating-column cases. End bearing encased columns benefit more from encasement than floating encased columns in most tested configurations.

The installation of stone columns greatly increases the load carrying capability of soft clay beds, as confirmed by the overall experimental and computational research. End bearing columns regularly outperform floating columns. Regarding load-settlement response, both methods demonstrated strong agreement, confirming the accuracy of the numerical model in representing field behavior. By decreasing bulging and offering lateral confinement, the use of geosynthetic encasement enhanced performance and increased the composite ground's stiffness and strength. Between the two types of geosynthetics, geotextile consistently yielded greater improvement than geogrid, particularly for end bearing columns, while geogrid occasionally gave comparable performance for floating columns.

In group configurations, triangular and square patterns with closer spacing (S/D = 2) demonstrated superior efficiency compared to hexagonal patterns with wider spacing (S/D = 3). The highest improvements were observed for end bearing columns encased with geotextile in triangular and square arrangements, showing increases of more than 70% over the unreinforced clay bed. Floating columns also benefited substantially, though to a lesser degree than end bearing columns.

Overall, the study finds that both numerical and experimental evaluations demonstrate how well stone columns improve soft soils, with encasement—particularly with geotextile—offering the biggest advantage. The most effective arrangement for increasing the load carrying capacity of soft clay deposits is end bearing encased columns in compact group layouts.

### 4.5 Comparative Analysis of Experimental and Numerical Outcomes of Tests Performed on individual Stone Column and Group of Stone Columns

To confirm the experimental findings, a comparison with the numerical data acquired by Plaxis 3D was also carried out. Both situations have a similar failure mechanism, which can be highly clearly shown in Figures 4.25. Unreinforced soil underwent more deformation than reinforced soil (OSC). However, bulging was the cause of the OSC's failure, which was managed by encasing the OSC. The geotextile and geogrid encasement was supplied vertically. When it came to failure mechanisms, the numerical and experimental investigations showed the same pattern.

**Table 4.1: Comparing the experimental and numerical measurements of the load capacities of stone columns for a single column**

| Dia of the stone column | Type of Column | Experimental Results (kN) | Numerical Results (kN) | Coefficient of variation (%) |
|---|---|---|---|---|
| D=70mm | End Bearing | 7.2 | 7.15 | 0.49 |
| | Floating | 6.5 | 6.3 | 2.21 |
| | End Bearing encased with geogrid | 7.7 | 7.52 | 1.67 |
| | End bearing encased with geotextile | 8.15 | 7.85 | 2.65 |
| | Floating with Geogrid | 7.6 | 7.25 | 3.33 |
| | Floating with Geotextile | 7.9 | 7.45 | 4.15 |

Table 4.1 The low coefficients of variation indicate a close agreement between the experimental and numerical results for stone columns with a diameter of 70 mm. For the end bearing column, the experimental load capacity was 7.2 kN against 7.15 kN from numerical analysis, giving a variation of only 0.49%. Similarly, the floating column recorded 6.5 kN experimentally and 6.3 kN numerically with a variation of 2.21%. The load capacity of both end bearing and floating columns was further enhanced by the addition of geogrid and geotextile encasement; experimental results were consistently marginally higher than the numerical projections. For end bearing columns, geogrid and geotextile encasement increased the load to 7.7 kN and 8.15 kN, respectively, with variations of 1.67% and 2.65%. For floating columns, geogrid and geotextile encasement enhanced the capacity to 7.6 kN and 7.9

kN, with variations of 3.33% and 4.15%. Overall, the results confirm that the numerical model reliably simulates the experimental behaviour of stone columns, while also demonstrating the effectiveness of geosynthetic encasement, particularly geotextile, in improving load carrying capacity.

**Table 4.2: Comparing the experimental and numerical measurements of the load capacities of stone columns for group columns arranged in a triangle (s/d=2)**

| Dia of the stone column | Type of Column | Experimental Results (kN) | Numerical Results (kN) | Coefficient of variation (%) |
|---|---|---|---|---|
| D=50mm | End Bearing | 9.10 | 8.75 | 2.77 |
| | Floating | 9.6 | 9.1 | 3.78 |
| | End Bearing encased with geogrid | 9.2 | 8.75 | 3.55 |
| | End bearing encased with geotextile | 9.8 | 9.3 | 3.70 |
| | Floating with Geogrid | 8.8 | 8.65 | 1.22 |
| | Floating with Geotextile | 9.2 | 8.75 | 3.55 |

For stone columns with a diameter of 50 mm, the numerical and experimental findings demonstrate good agreement, with coefficients of variation often less than 4% (see table 4.2). For the end bearing column, the experimental load capacity was 9.10 kN compared to 8.75 kN from numerical analysis, yielding a variation of 2.77%. The floating column showed a slightly higher experimental capacity of 9.6 kN against 9.1 kN numerically, with a variation of 3.78%. With geogrid encasement, the load capacity of end bearing and floating columns was 9.2 kN and 8.8 kN, respectively, while geotextile encasement further enhanced the performance to 9.8 kN for end bearing and 9.2 kN for floating columns. The variations for these encased conditions ranged between 1.22% and 3.70%, confirming close correspondence between experimental and numerical outcomes. Overall, the findings show that the numerical model can accurately simulate load-settlement behavior. When compared to geogrid, geotextile encasement offers a more notable increase in load carrying capacity.

**Table 4.3: Comparing the numerical and experimental measurements of the load capacities of stone columns for group columns in a square pattern (s/d=2)**

| Dia of the stone column | Type of Column | Experimental Results (kN) | Numerical Results (kN) | Coefficient of variation (%) |
|---|---|---|---|---|
| D=50mm | End Bearing | 9.60 | 9.15 | 3.39 |
| | Floating | 8.10 | 7.45 | 5.91 |
| | End Bearing encased with geogrid | 8.60 | 8.15 | 3.8 |
| | End bearing encased with geotextile | 9.10 | 8.70 | 3.18 |
| | Floating with Geogrid | 8.6 | 7.35 | 11.08 |
| | Floating with Geotextile | 8.7 | 8.4 | 2.48 |

The results for stone columns of 50 mm diameter showed in table 4.3, show a consistent correlation between experimental and numerical findings, with coefficients of variation generally within an acceptable range. For the plain end bearing column, the experimental load capacity was 9.60 kN compared to 9.15 kN numerically, yielding a variation of 3.39%. The floating column exhibited a lower experimental capacity of 8.10 kN against 7.45 kN numerically, with a variation of 5.91%. With geogrid encasement, the end bearing and floating columns showed capacities of 8.60 kN and 8.60 kN experimentally, which were slightly lower than the plain end bearing case, while the numerical values were 8.15 kN and 7.35 kN, giving variations of 3.80% and 11.08%, respectively. Geotextile encasement improved the performance, raising the capacity to 9.10 kN for end bearing and 8.70 kN for floating columns, with variations of 3.18% and 2.48%. These findings demonstrate that the numerical model accurately predicts experimental behavior. Furthermore, geotextile encasement proved more effective than geogrid in enhancing column performance, with the plain end bearing column achieving the highest load carrying capacity overall.

**Table 4.4: Comparing the experimental and numerical measurements of the load capacities of stone columns for a hexagon-shaped group column (s/d=3)**

| Dia of the stone column | Type of Column | Experimental Results (kN) | Numerical Results (kN) | Coefficient of variation (%) |
|---|---|---|---|---|
| D=50mm | End Bearing | 7.9 | 7.65 | 2.27 |
| | Floating | 7.3 | 6.45 | 8.74 |
| | End Bearing encased with geogrid | 7.9 | 7.45 | 4.15 |
| | End bearing encased with geotextile | 8.5 | 8.22 | 2.37 |
| | Floating with Geotextile | 9.10 | 8.42 | 5.49 |
| | Floating with Geogrid | 7.9 | 7.45 | 4.15 |

For the stone columns of 50 mm diameter, the comparison between experimental and numerical results shows close agreement with relatively small coefficients of variation, indicating the numerical model's dependability as shown in table 4.4. The plain end bearing column exhibited an experimental load capacity of 7.9 kN compared to 7.65 kN numerically, with a variation of 2.27%. The floating column, however, recorded a lower capacity of 7.3 kN experimentally and 6.45 kN numerically, showing a higher variation of 8.74%. With geogrid encasement, both end bearing and floating columns displayed a capacity of 7.9 kN experimentally and 7.45 kN numerically, each with a variation of 4.15%. Geotextile encasement proved more effective, as the end bearing column reached 8.5 kN experimentally and 8.22 kN numerically (2.37% variation), while the floating column achieved the highest capacity of 9.10 kN experimentally and 8.42 kN numerically (5.49% variation). Overall, the performance of both end bearing and floating columns was greatly improved by geotextile encasement, especially in the floating instance, but geogrid encasement only little improved.

The type, diameter, and reinforcing of stone columns all have a substantial impact on their load-carrying ability. For a diameter of 50 mm, end bearing columns exhibit higher load capacity (7.9 kN) compared to floating columns (7.3 kN), highlighting the efficiency of direct end bearing in transferring loads to the underlying firm layer. Reinforcement further

enhances performance, as end bearing columns enclosed with geotextile show a notable increase in load capacity to 8.5 kN, representing approximately a 7.6% improvement over unreinforced columns, while geogrid encasement provides a marginal increase of about 0.0–0.6%. Interestingly, when comparing diameters, the 50 mm end bearing columns carry slightly more load than the 70 mm columns (7.9 kN vs 7.2 kN), indicating potential experimental variability or the influence of soil conditions. Numerical analyses closely replicate the experimental results, generally slightly underestimating the load values, with low coefficients of variation, demonstrating good agreement between models and experiments. Floating columns consistently exhibit lower load capacity and higher deviations, reflecting their reliance on frictional resistance rather than end bearing. Overall, end bearing columns encased with geotextile consistently provide superior load-carrying performance, illustrating the combined effects of column type, diameter, and reinforcement in improving the strength and stability of soft soil foundations.

## 4.6 X-ray diffraction (XRD) and Scanning Electron Microscope (SEM) Analyses

### 4.6.1 General

In order to determine the crystalline minerals in the soil and materials utilized in the construction of columns, such as fly ash, stone dust, iron dust, and the mix design of the granular column, an X-ray diffraction test was performed using Bragg-Brentano in Bruker D8 advanced machines. A Jeol JSM-6610 LV operating in an extremely high vacuum was used for the Scanning Electron Microscope (SEM) investigation. Both normal plane and cross-section view modes were used to gather the SEM pictures. In accordance with the resolution criteria, the SEM's operating voltage was 5 kV.

### 4.6.2 X-ray diffraction (XRD)

The mineralogical makeup of the expanding soil and the additives used in column construction were determined by XRD analysis. In addition to lesser peaks linked to clay minerals like montmorillonite and kaolinite, which give expansive soil its expansive behavior, the diffraction pattern of expansive soil displays a significant crystalline peak about $2\theta = 27–28°$, showing the dominance of quartz. Fly ash's pozzolanic character is reflected in the broad hump in the 20–35° $2\theta$ range, which shows the presence of an amorphous glassy phase together with small crystalline peaks of quartz and mullite.

Stone dust exhibits sharp and well-defined crystalline peaks, particularly around 27–28° 2θ, confirming the presence of quartz and feldspar minerals, which contribute to its inert and stable behaviour. The additional mix shows a relatively diffused pattern with lower intensity peaks, suggesting partial amorphous characteristics and mineral dispersion. Finally, the XRD spectrum of the multi-blended column mix displays a combination of crystalline peaks from quartz and feldspar along with amorphous humps, indicating the integration of soil, fly ash, and stone dust. This confirms that the blended column mix achieves both reactive and inert mineral phases, enhancing pozzolanic activity and improving soil stabilization potential.

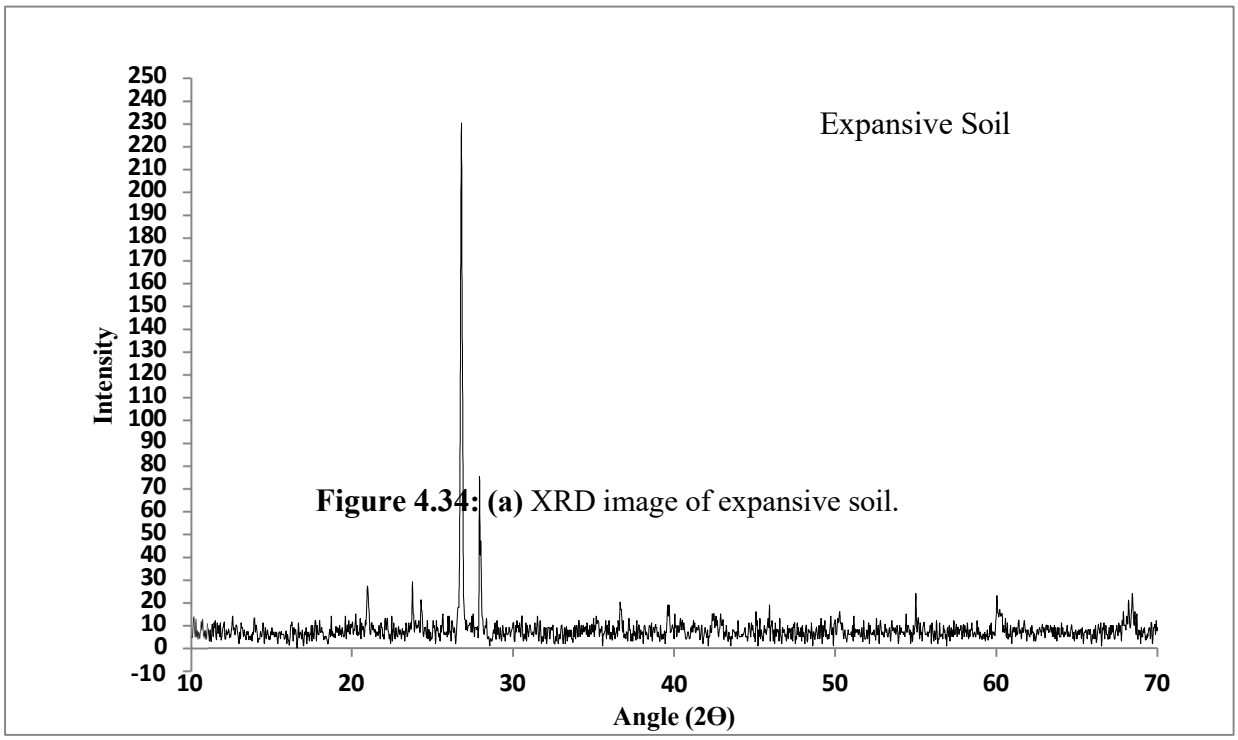


**Figure 4.34: (a)** XRD image of expansive soil.

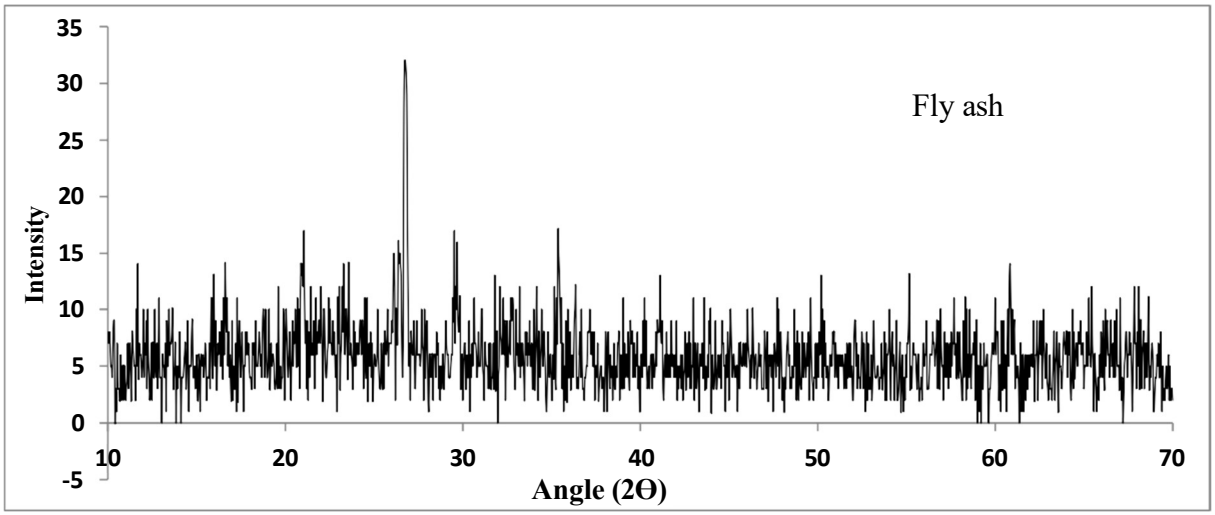


**b)** XRD image of Fly ash.

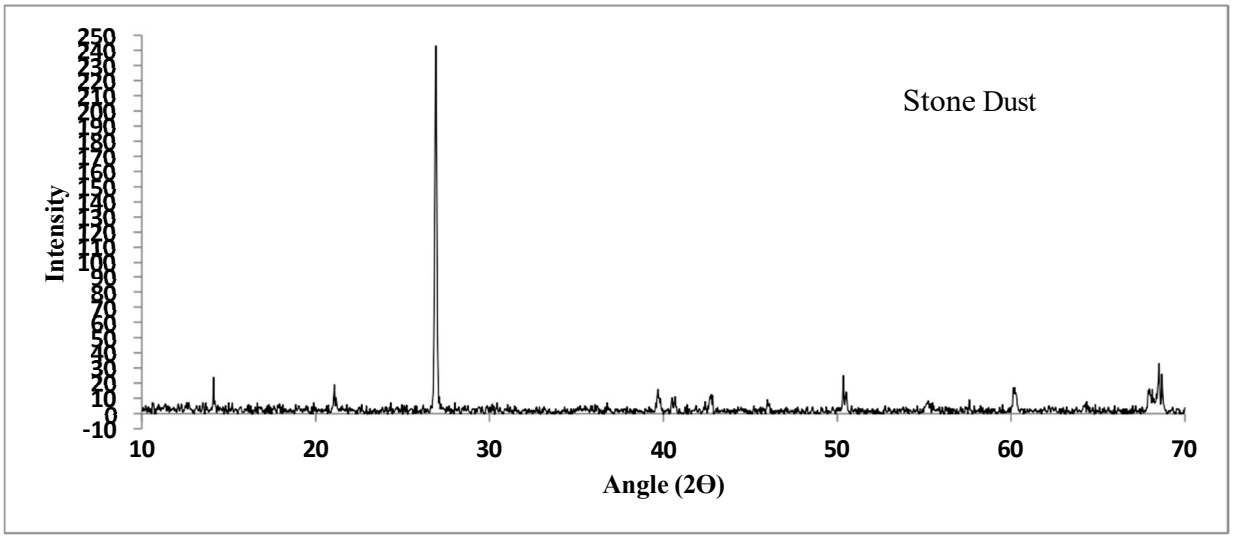


**c)** XRD image of Stone dust.

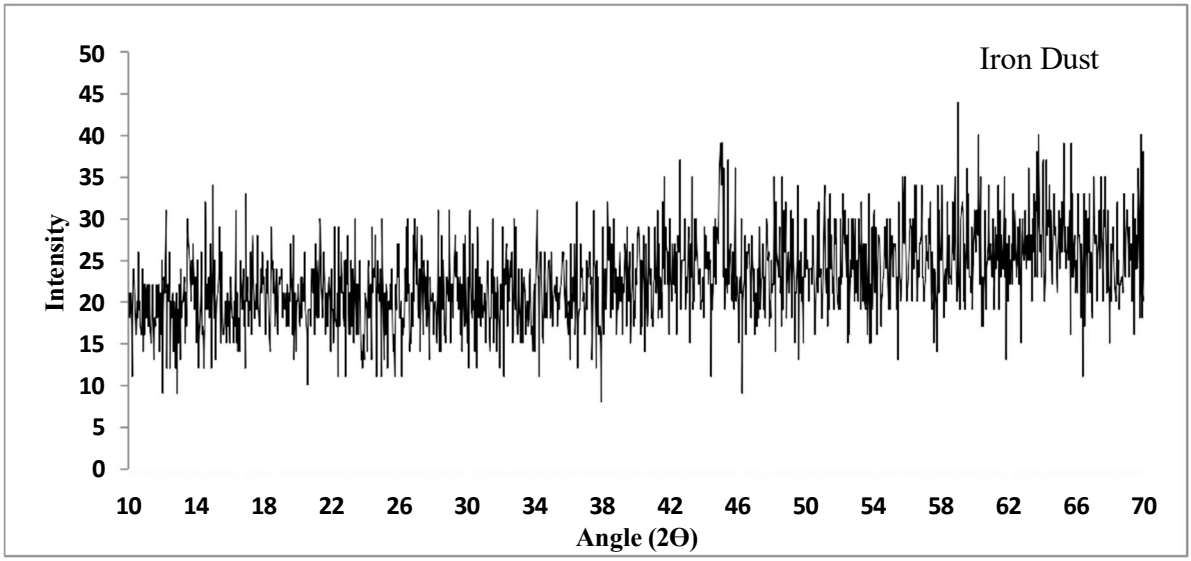


**d)** XRD image of Iron dust.

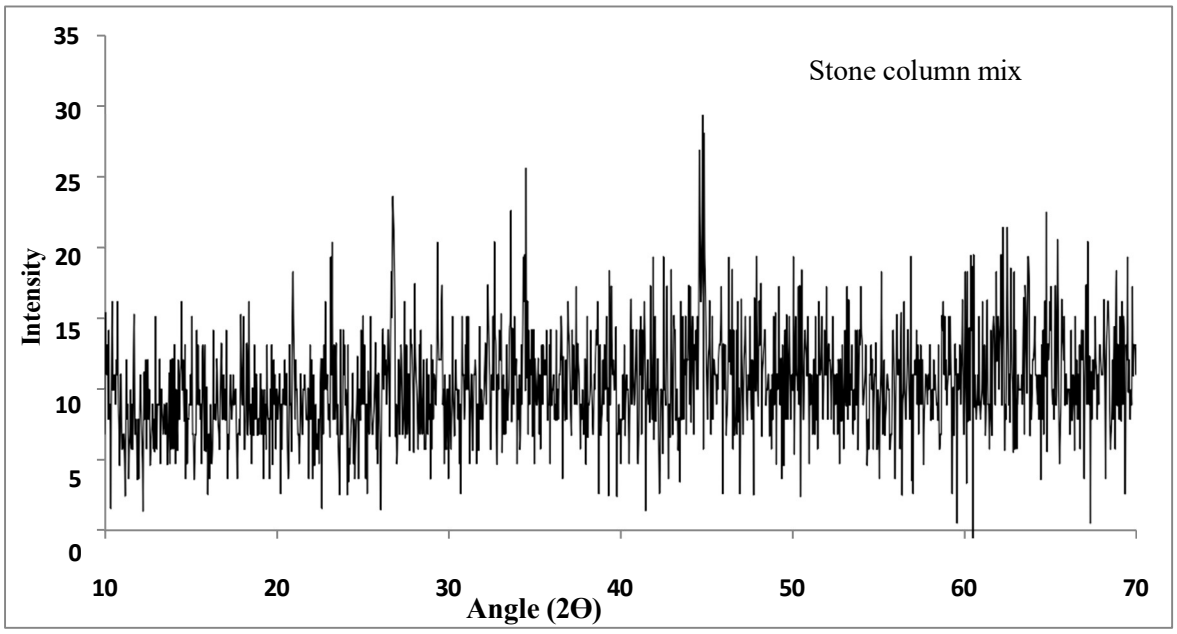


**e)** XRD image of column mix with iron dust

201

#### 4.6.3 Scanning Electron Microscope (SEM)

The SEM micrographs (Figure a–e) illustrate the microstructural variations in the tested soil samples. Images (a) and (c) exhibit aggregated clay particles forming dense flocculated clusters with visible inter-particle voids, indicating a relatively compact fabric that contributes to higher strength and lower compressibility. In contrast, image (b) shows a more dispersed arrangement of fine particles with an open structure, reflecting weaker inter-particle bonding and higher porosity, which can reduce load-bearing capacity. Image (d) reveals a

9

distinct plate-like or flaky morphology, feature of clay minerals like montmorillonite or kaolinite, which are recognized for their propensity to change volume and absorb water. Image (e) presents a mixed microstructure comprising aggregated lumps interspersed with pores, suggesting partial cementation and heterogeneous packing. Overall, the SEM observations highlight the differences in soil fabric, where denser and more aggregated structures correspond to improved load resistance, while loose and flaky arrangements result in higher compressibility and reduced stability.

Together, the XRD and SEM analyses provide complementary insights: SEM highlights the morphological arrangements and bonding of soil particles, while XRD confirms the mineralogical composition and reactivity of the materials. The combined findings confirm that adding fly ash and stone dust to the column mix enhances the soil–column system's overall load-bearing capability by improving the microstructural integrity and mineralogical interactions.

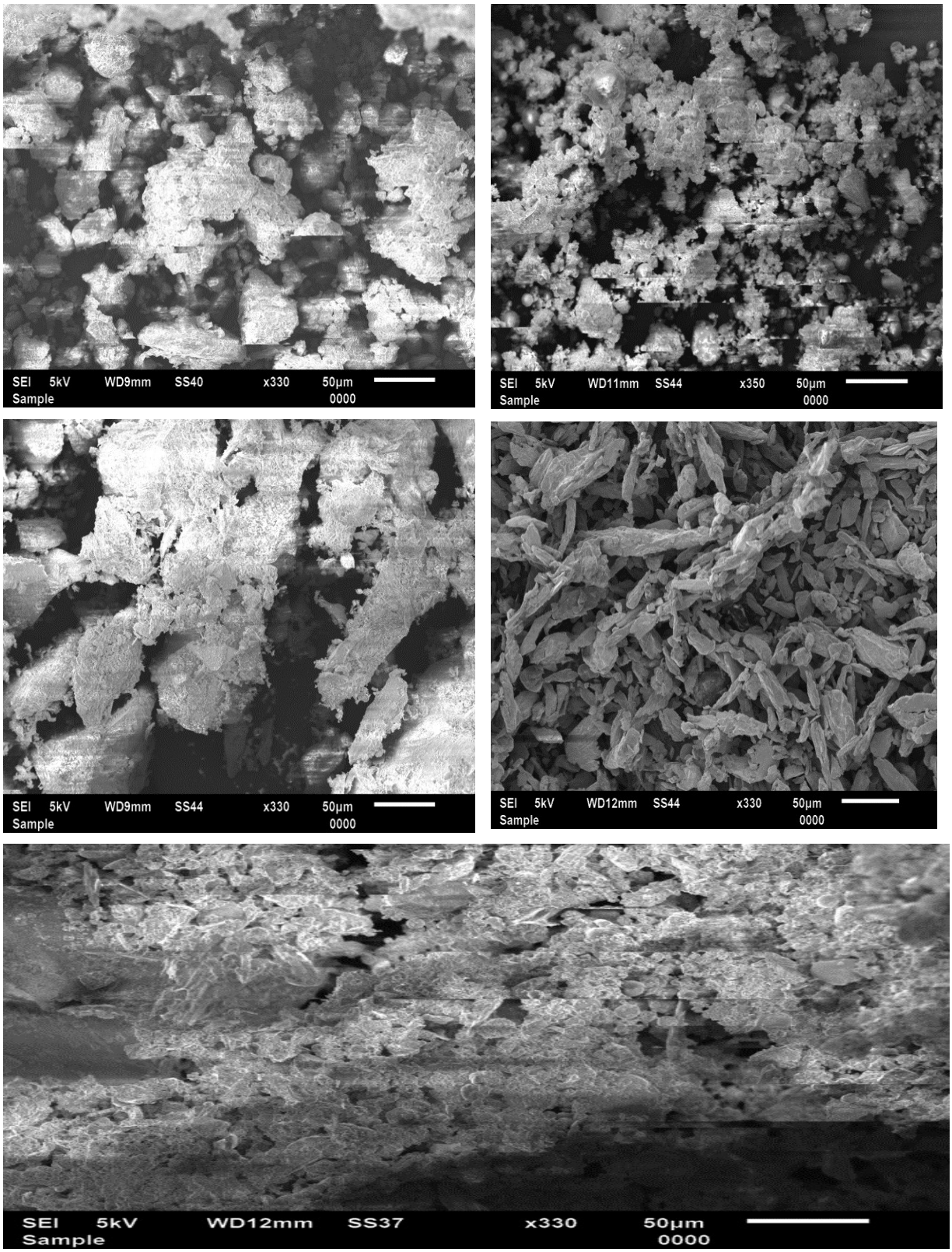


**Figure 4.35** SEM images of (a) expansive soil, (b) fly ash, (c) stone dust, (d) iron dust and (e) column mixes with iron dust

# CHAPTER 5

# CONCLUSIONS

## 5.1 GENERAL

The main conclusions from the testing and finite element analysis are presented in this chapter, along with a brief synopsis of the study. It also makes suggestions for further study.

## 5.2 CONCLUSIONS

1. Stone columns for ground improvement tested in this study were made utilising industrial waste products such as iron dust and fly ash; sand was replaced with stone dust.
2. End bearing column shows failure in bulging while floating columns failed in punching failure.
3. In groups of columns three loading arrangements were tested, i.e. triangular, square and hexagonal. Triangular loading gives the best results compared to the two other loading arrangements with or without encasement.
4. Single columns are less efficient than to groups of columns. The loading arrangement in triangular groups gives optimum efficiency.
5. The column's bearing capacity is improved by the use of encasement using geosynthetics and reduces the settlement as compared to columns without encasement.
6. Geotextile shows better results than geogrid due to its grid size as the material used for column casting is fine grained. The slurry spills out or extrudes into the surrounding soil replaced for the column casting.
7. Plaxis 3D software was used to validate the experimental results.; experimental and modelled results are in good agreement.
8. XRD on powdered materials shows a predominance of quartz in both the expansive soil and the multi-blended material mix. The SEM analyses were performed on powdered materials. The microstructure and crystal structures of expanding soil, fly ash, iron dust, stone dust, and the column mix of fly ash, iron dust, stone dust, and cement as a binder were examined.

## 5.3 AREA OF FUTURE RESEARCH

There are significant gaps in this field's current development that must be filled in order to fully comprehend how stone column-reinforced ground behaves and to predict how it will react to applied loads. Further research can be undertaken on the following topics:

1. In the current study, a column mix is created using waste materials such fly ash, stone dust, and iron dust. The utilization of waste materials in the production of stone columns has received little research. Future research can use either small-scale or field-scale testing to examine the necessity to use industrial and agricultural waste due to land shortage.
2. 2. More thorough research is conducted on the various column diameters, group column spacing, and S/D ratio.
3. While the present study examines the use of vertical encasement only, findings indicate that stone columns reinforced in vertical and horizontal directions exhibit comparable load-bearing capacity. Moreover, there is a lack of field investigations exploring the combined application of vertical and horizontal reinforcement. Future research could therefore focus on stone columns reinforced in both orientations, assessed through either small-scale or full-scale field testing.
4. In present encasement is provided to column length. In future investigations the impact of variation of encasement length can also be done. More detailed investigation is necessary.
5. Future research could examine how well reinforced stone columns function in soil profiles with many layers.. In many real-world scenarios, site conditions include a sand layer between clay layers or the reverse. While stone columns have been observed to perform effectively in such configurations, the application of reinforced stone columns under these conditions has received little attention and remains insufficiently analysed.
6. 6. A more thorough analysis of the stress concentration on the column and the surrounding soil is made possible by the use of pressure cells. As a result, it becomes easier to comprehend how the load is distributed between the nearby earth and the columns.
7. Only the utilization of geotextile and geogrid has been employed in the current investigation. Any other type of geosynthetic material can also be substituted. More detailed experimental investigation is necessary.

# CHAPTER 6
# ADDITIONAL WORK

## 6.1 General

Due to land scarcity, civil engineers have developed methods for improving the ground so that construction is possible, for example, on areas with expansive soils. This is often accomplished by inserting granular or stone columns into the soft soil. In this study, we look into a method of ground improvement that makes use of stone columns. Instead of using sand and cement as a binder, stone columns use a mixture of industrial waste, such as fly ash, iron dust, or stone dust. Engineers find it appealing to use the ever-growing amount of waste material for building projects. In the current project, we attempted to use the waste in specific mixes and cast columns in expanding soil using these particular mixes. The various waste material blends used in column design, the diameters of individual stone columns, and the bearing strength of individual columns as opposed to groups of columns were all taken into account. A mold measuring 150 mm in diameter and 170 mm in height was used for the laboratory trials. Granular columns were cast in molds with a diameter of 20, 30, and 50 mm utilizing waste materials such as fly ash, stone dust, iron dust, and cement as a binder. The columns were installed on expanding soil using the replacement approach. The compressive strength of the column was evaluated both with and without iron dust. A 50 mm plunger in the CBR machine was used to obtain the load-deformation curve. Geogrid and geotextile were the two types of geosynthetics used to make the encasements. UCS (unconfined compressive strength) tests on soil samples and granular mixes in various ratios with and without iron dust were conducted after the mix design. In comparison to the expansive soil, the mix utilized for the stone column design demonstrated optimal compressive strength. When columns are separated more than three times their diameter, there is no discernible advantage. Based on the results, design charts are made, and a design process is provided.

## 6.2 Methodology

### 6.2.1 Test program:

The clay chunks that were taken from the paddy fields were ground up, cleaned of undesired items including grass, plant roots, stones, and pebbles, and then allowed to dry in the sun. To get a soft consistency, the necessary amount of water was completely combined with the fine clayey soil. The granular column was inserted into the highly cohesive expansive soil. The waste material used for

column fill was a mix of stone dust, fly ash, ordinary Portland cement (OPC), and/or iron dust. The woven geosynthetics were used for the encasement of the granular column for single and groups of columns.

The 31 experiments were carried out in the current study, 12 of which were on a set of columns, 18 of which were on individual columns with diameters of 20, 30, and 50 mm, and one test on virgin soil. The experimental program showed in table 3.

**Table 6.1: summary of an experimental program**

| Test series | Reinforcement type | Detailed parameters | | No of tests |
|---|---|---|---|---|
| | | Single stone column | Group stone column | |
| 1 | Natural expansive soil | - | - | 1 |
| 2 | Expansive Soil + stone column (end bearing without iron dust) | l = 170 mm (end bearing)<br>Diameter = 20, 30 and 50 mm<br>No of experiment = 3 | l = 170 mm (end bearing)<br>Diameter 30 mm, s/d = 1<br>No of experiment = 2 | 5 |
| 3 | Expansive Soil + stone column (end bearing with iron dust) | l = 170 mm (end bearing)<br>Diameter = 20, 30 and 50 mm<br>No of experiment = 3 | l = 170 mm (end bearing)<br>Diameter = 30 mm,<br>s/d = 1.<br>No of experiment = 2 | 5 |
| 4 | Expansive soil + stone column (end bearing with iron dust) with geosynthetics (geogrid or geotextile) encasement | l = 170 mm (end bearing)<br>Diameter = 20, 30 and 50 mm<br>No of experiment = 6 | l = 170 mm (end bearing)<br>Diameter = 30 mm,<br>s/d = 1<br>No of experiment = 4 | 10 |
| 5 | Expansive soil + stone column (end bearing without iron dust) with geosynthetics (geogrid or geotextile) | l = 170 mm (end bearing)<br>Diameter = 20, 30 and 50 mm<br>No of experiment = 6 | l = 170 mm (end bearing)<br>Diameter = 30 mm,<br>s/d = 1<br>No of experiment = 4 | 10 |

### 6.2.2 Test setup:

Every experiment was carried out in a cylindrical mold that measured 150 mm in diameter and 170 mm in height. According to Shahu and Reddy (2011), the tank borders were built to minimize induced stresses. In accordance with IS 2720-16 (2016), the soil sample was prepared. A 25 kg rammer was used to fill the three layers of 5 kg soil and compact them with 56 blows per layer. The mold's interior was greased with oil to prevent wall friction. In this case, 20% of the soil weight water—that is, the ideal moisture content obtained from a typical proctor test conducted in the lab—was added to the sample. The soil sample with mould soaked in water for 96 hours as per IS 2720-16 (2016). The mould was pulled out of the water and left for 10 to 15 minutes so that the excess water could be removed. The expansion ratio procured for soil sample was 1.23%. The 50 mm diameter plunger in the CBR machine applied the footing load at a constant speed of 1.25 mm/min. A two-dial gauge with a sensitivity of 0.02 mm placed above the testing plate and the mold was used to observe the deformation.

An area replacement ratio of (Ar) 10%, 14%, and 23% for a single column with a diameter of 20, 30, and 50 mm was selected for all model tests, with a footing diameter roughly equivalent to twice the diameter of the stone column. The area replacement ratio is the area of the column divided by the area of the surrounding expansive soil. According to IS 15284-1 (2003), the settlement measured between 20 and 40 mm when the column failed. As a reference, the soft clay bed without a stone column loaded with a 50 mm diameter footing was performed. A load-deformation curve was obtained between loadings via settlement.







**Figure 6.1:** sample soaked in water for 96 hours, **Figure 6.2:** sample after soaking for 96 hours with single end bearing column, **Figure 6.3**: failed sample after loading with single column, **Figure 6.4:** column casing with encasement using geotextile, **Figure 6.5 & Figure 6.6**: column casing with geogrid, **Figure 6.7:** placing of encasement with casing in expansive soil.

### 6.2.3 Forming of the granular column:

The stone columns were designed as per IS 15284-1 (2003). The end-bearing columns were designed for the present study. The single columns of 20, 30, and 50 mm diameter were cast

in the centre of the cylindrical mould. For groups, double columns and triangular pattern columns of 30 mm diameter are designed. The replacement technique was used for the design of the column. The pipes of 20, 30, and 50 mm diameter were inserted into the soil bed at the desired spacing between the columns. The pipe was lubricated with oil inside and outside perimeter to avoid friction between the soil and the pipe. With the help of an auger and spatula, the soil was removed from the pipe. The desired depth of the column was checked on the scale. The column was filled with a mix of stone dust, fly ash, and cement and 12% water compared with the mix of stone dust, fly ash, cement, and iron dust, and 12% water. After the column was prepared, the pipe was removed carefully. Water content = P/4 + 3 where P is the cement consistency of OPC used for a mix. The cement consistency is 36%, calculated by the Vicat apparatus in the laboratory. The column mix is determined by the (unconfined compressive strength) UCS test. The UCS samples of a different mix are prepared in the sampler and left for 7 days in desiccator for curing and tested as per IS 2720-10 (1991). The mix gives optimum compressive strength compared to the soil used for the column mix. The average of three samples of each mix with different percentages of fly ash, stone dust, and cement compared with mix with iron dust was prepared and tested in the laboratory.

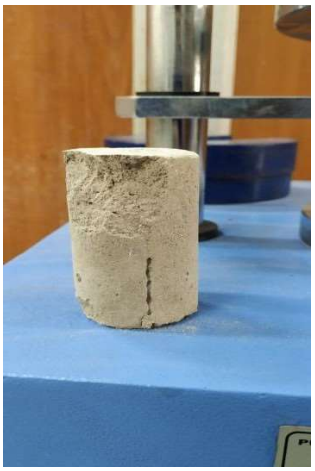

**Figure 6.8**: sample prepared for UCS test with the help of sampler, **Figure 6.9:** Loading cell with failed sample, **Figure 6.10:** failed sample.

For the encasement of the column, geosynthetics were applied to the perimeter of the column. The geosynthetics were rolled on the outside diameter of the pipe and inserted into the soil bed. The pipe used for column construction was lubricated inside and outside diameter so that can be easily removed. The soil was removed with the help of an auger and spatula, and then the granular mix was filled. The mix was tamped with the tamping rod. After the column was prepared, the pipe was removed carefully so that the column and the encasement were not

disturbed. Two types of geosynthetics are compared in the present study, i.e. geogrid and geotextile. The geosynthetics were tied with thread so that they were properly rolled up.

### 6.3 Column exhumation:

After the test, the column mix was carefully removed, and the column's distorted shape was restored by adding a thin layer of plaster of Paris paste. The surrounding dirt was then removed in order to isolate the cured plaster of Paris for additional examination. Following the test, measurements were made of the column's bottom penetration and the length of the distorted columns (Ali et al. 2012)

**Figure 6.11:** exhumed column with geotextile **Figure 6.12**: exhumed column with geogrid

### 6.4 Results and discussion:

To choose the optimum mix design the strength test was done on different column mixes. The unconfined compressive strength tests results showed in figure 13 and 14.

The average compressive strength of soil was 642 kPa. The experimental result verified with the equation (O'Flaherty et al., 1961)

$$\log CBR = 1.115 + 0.660 \log UCS$$

a working relationship between California bearing ratio and unconfined compressive strength under varying experimental conditions. The mix of 1:3 prepared to cast the stone column i.e. 1 part cement and fly ash and 3 part stone dust tested. The optimum results considered was 45% cement + 55% fly ash added with 3 part of stone dust used for column mix.

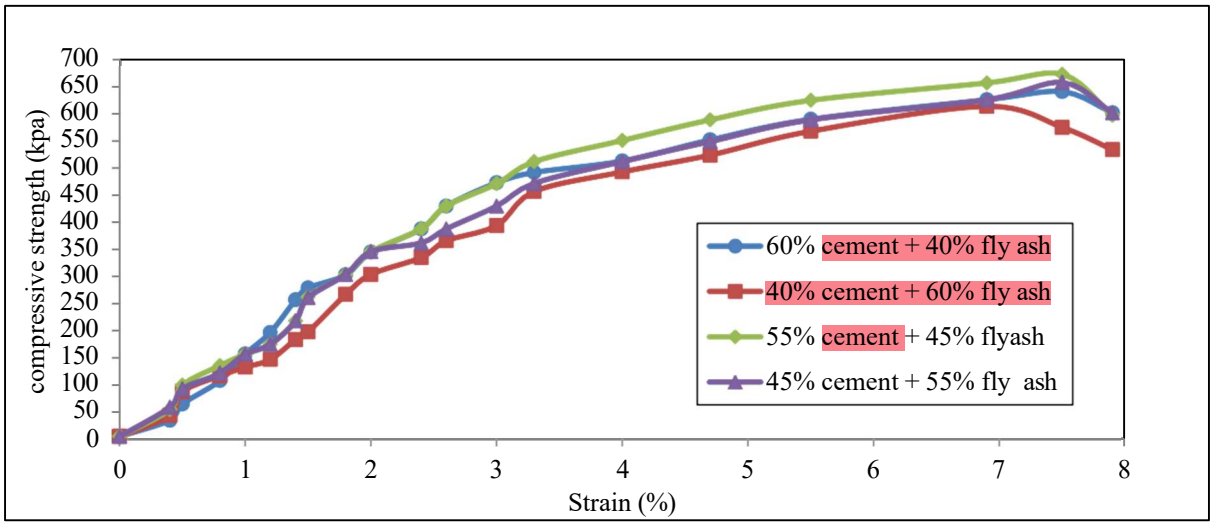


**Figure 6.13:** UCS tests mix designed for granular column without iron dust

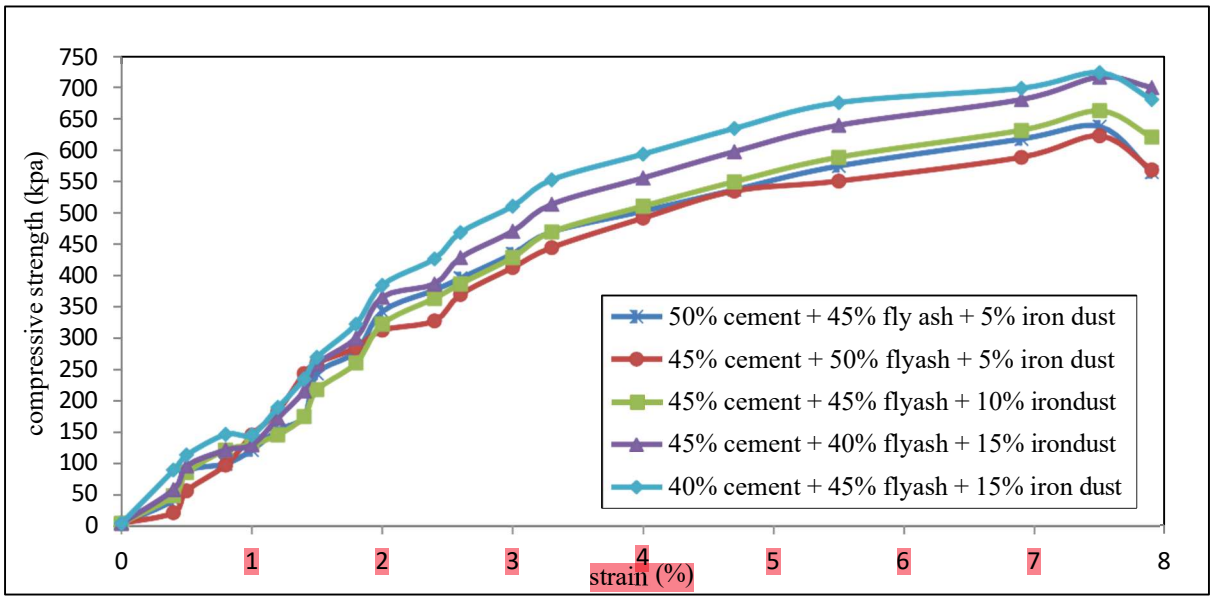


**Figure 6.14:** UCS tests mix designed for granular column with iron dust

The average compressive strength of the column mix without iron dust was 657 kPa. Similarly for iron dust mix 45% cement + 45% fly ash + 10% iron dust mix used for construction of column in the mould. The average compressive strength of the column mix with iron dust was 662 kPa. The mix design used for the column construction was in range of the compressive strength of the expansive soil used and also economical to the environment.

**6.4.1 Granular column without iron dust:** The load was shared between the soil and the granular column designed without iron dust.

**6.4.1.1 Granular unencased single column:** The load settlement graph procured as shown in fig 15. With the increase in load settlement also increases for certain time after that failure is shown and the readings in proving ring decreases as shown in graph. For 20 mm column

failure is at 40 mm settlement while for 30 mm and 50 mm settlement is at 60 and 50 mm. Failure pattern is obtained with the help of exhumed columns using plaster of Paris. Bulging failure is obtained in end bearing columns.

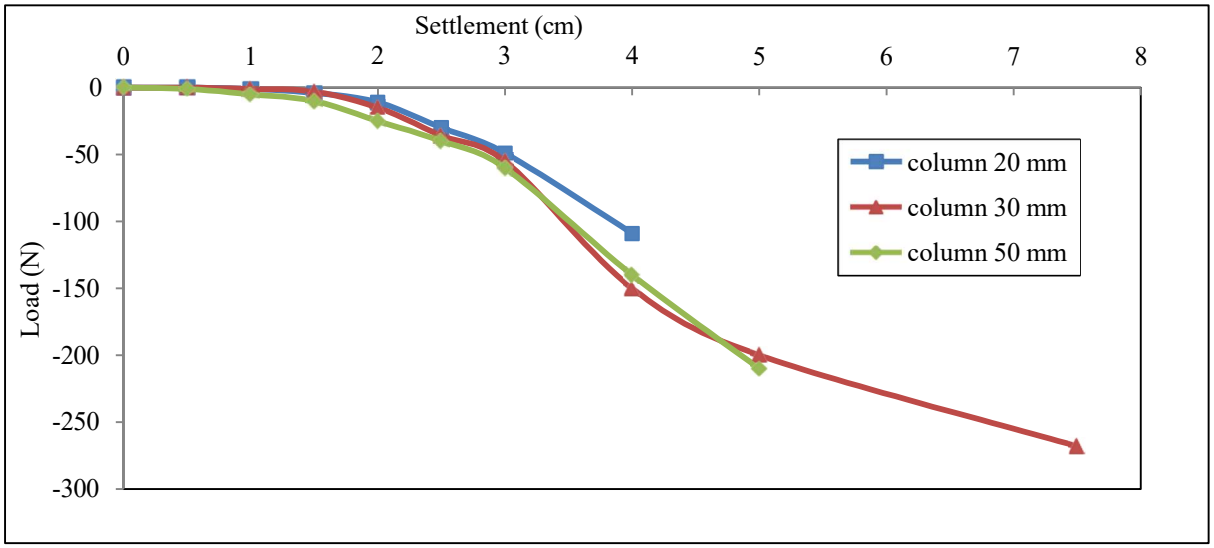


**Figure 6.15**: Granular unencased single column without iron dust

The load–settlement behaviour of stone columns with varying diameters (20 mm, 30 mm, and 50 mm) is presented in the graph. It is evident that the load-carrying capacity improves significantly with an increase in column diameter. The 20 mm diameter column exhibited the lowest resistance, reaching a maximum load of approximately 100 N at a settlement of about 30–40 mm, after which it failed rapidly. In contrast, the 30 mm diameter column demonstrated the highest load-bearing capacity, sustaining up to 280 N at a settlement of nearly 120 mm, indicating superior performance compared to the other diameters. The 50 mm diameter column also showed improved behaviour compared to the 20 mm column, resisting up to 200 N at a settlement of around 50 mm before declining. These results highlight that while an increase in diameter enhances load-carrying capacity, an optimum diameter exists, with the 30 mm column emerging as the most effective in this study.

**6.4.1.2 Granular encased single column:** The columns are encased with using geosynthetics i.e. geotextile and geogrid shown in figure 5 and 6. As the load increases settlement also increases with a certain amount of time. After which failure of the encased column obtained. The load bearing capacity of the column increases with the encasement of the column. Geotextile gives better results as compared to geogrid. After test completed exhumed column obtained as shown in figure 12 and 13 for both geogrid and geotextile.

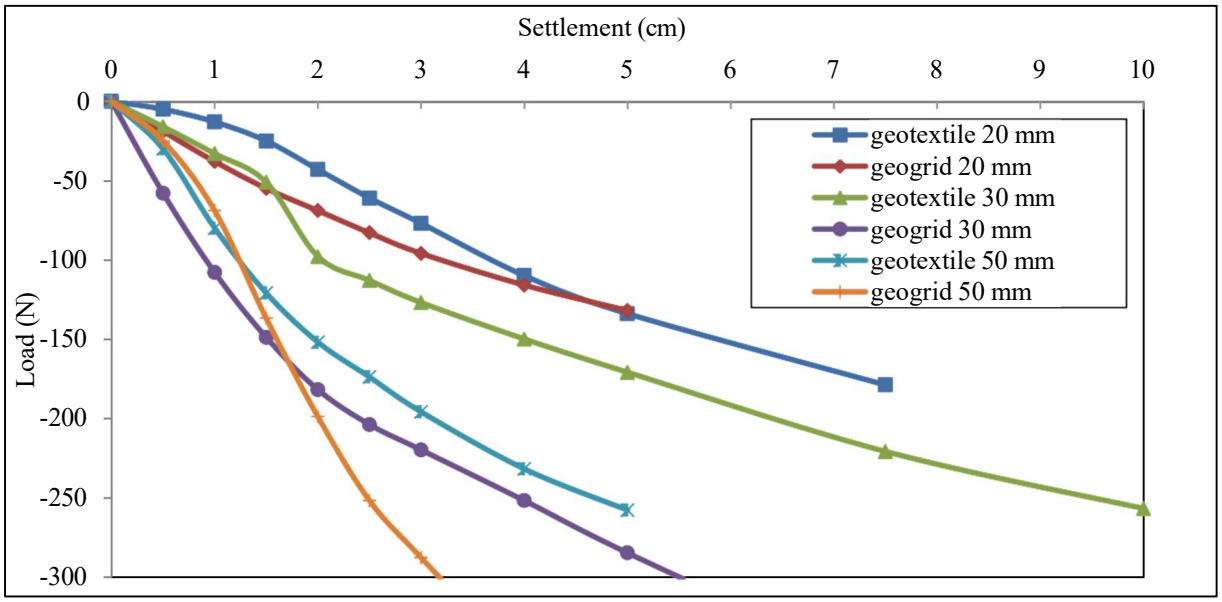


**Figure 6.16:** Granular encased single column without iron dust

19

The load–settlement behaviour of stone columns encased with geotextile and geogrid for different diameters (20 mm, 30 mm, and 50 mm) is shown in the graph, and the results clearly highlight the superiority of geotextile encasement over geogrid. For the 20 mm column, the geotextile-encased specimen exhibited the highest load resistance and sustained loading at lower settlements, whereas the geogrid-encased column failed earlier, indicating inadequate confinement. A similar trend was observed for the 30 mm diameter columns, where the geotextile-encased column demonstrated gradual load improvement and higher performance compared to the geogrid-encased column, which showed early settlement and reduced resistance. In the case of 50 mm diameter columns, the geotextile encasement again provided greater confinement and improved load resistance, while the geogrid encasement exhibited rapid settlement and the lowest capacity among all cases. Overall, geotextile encasement proved to be significantly more effective across all diameters, with the 20 mm geotextile column even outperforming larger geogrid-encased columns. These findings emphasise that the type of encasement plays a more decisive role in enhancing column performance than the diameter alone, with geotextile providing superior confinement, reduced settlement, and greater load-carrying efficiency.

### 6.4.1.3 Granular column in group

In group of granular column two columns placed along the diameter of the mould and other was triangular pattern designed with s/d = 1 with or without encasement. In group of two columns the settlement for without encasement showed 220 mm and for with encasement was 200 and 230 mm for geotextile and geogrid. In case of triangular pattern, settlement showed

without encasement 240 mm and with encasement provided using geotextile and geogrid was 260 and 230 mm. In group of columns triangular arrangement gives better results as compared to double columns. By providing encasement settlement reduces with the increase in load. In group of columns geogrid gives better results in both the geosynthetics used for the encasement.

**6.4.2 Granular column with iron dust:** In this case the iron dust is also added to the columns and the results are obtained.

**6.4.2.1 Granular unencased single column**

With the addition of iron dust the granular columns are casted using diameter of 20 mm, 30 mm and 50 mm, respectively. With the increase in load, settlement also increases upto certain time. When failure is obtained proving ring reading started reducing. The obtained results are shown in fig 17. The bulging failure is obtained in end bearing columns. Exhumed columns taken with the help of plaster of Paris.

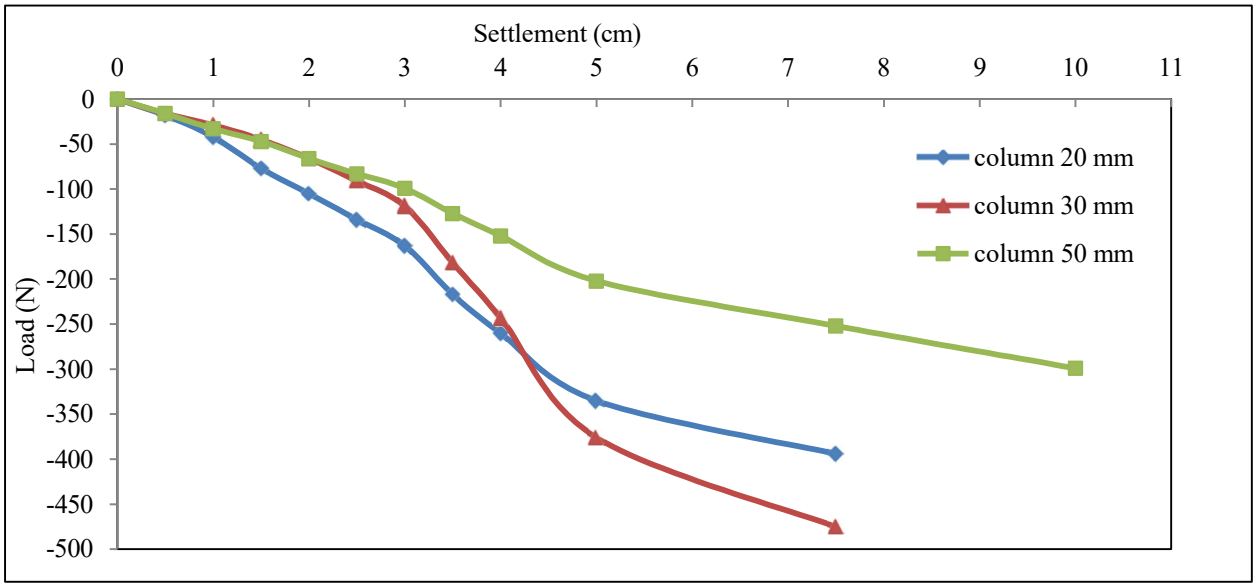


**Figure 6.17**: Granular unencased single column with iron dust

The load–settlement behavior of stone columns with varying diameters (20 mm, 30 mm, and 50 mm) is illustrated in the graph. It is observed that the 20 mm diameter column sustains a maximum load of about 400 N at a settlement of nearly 70 mm, showing a steeper load reduction pattern and indicating limited load-bearing capacity. In contrast, the 30 mm diameter column demonstrates superior performance, withstanding a maximum load of approximately 470 N at around 70 mm settlement, thereby highlighting it as the optimum column size in terms of load resistance. On the other hand, the 50 mm diameter column exhibits the ability to accommodate larger settlements up to 100–110 mm; however, its load-bearing capacity remains lower at around 300 N. These results clearly indicate that increasing

column diameter does not linearly improve the load capacity, and while the 50 mm column provides greater settlement tolerance, the 30 mm column offers the most efficient performance in terms of maximum load resistance.

### 6.4.2.2 Granular encased single column

The columns are encased with using geosynthetics i.e. geotextile and geogrid shown in fig 5 and 6. As the load increases settlement also increases with a certain amount of time. After which failure of the encased column obtained. The load bearing capacity of the column increases with the encasement of the column. Geotextile gives better results as compared to geogrid. After test completed exhumed column obtained as shown in fig 12 and 13 for both geogrid and geotextile.

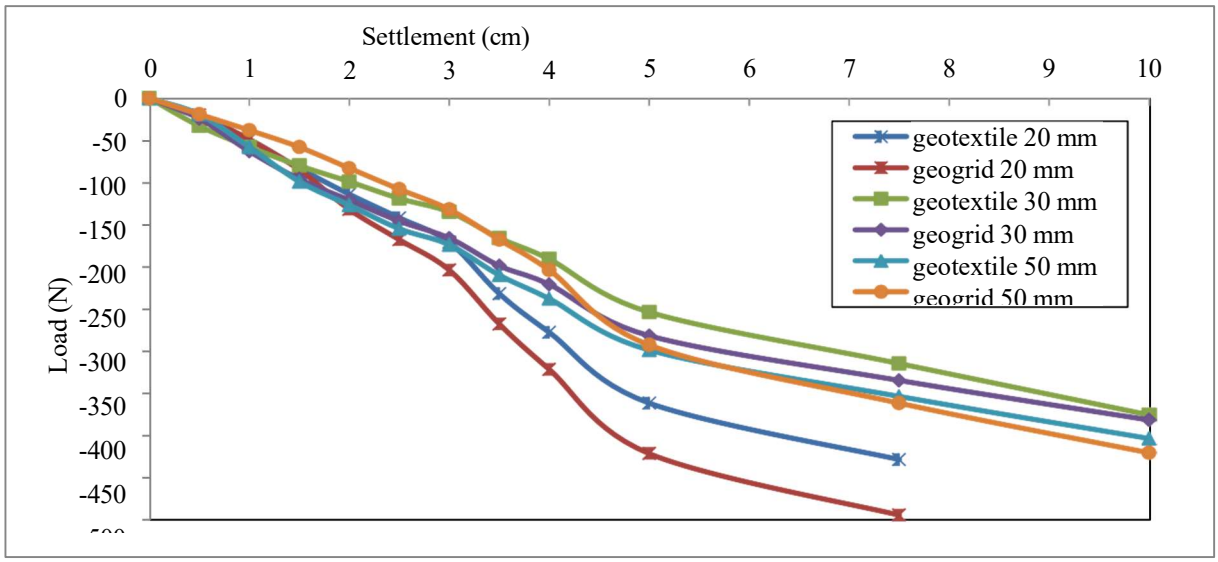


**Figure 6.18:** Granular unencased single column with iron dust

The graph illustrates the load–settlement response of stone columns of varying diameters (20 mm, 30 mm, and 50 mm) when encased with two different types of geosynthetics: geotextile and geogrid. The performance trends reveal that geosynthetic encasement significantly improves the load-bearing capacity of the columns compared to unreinforced ones, but the effectiveness depends on both the diameter and the type of encasement. For the 20 mm diameter column, the geotextile-encased column carries higher loads than the geogrid-encased one, with the latter showing the lowest capacity overall (≈ –470 N at 70 mm settlement). In the case of 30 mm diameter columns, both geotextile and geogrid encasements perform better, with the geotextile-encased column achieving higher resistance (≈ –300 N at 90 mm settlement) than the geogrid counterpart. Similarly, for 50 mm diameter columns, both encasement types show improved settlement tolerance, but the geotextile-encased column again provides slightly higher load-bearing capacity throughout the settlement range.

Overall, it can be concluded that geotextile encasement generally outperforms geogrid encasement across all diameters, with the most effective performance observed in the 30 mm geotextile-encased column, which shows the best balance between load resistance and settlement control. This indicates that the choice of both column diameter and encasement material plays a critical role in enhancing soil reinforcement efficiency.

The comparative evaluation of unreinforced and geosynthetic-encased columns clearly demonstrates that encasement significantly enhances the load-bearing performance. For the 20 mm column, geogrid encasement improved the load capacity by about 15%, while geotextile provided a 7.5% increase over the unreinforced case. In the 30 mm column, geotextile proved more effective with a 6.4% improvement, whereas geogrid contributed only a marginal 2.1% gain. The most notable enhancement was observed in the 50 mm column, where geotextile increased the load capacity by nearly 20% compared to 13.3% for geogrid. These results indicate that while both geotextile and geogrid contribute to improved strength and deformation control, geotextile encasement consistently outperforms geogrid, particularly for larger diameter columns. Overall, the findings highlight that geosynthetic encasement not only increases load resistance but also ensures better settlement control, with geotextile encasement emerging as the most efficient reinforcement option for optimizing column performance.

#### 6.4.2.3 Granular column in group

For group of columns, two columns placed along the diameter of the mould and other was triangular pattern designed with s/d = 1 with or without encasement. In group of two columns of diameter 30 mm the settlement for without encasement showed 200 mm and for with encasement was 180 and 220 mm for geotextile and geogrid. In case of triangular pattern settlement showed without encasement 220 mm and with encasement provided using geotextile and geogrid was 240 and 230 mm. In group of columns triangular arrangement gives better results as compared to double columns. By providing encasement settlement reduces with the increase in load. In group of columns geogrid gives better results in both the geosynthetics used for the encasement.

From these observations, it is evident that the triangular arrangement consistently performs better than the double column arrangement, as it shows reduced settlements under similar conditions. The addition of iron dust further enhances performance, as it results in lower settlements compared to the corresponding cases without iron dust, particularly in the two-

column group. Moreover, geogrid encasement demonstrates better results than geotextile in both conditions, highlighting its superior confinement capability in group column behavior. Overall, the results confirm that the combination of triangular arrangement, iron dust inclusion, and geogrid encasement provides the most effective configuration for reducing settlements and improving the efficiency of group granular columns.

### 6.5 Comparison in casting of granular column with or without iron dust

The results showed that with the mix of iron dust gives better results as compared to without iron dust. With using iron dust settlement reduces which cause increase in load capacity of the granular column. As the load increases, bearing capacity of the column increases for both the cases with or without encasement.

The experimental and comparative study on granular columns demonstrates that both column arrangement and encasement significantly influence load-bearing capacity and settlement behavior. For single columns, geotextile encasement proved more effective in enhancing load resistance, with the 30 mm diameter column showing optimum performance. In contrast, for group columns, the triangular arrangement consistently outperformed the double-column arrangement, offering better settlement control and load distribution. Between the two geosynthetics, geogrid provided superior results in group columns, while geotextile showed advantages in single columns. The inclusion of iron dust further improved the performance of both single and group columns, reducing settlements and enhancing overall strength, with the effect being more pronounced in group configurations.

Overall, it can be concluded that the most effective configuration is the triangular group arrangement of granular columns with geogrid encasement and iron dust inclusion, which ensures the highest load-bearing efficiency and minimum settlement.

### 6.6 Conclusion

1. The stone column for the ground improvement is made utilising industrial effluents products such as, iron dust, fly ash and sand is replaced with stone dust.
2. End bearing column shows failure in bulging.
3. The 30 mm column diameter gives better results as compared to others.
4. With the use of iron dust bearing capacity increases more as compared to without iron dust.
3. In group of columns two loading arrangements are used i.e. double columns placed along with the diameter of the mould and triangular pattern columns. In both the above triangular

loading gives the best results compared to two column loading arrangements with or without encasement.

4. The efficiency of the single column is less as compared to the group of columns. The triangular loading arrangement in groups gives approachable efficiency.

5. The column's bearing capacity is improved by the use of encasement using geosynthetics and reduces the settlement as compared to without encasement.

6. Geotextile shows better results as compared to geogrid due to its grid size as the material is fine used for column casting. The refined substance spills out or gets punched in the surrounding soil replaced for the column casting.